Euscorpius

Occasional Publications in Scorpiology

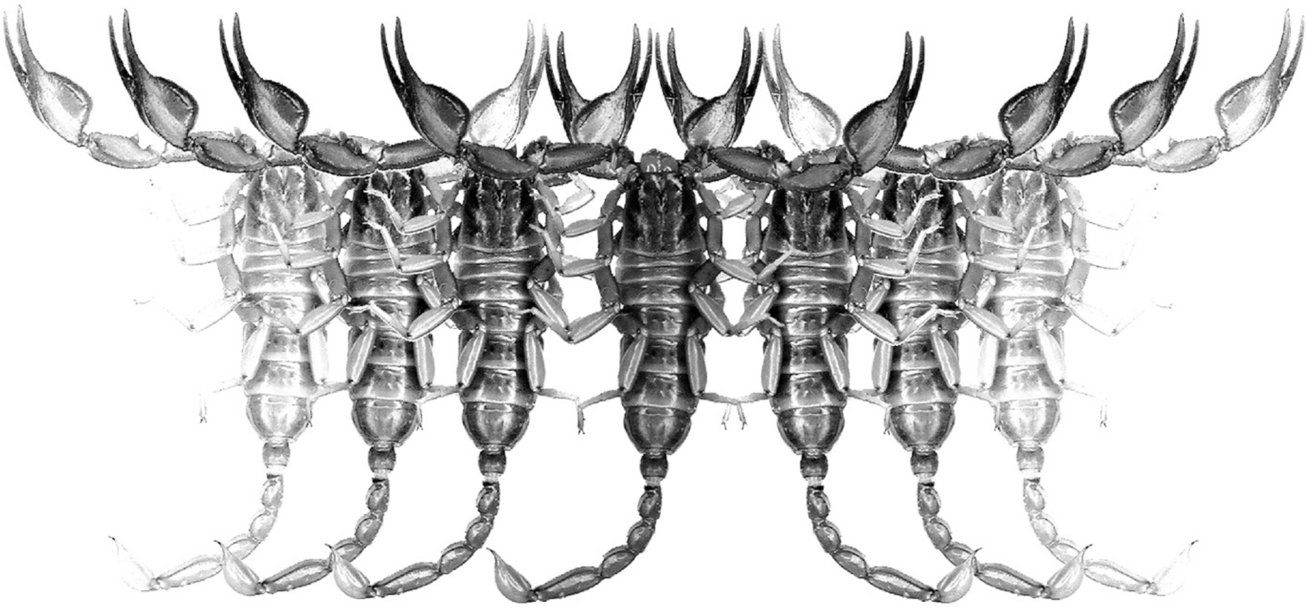

A new monotypic genus and species from China, *Langxie feti* gen. et sp. n. (Scorpiones: Buthidae)

Victoria Tang, Qingquan Jia & Leonhard Liu

April 2023 — No. 370

Euscorpius

Occasional Publications in Scorpiology

Euscorpius is the first research publication completely devoted to scorpions (Arachnida: Scorpiones). ***Euscorpius*** takes advantage of the rapidly evolving medium of quick online publication, at the same time maintaining high research standards for the burgeoning field of scorpion science (scorpiology). ***Euscorpius*** is an expedient and viable medium for the publication of serious papers in scorpiology, including (but not limited to): systematics, evolution, ecology, biogeography, and general biology of scorpions. Review papers, descriptions of new taxa, faunistic surveys, lists of museum collections, and book reviews are welcome.

Derivatio Nominis

The name ***Euscorpius*** Thorell, 1876 refers to the most common genus of scorpions in the Mediterranean region and southern Europe (family Euscorpiidae).

Euscorpius is located at: https://mds.marshall.edu/euscorpius/
Archive of issues 1-270 see also at: http://www.science.marshall.edu/fet/Euscorpius

(Marshall University, Huntington, West Virginia 25755-2510, USA)

ICZN COMPLIANCE OF ELECTRONIC PUBLICATIONS:

Electronic ("e-only") publications are fully compliant with ICZN (*International Code of Zoological Nomenclature*) (i.e. for the purposes of new names and new nomenclatural acts) when properly archived and registered. All ***Euscorpius*** issues starting from No. 156 (2013) are archived in two electronic archives:

- **Biotaxa,** http://biotaxa.org/Euscorpius (ICZN-approved and ZooBank-enabled)
- **Marshall Digital Scholar**, http://mds.marshall.edu/euscorpius/. (This website also archives all *Euscorpius* issues previously published on CD-ROMs.)

Between 2000 and 2013, ICZN ***did not accept online texts*** as "published work" (Article 9.8). At this time, *Euscorpius* was produced in two ***identical*** versions: online (*ISSN 1536-9307*) and CD-ROM (*ISSN 1536-9293*) (laser disk) in archive-quality, read-only format. Both versions had the identical date of publication, as well as identical page and figure numbers. ***Only copies distributed on a CD-ROM*** from ***Euscorpius*** in 2001-2012 represent published work in compliance with the ICZN, i.e. for the purposes of new names and new nomenclatural acts.

In September 2012, ICZN Article 8. What constitutes published work, has been amended and allowed for electronic publications, disallowing publication on optical discs. From January 2013, ***Euscorpius*** discontinued CD-ROM production; only online electronic version (ISSN 1536-9307) is published. For further details on the new ICZN amendment, see http://www.pensoft.net/journals/zookeys/article/3944/.

Publication date: 14 April 2023

http://zoobank.org/urn:lsid:zoobank.org:pub:117D9DDD-6F32-4E2C-BC09-D66B8D6265A4

Euscorpius — Occasional Publications in Scorpiology. 2023, No. 370

A new monotypic genus and species from China, *Langxie feti* gen. et sp. n. (Scorpiones: Buthidae)

Victoria Tang[1], Qingquan Jia[2] & Leonhard Liu[3]

[1] Zhangyang Rd. 200120, Pudong New District, Shanghai, China; email: jibril.flueqel@gmail.com
[2] Modern College of Northwest University, Changan District, Xian, Shaanxi, China; email: xinandaixy@126.com
[3] Guilin Medical University, Lingui District, Guilin, Guangxi, China; email: maziyuu.helgen@gmail.com

http://zoobank.org/urn:lsid:zoobank.org:pub:117D9DDD-6F32-4E2C-BC09-D66B8D6265A4

Summary

A new monotypic genus, *Langxie* **gen. n.**, is described from Xizang (Tibet), China. The new genus shares an important morphological character with *Afrolychas* Kovařík, 2019: absence of external accessory denticles (EADs) along the sixth row of median denticles (MDs) on the pedipalp movable finger. *Langxie* **gen. n.** is different from *Afrolychas* in the following aspects: loss of EAD near the proximally enlarged MD within each row (i. e., loss of all EAD on the movable finger; this also distinguishes the new genus from other related genera in the "(*Ananteris* + *Isometrus*)" clade (Štundlová et al., 2022)), subaculear tubercle armed with or without a secondary tubercle dorsally, immaculate color pattern, more slender appendages and metasoma, and less sexually dimorphic pectines. *Langxie* **gen. n.** further differs from another geographically close genus, *Himalayotityobuthus* Lourenço, 1997, by the presence of highly developed pectinal fulcra (vs. absent in *Himalayotityobuthus*), six rows of MDs on the pedipalp movable finger (vs. 7–8 in *Himalayotityobuthus*) and five pairs of lateral ocelli (vs. 3 in *Himalayotityobuthus*). The new species, *Langxie feti* **sp. n.**, is small and slender, exhibiting no obvious sexual dimorphism in pedipalp and metasoma, but the sexes are visibly different in the relative size of median ocelli and coarseness of carapacial granulation. Lattice microstructures are prominently developed on its cuticle.

Introduction

Xizang (or the Tibet Autonomous Region) has the most diverse scorpiofauna in China (30 species) (Tang, 2022d; Lv & Di, 2022), followed by Yunnan and Xinjiang Provinces. Six genera of five families have been recorded in this area: *Hottentotta* Birula, 1908 (Buthidae; 1 sp.), *Reddyanus* Vachon, 1972 (Buthidae; 1 sp.), *Chaerilus* Simon, 1877 (Chaerilidae; 8 spp.), *Scorpiops* Peters, 1861 (Scorpiopidae; 18 spp.), *Tibetiomachus* Lourenço & Qi, 2006 nomen dubium (see Kovařík, 2009: 27) (Hormuridae; 1 sp.), and *Deccanometrus* Prendini & Loria, 2020 (Scorpionidae; 1 sp.), all distributed in the south range along the national border. In this study, the seventh genus is described from Xizang (and the 14th genus for China), *Langxie* **gen. n.**, represented by a distinctive new species, *L. feti* **sp. n.** Within the Chinese scorpion fauna, the new species also represents the 13th species of Buthidae, and the 22nd species of parvorder Buthida (Tang, 2022b), if one were to ignore an isolated record of *L. scutilus* C. L. Koch, 1845 that was never confirmed again.

Kovařík (2019) conducted a taxonomic reassessment of the genus *Lychas* C. L. Koch, 1845 and established three new genera (*Afrolychas*, *Janalychas*, *Spelaeolychas*) based on the length of tibial spur on legs III and IV; the presence/absence of external accessory denticles on the pedipalp movable finger along the sixth row of denticles; the density of ventral setation of tarsomeres II of the legs; and the morphosculpture of the telson (presence or absence of granulation and lateral furrow). The validity of *Janalychas* was subsequently supported by a molecular analysis by Štundlová et al. (2022). The genus *Lychas* currently comprises 33 species, known mostly from the south and southeast Asia, Africa, Australia, and Oceania (Kovařík, 2019; Ythier & Lourenço, 2022; Kovařík, 2023). However, a more detailed revision is yet to be published and some dubious species could be transferred to other genera (e. g., some species from Africa, Australia, and Oceania currently placed in this genus). According to Kovařík (2019), the genus *Afrolychas* shares three characters with the genus *Lychas*: (1) tibial spurs reduced to moderate on leg III and leg IV; (2) ventral surfaces of tarsomeres II of legs densely equipped with two rows of setae; (3) telson smooth or granulated with the furrow absent or only indicated. One character differentiates the two genera: in *Afrolychas*, the external accessory denticle (EAD) is absent along the sixth row of median denticles (MDs) of the pedipalp movable finger; however, in *Lychas*, this row is flanked by 1–4 EADs. The absence of these EADs is also

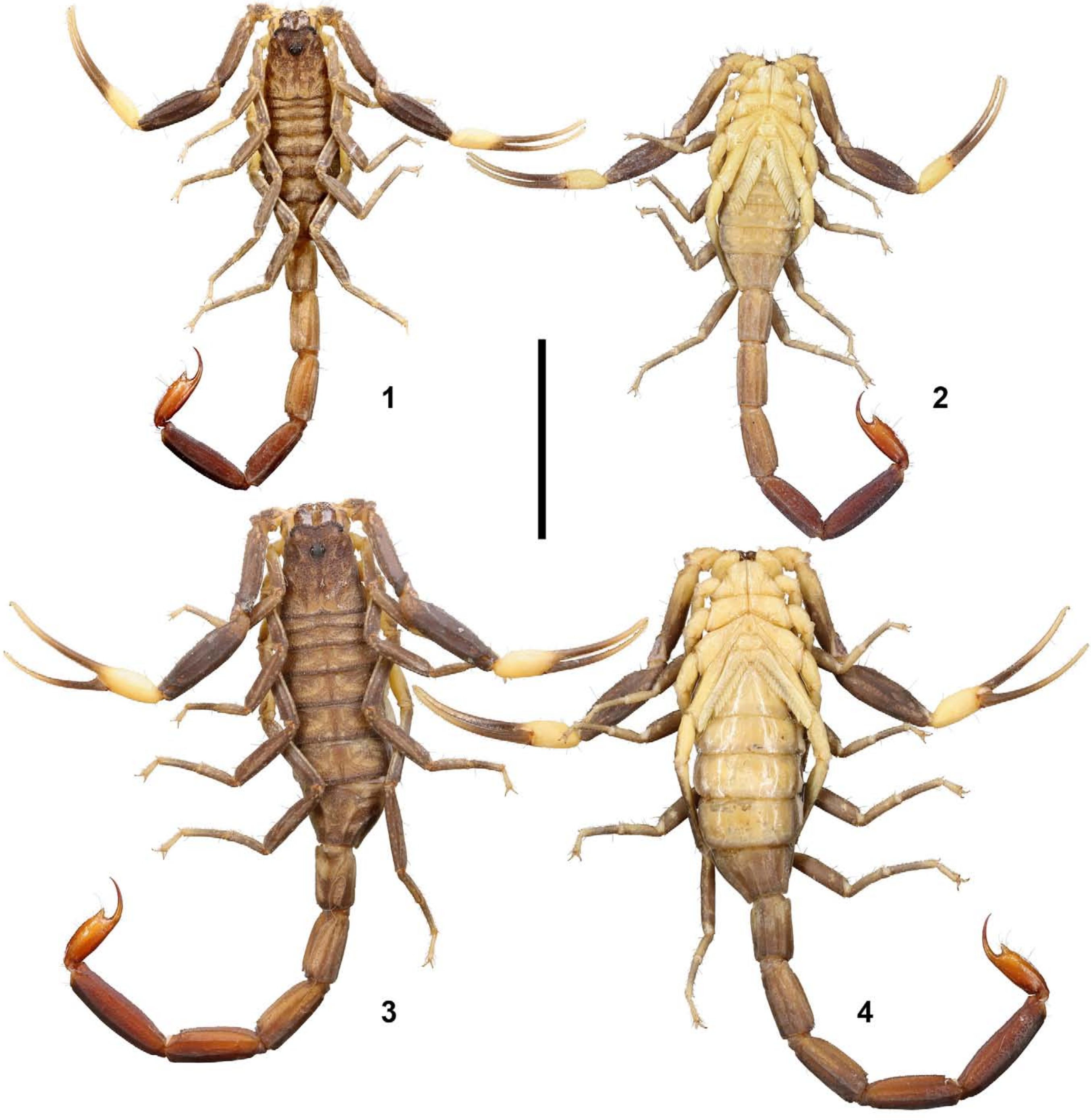

Figures 1–**4**: *Langxie feti* **gen**. et **sp**. **n**., habitus under white light. **Figures 1**–**2**. Male holotype in dorsal (1) and ventral (2) views. **Figures 3**–**4**. Female paratype in dorsal (3) and ventral (4) views. Scale bar = 10 mm.

a character of *Janalychas*, which differs from the previous two genera in: (1) tibial spurs elongated, and (2) telson in male laterally strongly bumpy with a developed longitudinal furrow (not verified for *J. albimanus* (Henderson, 1919)). The monotypic genus, *Spelaeolychas*, is from Malaysia and differs from *Lychas* in the ventral surfaces of tarsomeres II (with only 5–7 spiniform setae in two rows vs. densely equipped with two rows of setae).

Previously, the two most widespread species of *Lychas*, *L. mucronatus* (Fabricius, 1798) and *L. scutilus*, have been recorded in China and considered as the only two species of this genus in this country (Tang, 2020b). The former species is abundantly found in the provinces of Yunnan and Hainan, as well as in some parts of Guangxi, Guangzhou and Fujian Provinces (Tang, 2022b; probably in Taiwan as well, based on recent local observations); however, it is important to reiterate that the latter was only recorded in Shanghai once, based on a single female specimen collected in 1878 and was subsequently assumed to be extinct (Fet et al., 2000; Kovařík & Whitman, 2005). In the present study, a new species that has been so far

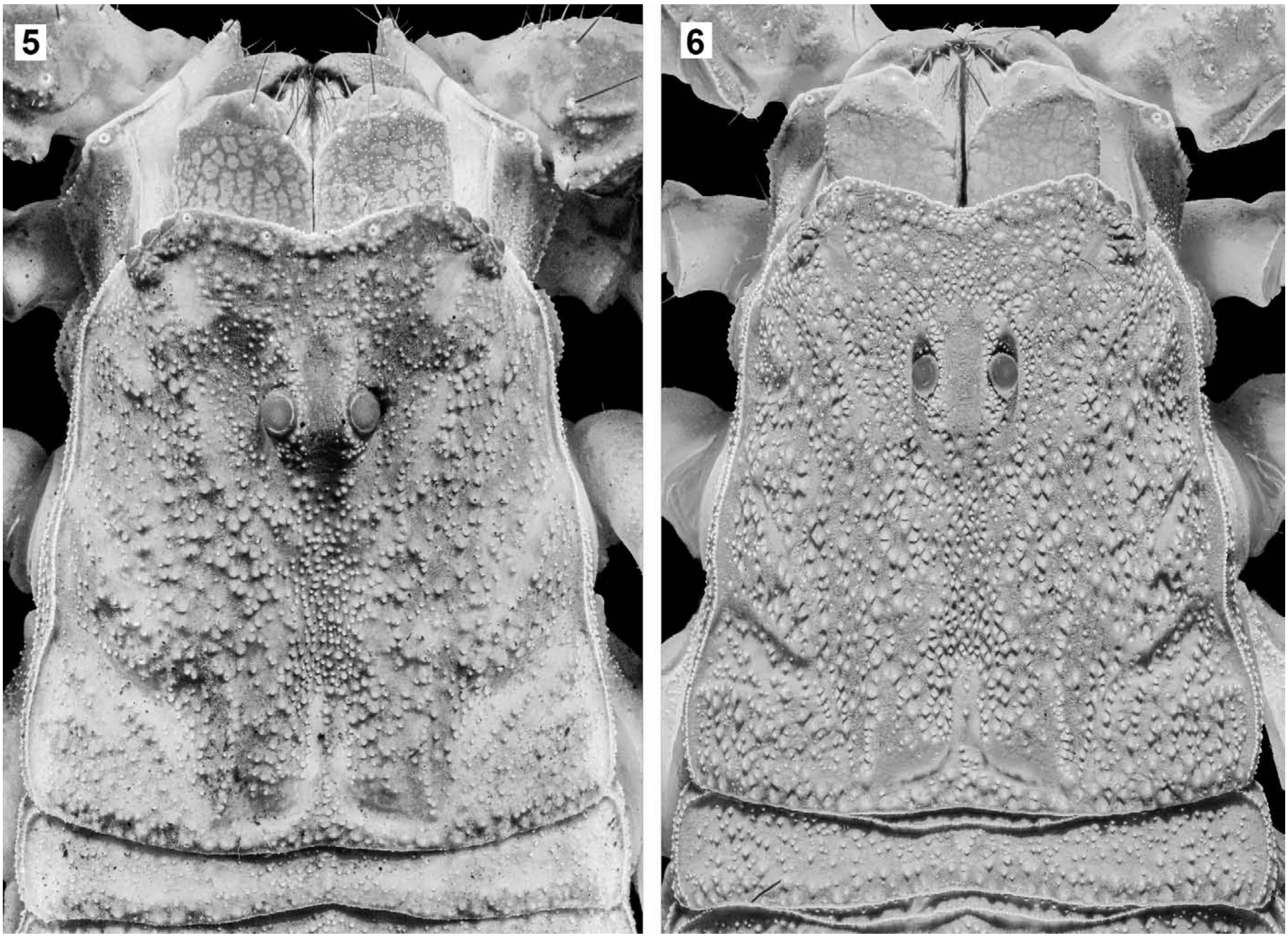

Figures 5–6. *Langxie feti* **gen**. et **sp**. **n**., carapace of female paratype (5) and male holotype (6) under UV light.

found only in China is described based on recently collected specimens from the southeastern region of Xizang. The new species is associated with some species of the "(*Ananteris* + *Isometrus*)" clade (Štundlová et al., 2022) in terms of its general morphological characters; Tang (2022b) mentioned this species based on several photographs and considered it to be the only endemic *Lychas* species of China (based on the presence of tibial spurs). However, after examination of the specimens, the new species keyed out as *Afrolychas* under the criteria of combinations of the four binary morphological characters defined by Kovařík (2019): no EADs were found along the sixth row of MDs of pedipalp movable finger. The geographic distribution and other characters suggest a new genus is required to accommodate this species, described here as *Langxie* **gen**. **n**. The validity of this new genus is also supported by a DNA analysis (in progress).

Langxie feti **gen**. et **sp**. **n**. was initially recorded from Gula Township and Chawalong Township, Chayu County, Linzhi Prefecture, Xizang, in August of 2019, by a group of college students during their expedition. However, those specimens were poorly preserved after a lengthy delay due to the dispute between the college students and the Chinese Academy of Sciences (the latter requested the former to donate the specimens free of charge for their publication; the students rejected, but even their own college would not provide the needed funds).

Methods, Material & Abbreviations

Morphology. Nomenclature and measurements mostly follow Stahnke (1971), Kovařík (2009), and Kovařík & Ojanguren Affilastro (2013), except for trichobothriotaxy (Vachon, 1974), sternum (Soleglad & Fet, 2003) and pedipalp patellar and femur carinae (Prendini et al., 2021). The detailed description of the new genus and species was based only on the holotype and allotypic paratype. However, in the differential diagnosis, the pectinal tooth count was based on all the type specimens studied (same with the coloration description) unless the structure was compromised; some pectinal teeth were lost or hidden and the count of those type specimens was inferred from the normal tooth size. The total length of the new genus and species is an approximated range of the minimal and maximal value (applying the retention method of "rounding") after roughly measuring the smallest and largest (visually determined) adults. For the measurement of the holotype and paratype, shrinkage due to dehydration prevented the posttergites and/or pretergites from being fully visible, and the measurement was directly applied upon the specimens along the central axis. Not until four months after the collection of the specimens by the second author (collector) did the first author (who examined the type specimens and wrote this paper) receive them (see Acknowledgements). Most of the specimens died during this period and as the second author had no previous experience in preserving scorpion specimens, the condition of the specimens was poor and most of them were nearly broken as the first author received them; more than half of the originally collected specimens were no longer useful and therefore were not sent to the first author. For the remaining six living specimens, the first author did not euthanatize or examine them (thus they will not be included in the type materials examined).

Photography. Photos of the specimens were taken by applying a different method from that of the previous papers by the first author. Previously, all the photos of detailed structures were taken by a microscope with a small camera attached to it, and photos at different focus distances were obtained by manual adjustments. In this study, a new setup was applied in order to obtain a higher resolution for minute details. This setup included two vertical stands, both mounted to a horizontal plane base, each carrying a camera (lens facing the base; Canon 5DsR, paired with Sigma or Laowa macro lens depending on the size of the target, and Kenko extension tube, if necessary) and a focus stacking rail (parallel to the stand; purchased from MJKZZ.de), respectively. A platform holding a board that carried the specimen was mounted perpendicularly to the rail. The rail carried the platform to move upwards and downwards at desired distances, and the camera took photos automatically after setting up the parameters in the MJKZZ 3 axes motion controller. The photos were then processed in two computer software, ZereneStacker and Photoshop. This setup was enlightened by the advice of Dr. Graeme Lowe (pers. comm. to V. Tang) but simplified.

Abbreviations. D, depth; L, length; W, width; PTC, pectinal tooth count; IAD, internal accessory denticle; MD, median denticle; EAD, external accessory denticle; PLMa, posterolateral major ocellus; ADMi, anterodorsal minor ocellus; PDMi, posterodorsal minor ocellus.

Specimen Depositories. VT (Personal collection of Victoria Tang, Shanghai, China); BMNH (British Museum [Natural History], London, UK); FKCP (František Kovařík, private collection, Prague, Czech Republic); ZMUH (Zoologisches Institut und Zoologisches Museum der Universität von Hamburg, Germany).

Comparative material (VT). *Centruroides bicolor* Pocock, 1898, 1♂1♀; *C. gracilis* (Latreille, 1804), 1♂; *C. nigrimanus* Pocock, 1898, 1♂; *Heteroctenus garridoi* (Armas, 1974), 1♀; *H. junceus* (Herbst, 1800), 1♂1♀; *Isometrus maculatus* (DeGeer, 1778), 1♂1♀; *Janalychas tricarinatus* (Simon, 1884), 1♀; *Lychas mucronatus* (Fabricius, 1798), 1♂1♀; *L. scutilus* C. L. Koch, 1845, juv. (sex no longer determinable); *Tityus footei* Chamberlin, 1916, 1♂; *T. smithii* Pocock, 1893, 1♀; *T. stigmurus* (Thorell, 1876), 1♀; all are dry specimens obtained as either pets or caught in the wild.

Systematics

Family Buthidae C. L. Koch, 1837

Langxie **Tang, Jia & Liu, gen. n.**

(Figures 1–63, 65, 82–155; Tables 1–3)

http://zoobank.org/urn:lsid:zoobank.org:act:50719AD2-C340-417F-A26F-B4D80DE62D88

TYPE SPECIES. *Langxie feti* **sp. n.**

ETYMOLOGY. The generic epithet is a noun in apposition, the Pinyin for "狼蝎" (láng xiē) in Chinese. Lang (狼) is the Chinese equivalent for "wolf", and xie (蝎) is that for "scorpion". This name is coined for three reasons: (1) the erroneous formal Chinese name for *Lychas* needs to be replaced (Tang, 2022a); (2) the new genus was found to be very abundant in the region and exhibited high tolerance to conspecifics, zooming among rock crevices like wolf packs; (3) the new genus was dominant in its habitat, and fed on a variety of prey, including other predatory arthropods.

DIAGNOSIS. Total length ca. 27–38 mm in adult males and ca. 38–45 mm in adult females. General coloration brownish, with whitish yellow pedipalp manus and reddish telson. Pedipalps, metasoma and telson rather slender. Cuticle furnished with prominently developed lattice microstructures. Carapace granular, lacking distinct carinae (except for a pair of posterior median carinae sometimes moderately indicated by granules, but the superciliary carinae constantly appear), flat, isosceles trapezoidal with concave anterior margin. Median eyes very small, situated anteriorly in the ratio ca. 2: 7 to 1: 3. Five pairs of lateral eyes (three major ocelli, two minor ocelli). Tergites I–VI granular, with single median carina, tergite VII with 5 carinae. Sternum type 1, sub-triangular in shape. Pectinal tooth counts 18–21 in males and 16–19 in females. Pectines with conspicuous fulcra. Chelicerae with typical buthid dentition with a single enlarged denticle on ventral side of fixed finger. Metasoma elongate, segment I with 10 carinae, II–IV with 8–10 carinae, lateral median carina can be lacking. Telson elongate, ellipsoidal in shape, with distinct, triangular, subaculear tooth which sometimes presents a secondary tubercle on dorsal surface. Pedipalps orthobothriotaxic, type Aβ, femur trichobothrium d_2 prolateral to prodorsal carina, patella d_3 between retrodorsal and dorsomedian carina. Dentate margin of chela movable finger comprises 6 non-imbricated rows of MDs, row 1 to 5 terminate proximally in a moderately enlarged MD which is flanked by an IAD; apical row anterior to the 1st row very short, composed of less than 5 subterminal denticles, distal end flanked by one or two terminal denticles; EAD absent from all margins of both fixed and movable fingers. Short tibial spurs present on leg III and leg IV, tibia and tarsus without bristle combs, ventral surfaces of tarsomeres II equipped with 2 rows of short setae (ca. 9–12 for each row), ungues stout.

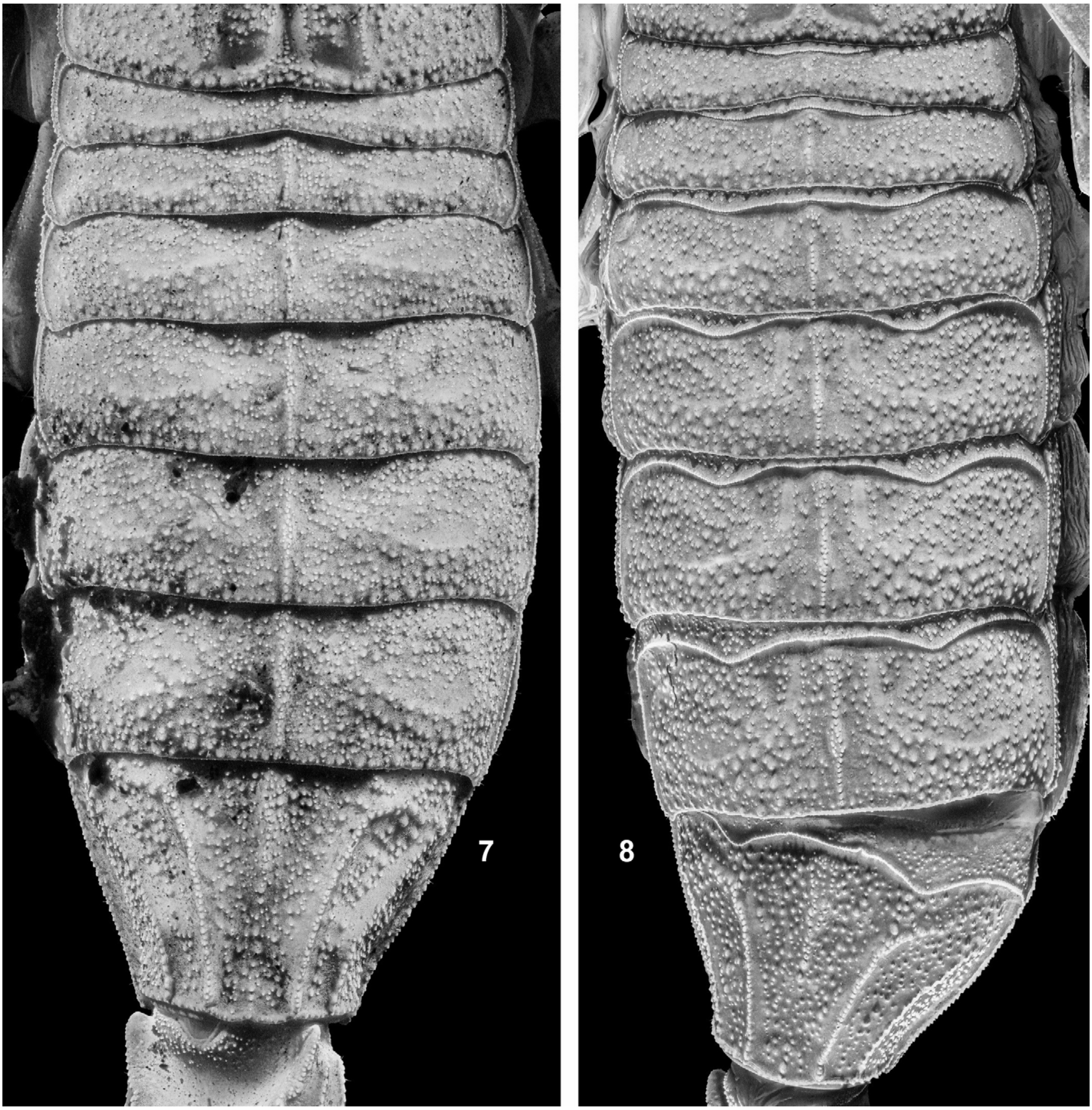

Figures 7–8. *Langxie feti* **gen**. et **sp**. **n**., tergites of female paratype (7) and male holotype (8) and under UV light.

Affinities. There are eight characters, which in combination differentiate *Langxie*, **gen**. **n**. from all other buthids: pedipalps orthobothriotaxic, type Aβ (*beta*-configuration); legs III and IV with tibial spurs; pedipalp movable fingers with six non-imbricated rows of denticles; pedipalp movable fingers without EAD; carapace flat; cheliceral fixed finger with a single ventral denticle; telson with a distinct subaculear tooth; metasoma V smooth or granulated without punctate.

The new genus is most similar to both *Afrolychas* and *Lychas* in its diagnostic characters. Only two species were included in *Afrolychas* by Kovařík (2019): *A. braueri* (Kraepelin, 1896) and *A. burdoi* (Simon, 1882). Both species are small-sized and they apparently also differ from the new genus in the following aspects: (1) maculate color pattern; (2) appendages relatively short; (3) metasoma relatively robust; (4) pectines more sexually dimorphic. In *A. braueri*, the dorsosubmedian carinae of metasoma II–III are armed with prominently enlarged posterior teeth (Kovařík, 2019: figs. 130–133), which is not the case for the new genus. The pectines of *A. braueri* is obviously sexually dimorphic (Kovařík, 2019: figs. 131, 133), but similar intersexually in *L. feti* **gen**. et **sp**. **n**. Additionally, the subaculear tubercle of the new genus is either

Dimensions (mm)		*Langxie feti* **gen**. et **sp**. **n**. ♂ HT	*Langxie feti* **gen**. et **sp**. **n**. ♀ PT
Carapace	L / W	3.66 / 3.29	4.64 / 3.86
Mesosoma	L	6.98	11.14
Tergite VII	L / W	1.96 / 3.13	3.06 / 3.78
Metasoma + telson	L	20.67	25.46
Segment I	L / W / D	2.46 / 1.68 / 1.47	2.93 / 2.01 / 1.88
Segment II	L / W / D	3.05 / 1.51 / 1.43	3.41 / 1.75 / 1.70
Segment III	L / W / D	3.16 / 1.42 / 1.40	3.92 / 1.66 / 1.67
Segment IV	L / W / D	3.59 / 1.35 / 1.38	4.75 / 1.62 / 1.64
Segment V	L / W / D	4.37 / 1.29 / 1.33	5.73 / 1.57 / 1.59
Telson	L / W / D	4.04 / 1.11 / 1.17	4.72 / 1.14 / 1.37
Pedipalp	L	15.24	18.79
Femur	L / W	3.66 / 0.78	4.76 / 1.16
Patella	L / W	4.74 / 1.16	5.37 / 1.72
Chela	L	6.84	8.66
Manus	L / W / D	2.35 / 0.93 / 0.88	3.19 / 1.15 / 1.24
Fixed Finger	L	4.49	5.47
Movable finger	L	4.77	6.21
Total	**L**	**31.31**	**41.24**
Pectine teeth number	left / right	20 / 19	18 / 18

Table 1. Comparative measurements of *Langxie feti* **gen**. et **sp**. **n**. male holotype and female paratype. Abbreviations: length (L), width (W, in carapace it corresponds to posterior width), depth (D).

armed with or without a secondary tubercle dorsally. On the other hand, this character is absent in *A. burdoi* (Kovařík, 2019: fig. 101) and present ventrally in *A. braueri* (at least visible in females; Kovařík, 2019: figs. 132–133). Due to the scarcity of subordinate taxa, the comparison of the new genus with *Afrolychas* can be easily biased. The four characters chosen by Kovařík (2019) in his matrix to diagnostically separate the genera may not be sufficient to indicate the phylogenetic relationships between these taxa. Although the new genus shares one more character with *Afrolychas*, it is hypothesized to be closer to *Lychas*, but this nonetheless requires a comprehensive phylogenetic study. Biogeographically, the highly disjunct distribution of *Afrolychas* vs. the new genus, which are isolated from each other by the Himalaya Mountain range, a major vicariant barrier, argues against inclusion of the new species in *Afrolychas*.

The new genus mainly differs from the *Lychas* by the loss of all EAD. These regular EADs are present in all the other known species of the "(*Ananteris* + *Isometrus*)" clade. Geographically (Fig. 86), the new genus is found most closely to five species of the genus *Lychas*: *L. brehieri* (Myanmar), *L. gravelyi* (Myanmar), *L. mucronatus* (China and Myanmar populations) and *L. scutilus* (Myanmar populations). However, both *L. brehieri* and *L. gravelyi* were described from Mon State in the south of Myanmar, and the former was discovered in the "Saddan Sin Gu" Cave, while the latter is only known from the Mawlamyine ("Moulmein"), Tenasserim. Moreover, the record of *L. scutilus* in Myanmar was from Maliwan Village ("Birma, Malewoon", No. VA2642, ZMUH), which is further south. As a result, the only closely distributed species of *Lychas* would be *L. mucronatus*, with the north-most record from Deqin (Dêqên) County, Diqing Tibetan Autonomous Prefecture (see figure 1 in Tang, 2022b). The Himalaya Mountain system may serve as an effective vicariant barrier blocking gene flow from the *Lychas* species in India as well. The new genus can be easily distinguished from the geographically close species, *L. mucronatus*, by a combination of evident characters besides the generic characters: (i) appendages and metasoma much more slender in the new species; (ii) pedipalp chelae do not create prominent gap between cutting edges when closed (in males) in the new species; (iii) coloration much darker, without conspicuous spots throughout the body and immaculate on pedipalp chelae in the new species; (iv) carapace without conspicuous median longitudinal groove posterior to the median ocelli in the new species; (v) carinae on metasoma more developed in the new species; (vi) telson more slender with a slightly less curved aculeus in the new species.

We further compared the new genus with another geographically close buthid genus, *Himalayotityobuthus* Lourenço, 1997, which also comprises only two species (*H. martensi* Lourenço, 1997 and *H. alejandrae* Lourenço, 2003). The original descriptions for those two species are poor with insufficient illustrations. The new genus clearly differs from *Himalayotityobuthus* by the presence of pectinal fulcra, and it may be different in other potential aspects (provided that

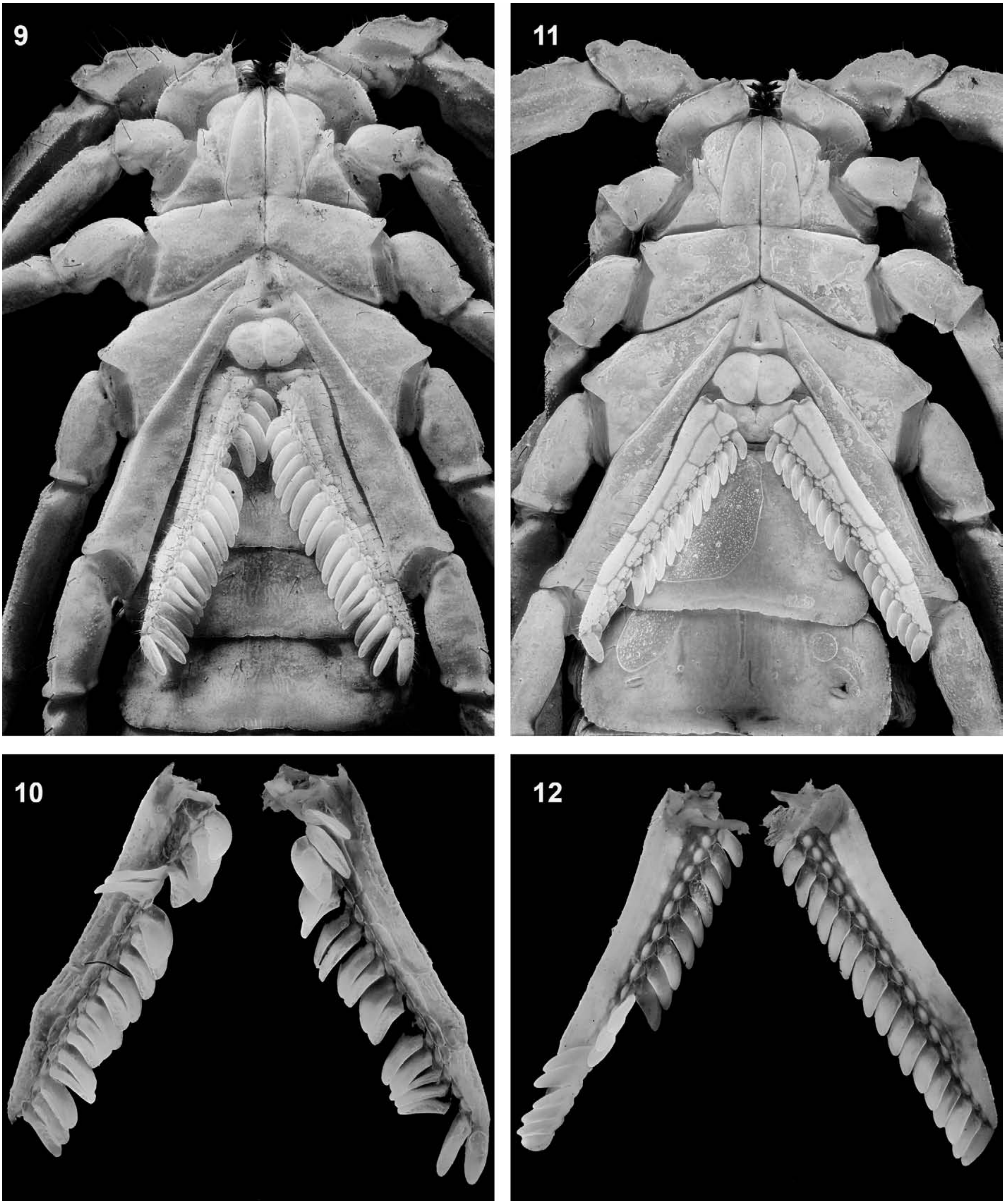

Figures 9–12: *Langxie feti* **gen**. et **sp**. **n**., coxal and sternopectinal regions (9, 11) and pectines in dorsal aspect (10, 12) under UV light (figures of left and right pectines in dorsal aspect mirrored to directly match the ones in ventral aspect in their above figures). **Figures 9–10**. Male holotype. **Figures 11–12**. Female paratype.

Figures 13–14: *Langxie feti* **gen**. et **sp**. **n**., sternites under UV light. **Figure 13**. Male holotype. **Figure 14**. Female paratype.

the documentation was correct; *Himalayotityobuthus* vs. *L. feti* **sp**. **n**.): (1) three lateral ocelli vs. five lateral ocelli (no illustrations); (2) 7–8 vs. 6 rows of denticle (based on the holotype male of *H. martensi*; F. Kovařík, pers. comm.); (3) accessory denticles present vs. absent (based on the holotype male of *H. martensi*; F. Kovařík, pers. comm.); (4) carapace anteriomedian notch present (e. g., *H. martensi*; based on the specimen MNHN-RS-RS8236) vs. absent; (5) spurs strong vs. moderate to weak (qualitative, no illustrations); (6) tarsus with numerous setae vs. two rows of setae comprised of ca. 12 setae (qualitative, no illustrations).

Distribution (Fig. 86). China (Tibet Autonomous Region).

Comments

Loss of accessory denticles.

Buthid scorpions are often characterized by their rows of denticles (or granules) on the pedipalp movable finger. Terminologies of these denticles varied in the past literature. Conventionally, the most distal denticle is called a terminal denticle, and those denticles just proximal to it are called subterminal denticles. The short row formed by those subterminal denticles is called an apical row, excluded

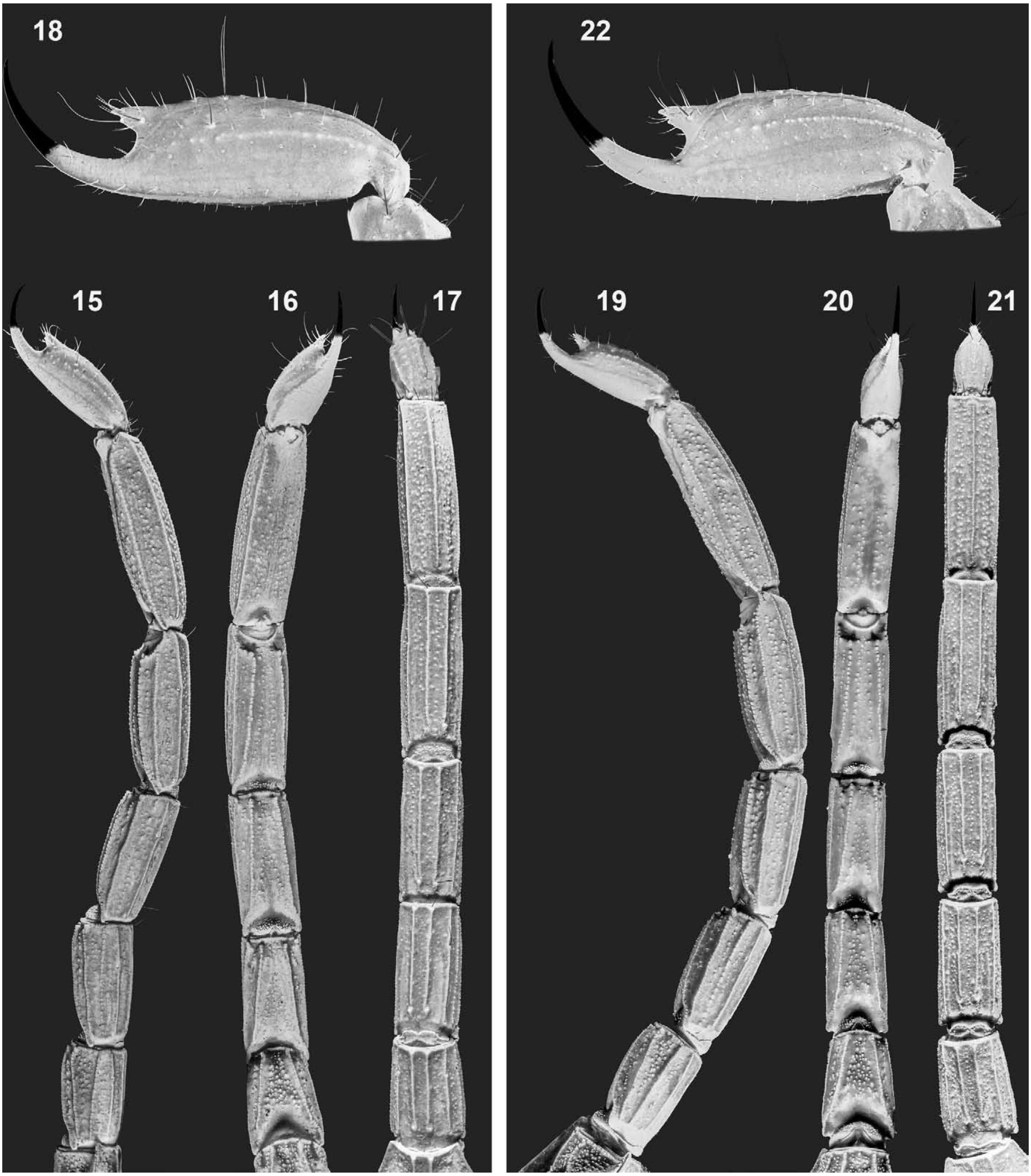

Figures 15–22: *Langxie feti* **gen**. et **sp**. **n**., metasoma and telson under UV light. **Figures 15–18**. Male holotype, metasoma and telson lateral (15), dorsal (16), and ventral (17) and telson lateral (18). **Figures 19–22**. Female paratype, metasoma and telson lateral (19), dorsal (20), and ventral (21) and telson lateral (22).

from the "primary denticle rows". We identify three types of denticles: internal accessory denticle (IAD), median denticle (MD) and external accessory denticle (EAD). For reference, these have the following notational equivalences in the literature: IAD = *gi* (*granule (accessoire) interne*; Vachon, 1950: figs. 72, 74) = *ia* (*inner accessory granules*; Stockwell, 1989: fig. 73) = *interior lateral granule* (Tikader & Bastawade, 1983: fig. 13) = *internal series* (Pocock, 1990:

fig. 3); MD = *pg* (*primary granules*; Stockwell, 1989: fig. 73) = *grr* (*granular row*; Sissom, 1990: fig. 3.17h) = *denticle series* (Levy & Amitai, 1980: fig. 8) = *median series* (Tikader & Bastawade (1983: fig. 13); Pocock (1900: fig. 3)); EAD = *ge* (*granule (accessoire) externe*; Vachon, 1950) = *oag* (*outer accessory granule*; Levy & Amitai, 1980: fig. 8; Sissom, 1990: figs. 3.17g, i) = *external series* (Pocock, 1990: fig. 3) = *exterior lateral granule* (Tikader & Bastawade, 1983: fig. 13) = *outer accessory denticle* (Levy & Amitai, 1980: fig. 8).. The definition of denticles in Soleglad & Sissom (2001: fig. 1) was different: their "outer denticles (OD)" on their left diagram integrated into the MD series, but separated therefrom on their right diagram. However, their scheme was defined for chactoids and iurids.

All three types of denticles are present in all the previously described species of *Afrolychas*, *Janalychas*, *Lychas* and *Spelaeolychas* (e. g., Kovařík, 1997: figs. 2–39; Kovařík, 2019: figs. 13–17). The presence of EAD was explicitly confirmed in Kovařík's (2019) generic diagnosis for all four genera: "…*terminated proximally flanked by two enlarged outer accessory denticles*…" (in reality, the "two enlarged outer accessory denticles" included one enlarged proximal MD, i. e., only one EAD flanks the denticle rows). The dentition pattern is very similar among all the species: each row of MD is terminated near an IAD distally and an enlarged MD within itself proximally, the latter of which is further flanked by an EAD. The identification and terminology of these denticles were mainly based on position, size and interdenticle spacing. The IAD and EAD always appear alone on the inner and outer margins respectively; usually, the IAD is obviously larger than all MD, while EAD is only slightly larger (if not identical with) than the proximally enlarged MD of each row. MDs of each row are always tightly positioned (contiguous) and the distal MD separates from IAD by a greater spacing. Soleglad & Sissom (2001: 33) wrote: "…*corresponding inner and outer denticles are paired for most of the length of the finger, forming denticle group (DG) boundaries within the median denticle row*…" in their revision of Euscorpiidae. Therefore, the IAD is conventionally paired with the MD row that is distal to it, i.e., the IAD near the distal end of an MD row is associated with the MD row anterior to this row; hence, the most proximal MD row does not have an IAD. However, the IAD may not always near the distal end of an MD row in buthids. An MD row may terminate distally at the proximal MD of the next distal MD row, and the IAD of the latter may be well separated from it (e. g., in *Butheolus* Simon, 1882; Lowe, 2018: figs. 41–42, 109–110). The most proximal MD of each row is often enlarged and this size increase is gradual from distal to proximal. In some species, the EAD flanks the enlarged MD on the same level or slightly distal to it, and the EAD is often separated by a larger gap than the interdenticle spacing within its adjacent MD row. However, an EAD can be difficult to discern from the MD row if this row is slanted and slightly imbricated. For example, in *Barbaracurus* Kovařík et al., 2018, each MD row is non-imbricated, almost linear and terminated by two conspicuously enlarged denticles (i.e., one enlarged MD + one EAD; Kovařík et al., 2018: figs. 1–10). However, in *Babycurus* Karsch, 1886, the increase of denticle size is gradual; typically, each row is terminated proximally by three more or less contiguous enlarged denticles (i.e., one enlarged MD + two EADs; Kovařík et al., 2018: figs. 11–23). The consideration of the enlarged MD and two EADs in *Babycurus* can be potentially defined by the linearity of the MD row. The short "row" comprised of the two EADs forms an obtuse angle against the MD row; the enlarged MD can be regarded as the apex of this angle. In the absence of these two EADs, the MD row is sublinear, which accords with other taxa that show a clear separation between the final MD and EAD, rendering the recognition of MD row feasible (e. g., Kovařík, 2019: fig. 13). However, this depends on how small the angle is (i.e., a larger angle renders the entire MD row plus the EAD(s) more sublinear). A similar consideration is proposed in Tang (2022c) for the identification of the denticle rows of *Scorpiops* Peters, 1861.

In our new genus, *Langxie* **gen**. **n**., all EADs are absent from the MD rows. This is a less common condition and so far known only from some "*Buthus* group" (sensu Fet et al., 2005; Štundlová et al., 2022) genera and species (e. g., *Anomalobuthus* Kraepelin, 1900 (Teruel et al., 2018), *Birulatus* Vachon, 1974 (Stathi & Lourenço, 2003), *Lissothus* Vachon, 1948 (Lourenço & Sadine, 2014), *Buthacus arenicola* (Simon, 1885) and *B. spatzi* (Birula, 1911) (Lourenço, 2006; Cain et al., 2021), a number of species of the "*werneri*" group of *Compsobuthus* Vachon, 1949 (Levy & Amitai, 1980), and a minority of *Orthochirus* Karsch, 1891 (as "outer denticles"; e. g., *O. formozovi* in Kovařík et al., 2020)), as well as in *Karasbergia methueni* Hewitt, 1913 (belonging to the "(*Charmus* + *Uroplectes*) group", sensu Štundlová et al., 2022); Hewitt, 1913: pl. XV, fig. 2; Prendini, 2004: 86). The absence of all EADs is unprecedented within *Lychas* and its three related genera, as well as in other closely related groups (e. g., *Isometrus* Ehrenberg, 1828 and *Reddyanus* Vachon, 1972; cf. Kovařík et al., 2016: figs. 241–259). The presence of imbricated MD rows and the number of enlarged EAD per row, are considered informative characters for discriminating buthid genera (Kovařík et al., 2018). The degree of "imbrication" of MD rows is defined by the length of the overlapping (but parallel) region in two adjacent rows (i.e., the posterior region of the anterior row and the anterior region of the posterior row). This can be recognized by how far the final MD of the anterior row extends to the posterior row. Few buthid genera have been considered with imbricated rows: *Ananteroides*, *Babycurus*, *Buthoscorpio*, *Centruroides*, *Egyptobuthus*, *Grosphus*, *Heteroctenus*, *Mesotityus*, *Odonturus*, *Tityus* and *Zabius* (Kovařík et al., 2018). If the final MD of the anterior row is on the same level with or above the first MD of the posterior row, then the denticle rows are considered non-imbricated. According to the figures in Kovařík (2019: figs. 13–17), the denticle rows of *Afrolychas*, *Janalychas*, *Lychas* and *Spelaeolychas* are non-imbricated, but there are slight differences: tighter rows (i.e., the final MD of the anterior row is on the same level with the first

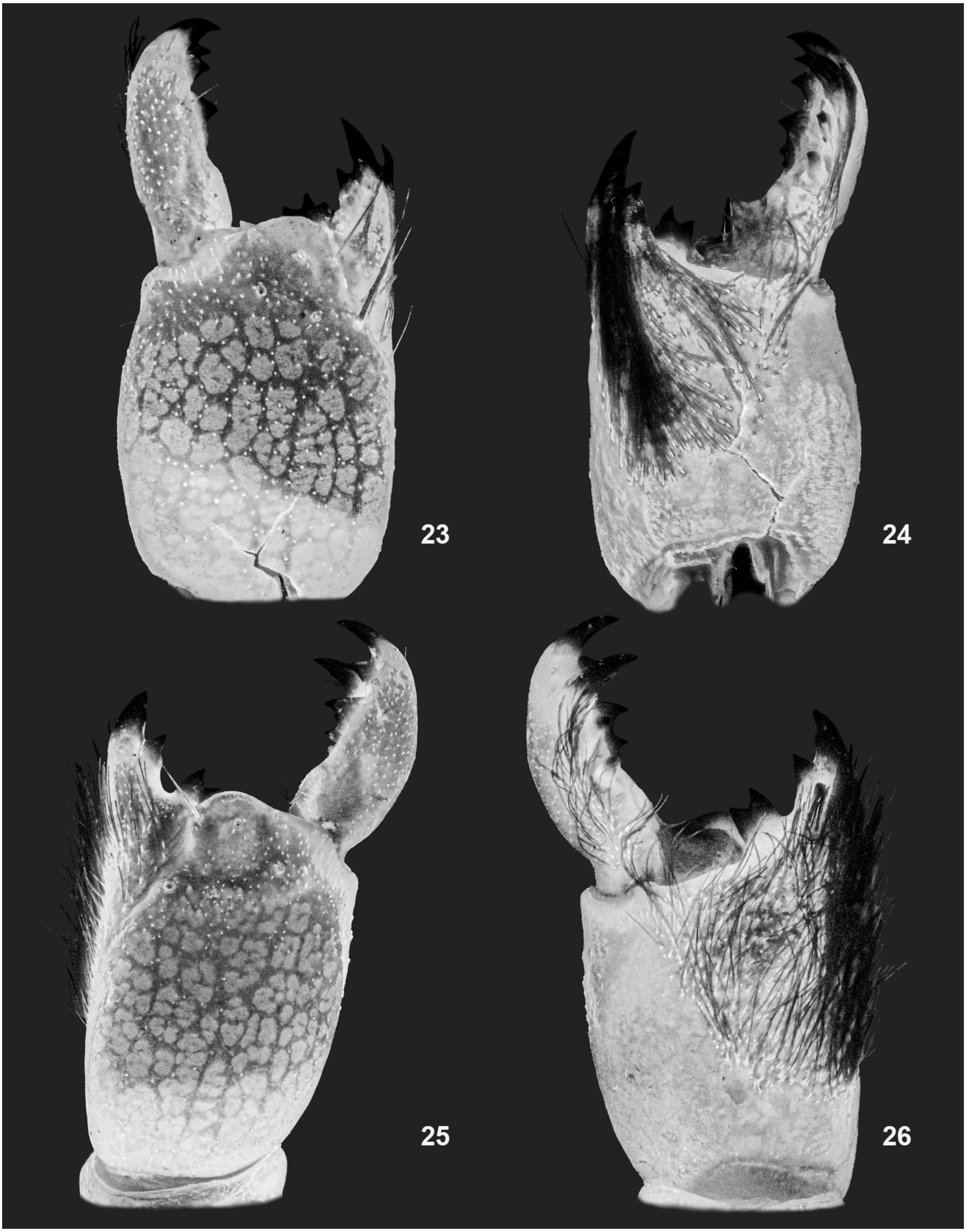

Figures 23–**26**: *Langxie feti* **gen**. et **sp**. **n**., chelicera in dorsal (23, 25) and ventral (24, 26) views under UV light. **Figures 23**–**24**. Male holotype. **Figures 25**–**26(change)**. Female paratype.

MD of the posterior row) are sometimes present in *Lychas*, *Janalychas* and *Spelaeolychas*, but never in *Afrolychas* (i. e., the two MDs are completely separated). In our new genus, each pair of adjacent MD rows are evidently separated by an obvious spacing, and the final MD is further above the IAD of its subordinate row. This renders a rather "loose" arrangement of MD rows. Pseudochactidae is hypothesized to be a basal scorpion family, sister to Buthidae (Prendini et al., 2021), so it can serve as an outgroup to polarize buthid characters (Kovařík et al., 2018). All pseudochactids exhibit non-imbricated linear series of MDs with a single EAD; this can be considered as a plesiomorphic state and is shared by many buthid taxa. Therefore, the imbricated rows and multiple EAD may both be derived characters in buthids. All the species in the "(*Ananteris* + *Isometrus*) group" (Štundlová et al., 2022) previously described also show non-imbricated MD rows and the presence of EAD. *Langxie* **gen**. **n**. apparently belongs to this group in terms of its general characters. However, the loss of all EAD suggests an autapomorphic condition, unique to itself. Phylogenetic relationships can only be analyzed by determining synapomorphies that are shared by more than one species. Hence, the phylogenetic position of this new genus is currently unknown until a more comprehensive study based on DNA sequences and a more detailed morphological character matrix is accomplished.

Sex and maturity determination.

The determination of sex and maturity in scorpions is crucial before any morphological description and/or comparison can be justified. This is partially because juveniles of different species can be very similar to each other, preventing differentiation. Asymmetrical comparison (between immature and mature specimens) can easily be biased since both quantitative (e. g., ratio, total length, density of granulation) and qualitative (e. g., development of carinae and lobes, coloration) characters are not fully developed in juveniles. Species descriptions based on immature specimens (or presumably so) have caused unnecessary inconvenience for subsequent authors, calling for re-examinations of types or extra efforts on collecting and reanalyzing topotypes (e. g., Kovařík & Lowe, 2022; Teruel & Turiel, 2022; Tang, 2022b). Correct sex determination is crucial as many taxa exhibit sexual dimorphism, often compared and used for differential diagnosis. Therefore, all available specimens of the new species were individually examined to ascertain their sex and development stage. These two conditions were evaluated on the basis of characters correlated with sexual maturity commonly observed in many other scorpion taxa.

For most of the Old World buthids, the pectinal morphology is often a useful character for determining sex regardless of the development stage. In some species, females have either enlarged basal teeth (e. g., *Grosphus* spp., *Teruelius* spp., *Uroplectes* spp.) or dilated basal lamellae (e. g., most *Parabuthus* spp.). However, this convenient character is not available for most other taxa. Male scorpions of the same species usually tend to possess more pectinal teeth (i.e., higher PTC) than females do, probably owing to their intense vagrancy during the mate season and thus requiring more sensorial organs (the greatest PTC disparity between sexes in ratio was found in *Liobuthus kessleri* Birula, 1898 (male 25–27, female 13–14; Vachon, 1958), followed by *Parabuthus cimrmani* Kovařík, 2004 (male holotype 62–61, female allotype 33–32; Kovařík, 2004)). No significant disparity of pectinal tooth count was found between the males and females of the new species (see below), and therefore this morphometric is not reliable for the sex determination in this new species. This condition has also been observed in *Lychas* species (e. g., Di et al., 2013: table 2; Kovařík, 1997: table 1). Males also tend to have relatively longer pectines; this dimensional increase is sometimes positively correlated with the proliferation of pectinal teeth. Absolute length is not applicable as it is influenced by the intraspecific variation and/or development stage. In terms of the new species, the relative length is recognized by whether or how far the distal tip of the marginal lamellae of pectine exceeds the distal end of the external margin of 4th leg coxae. Pectines of the surmised male specimens always conspicuously exceeded the external margin of 4th leg coxae, while those of the females may only exceed it a little, if at all (Figs. 55–56). One may refer to the separation boundary between the 3rd (distal) and 2nd (middle) marginal pectinal lamellae and see whether it is spatially within the length of the external margin of 4th leg coxae. This boundary was often beyond the articulation between the coxa and trochanter in the presumed males; should it retreat behind this articulation, it was always at the proximity thereof. Using the coxae as the reference system is more reliable than using the posterior margin of the 1st sternite; the coxae are very compact and stable, while the sternites may displace due to the shrinkage or dilation of the mesosoma (e. g., food consumption or pregnancy). However, the relative location of the lamella boundary may be unreliable because pectines can shrink in poorly preserved specimens, and in some females, it may exceed the distal end of the external margin of 4th leg coxae. Therefore, another index was considered as well – the shape and the relative length of pectinal teeth. In many Old World buthids, pectinal teeth of males are often longer than those of females and carry more peg sensillae for the same reason as having increased PTC. In the new species, the pectinal teeth of the presumed male specimens were conspicuously elongate (visually determining the ratio of the length and width of each tooth). Teeth of presumed females were usually shorter and proportionally wider, but there were many intermediate conditions. Nevertheless, our determination of the sex was based on both parameters. The relative length of the pectinal tooth was based on the basal and/or average width of the pectinal lamellae (visually determined). In some of the other Old World buthids, the distance between the basal tooth of each pectine (if the pectines were positioned without overlapping the inner margin of 4th leg coxae; greater in females) can also be useful as these females have shorter pectinal teeth and wider mesosoma, allowing the tips of the basal teeth to be separated from each other (Farzanpay & Vachon, 1979). However, this

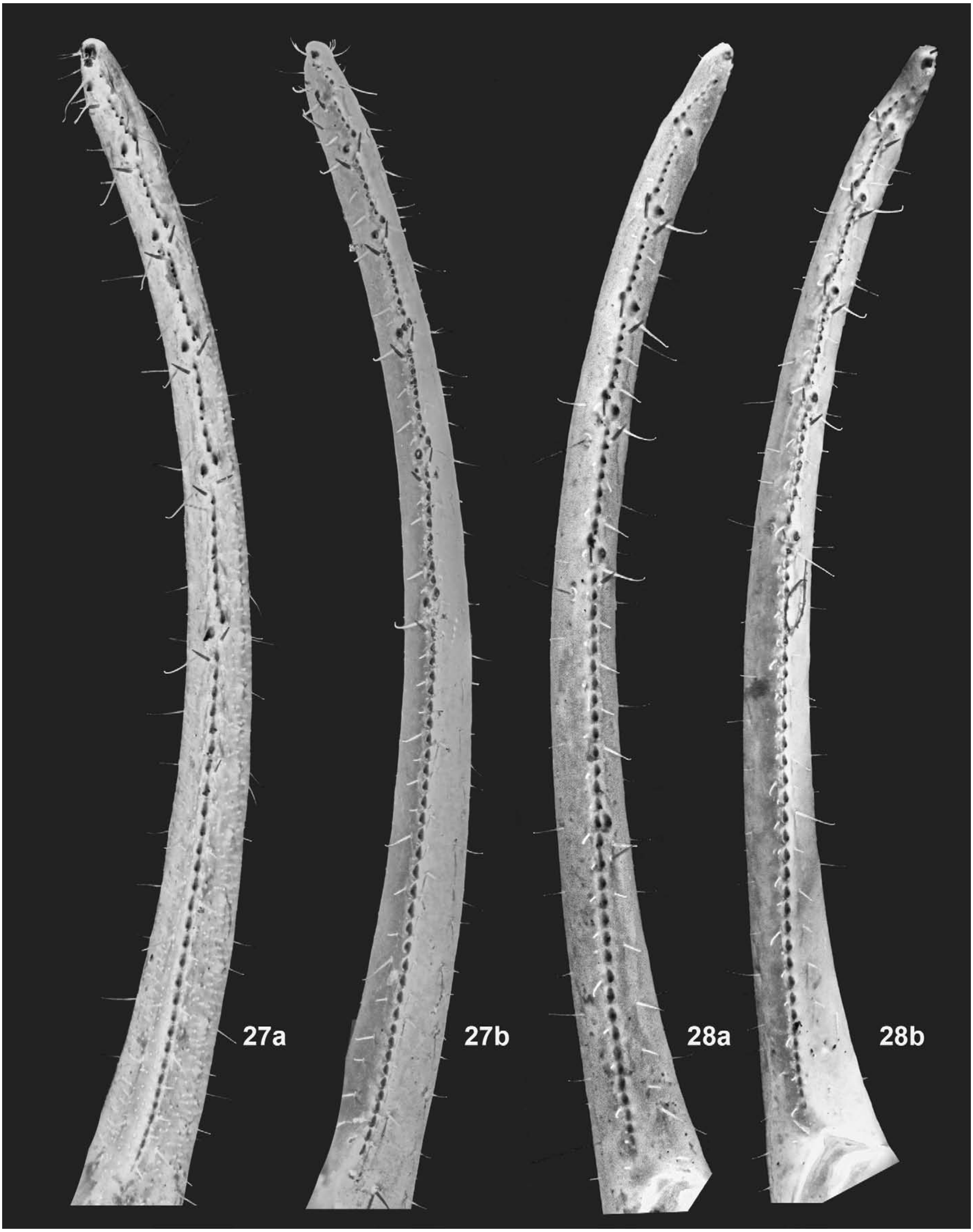

Figures 27–28: *Langxie feti* **gen**. et **sp**. **n**., pedipalp movable (27a–27b) and fixed (28a–28b) fingers under UV light. **Figures 27a–28a**. Male holotype. **Figures 27b–28b**. Female paratype.

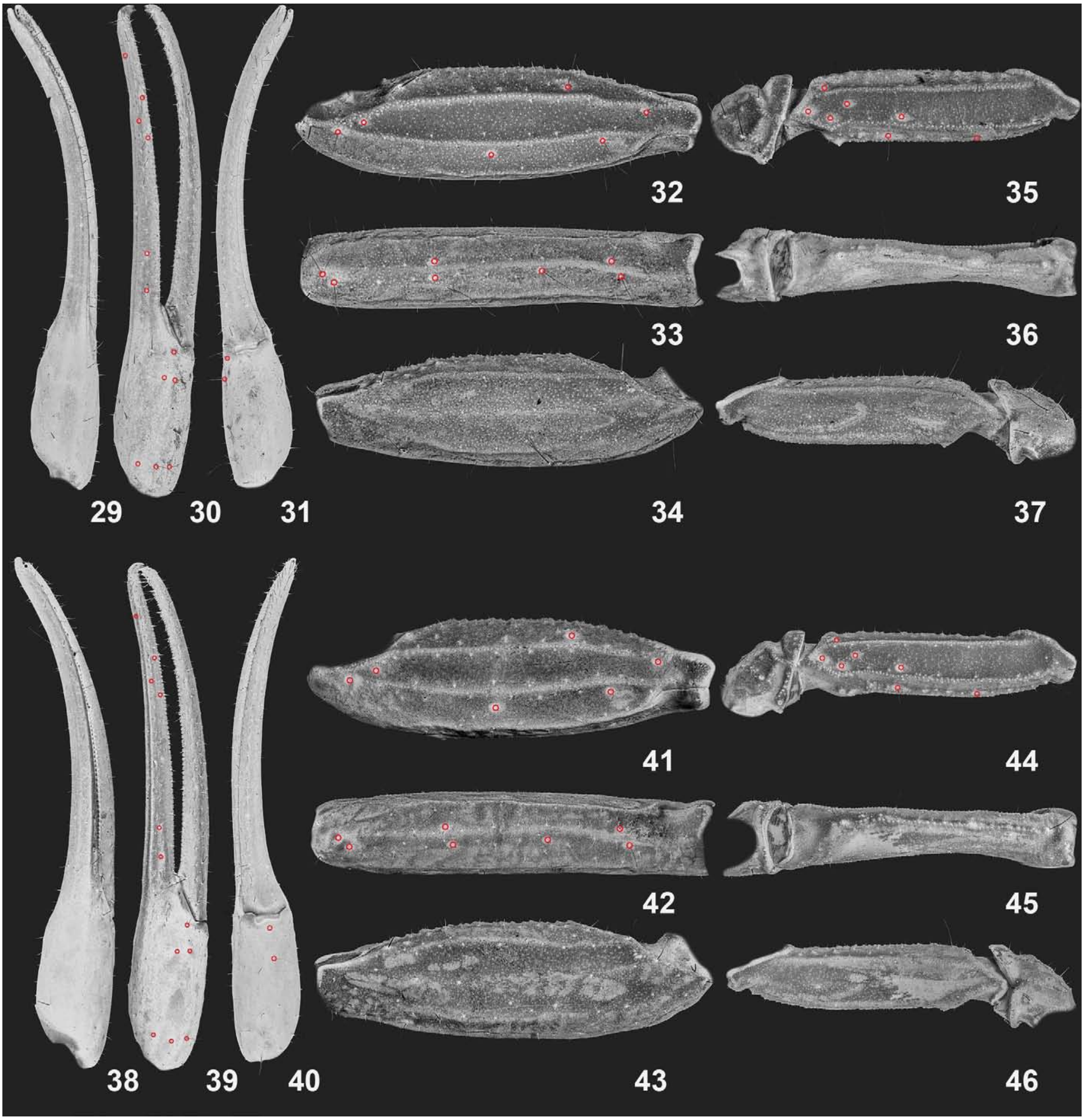

Figures 29–46. *Langxie feti* **gen**. et **sp**. **n**., pedipalp segments of male holotype (29–37) and female paratype (38–46) under UV light. Chela, dorsal (29, 38), external (30, 39) and ventral (31, 40) views. Patella, dorsal (32, 41), external (33, 42) and ventral (34, 43) views. Femur and trochanter, dorsal (35, 44), external (36, 45) and ventral (37, 46) views. The trichobothrial pattern is indicate in Figures 30–33, 35, 39–42, 44 (red circles).

was not always the condition in the new species, rendering it less informative. The ratios of pectine length (PL)/carapace width (CW) and pectine length (PL)/metasoma I width (MW) were calculated (Fig. 87a). Male scorpions tend to have a narrower carapace (i.e., lower CW value) than females since the posterior margin of the carapace matches in width the first mesosomal tergite (which in females tends to be wider). The assumption that males have proportionally longer pectines renders the value of R = PL/CW to be higher than that of female, exaggerating the sexual dimorphism. This ratiometric (R) is only applied as an amplification parameter for the final scatterplot, as R male > R female itself includes three different potential scenarios: (1) male PL > female PL; (2) male CW < female CW; (3) male PL > female PL, and male CW < female CW. If this value reveals a separation between sexes, it cannot explicitly indicate which of the two parameters shows the sexual dimorphism (or both of them), but only the fact that there is a sexual dimorphism regarding either or both of the characters in the target species. To clearly evaluate the sexual dimorphism of pectine length alone, a non-sexual dimorphic character should be selected as a reference system. In the morphometric analysis of another species of scorpion, *Hadrurus arizonensis* Ewing, 1928, the width of metasoma I was found to be the most sex-neutral character that can be potentially used to factor out static allometry in an unbiased way, in order to evaluate the sexual dimorphism of another variable (e. g., pectine length) (Fox et al., 2015). The final result suggested a general trend in this species: males tend to have proportionally longer pectines than females.

We also noticed that males tend to have proportionally larger median ocelli than females (Fig. 87b), and this sexual dimorphism that aids in visual capability may be relevant to their higher vagrancy. No significant or constant difference in carapace shape was discovered among all specimens, thus this character was assumed to be less instructive for the determination of sex and maturity (see Appendix). On the other hand, visual inspection suggested that carapace granulation was sexually dimorphic, being coarser in males than females. Surface morphosculpture such as granulation can be visualized by UV fluorescence imaging (Fig. 91), with most granules highlighted by small, localized areas of higher intensity fluorescence. To quantify sexual dimorphism of carapace morphosculpture, we implemented an image analysis procedure to detect and quantify those areas that roughly represent the size of granules in carapaces of males vs. females (most specimens photographed under the same UV illumination conditions). We applied the following sequence of image processing steps using the software, ImageJ (Schneider et al., 2012), on Fig. 91 (one injured adult female excluded; paratype no. F8): (1) apply a large radius (16 pixels) Gaussian low-pass spatial filter to suppress granules, which produces a map of larger scale (non-granule) background intensity variations; (2) subtract the result from the original image, yielding an image showing granule-scale highlights on a more uniform dark background; (3) apply automatic local thresholding with the Yen method (Yen et al., 1995) to segment and isolate regions-of-interest (ROIs) having higher intensity fluorescence; the Yen method was selected after it demonstrated its feasibility on a pair of carapaces to resolve and distinguish male larger granules from female smaller granules, consistent with differences perceived by the human eye; (4) analyze the numbers and sizes of the ROIs by applying particle detection limited to areas in the range 7–2,000 pixel^2, and circularity 0.50–1.00; these parameters were empirically chosen to reject: (i) very small pixel clusters that were unlikely to represent "granules"; (ii) very large pixel clusters that were larger than any visually perceived granules; and (iii) elongate pixel clusters that may represent either two or more fused (unresolved) "granules", or strips of bright fluorescence along the edges of the carapace. Our procedure provided a measure of surface morphosculpture that was related to the coarseness of granulation, although the detected ROIs did not exactly match the sizes and shapes of "granules" estimated by human visual perception and modeled by circular or elliptical profiles (Lowe et al., 2014) (Fig. 89). Its essence is the detection of highlights, as a kind of optical roughness measurement. The ROIs were smaller than human-perceived "granules" and were less round, because they only included highlight pixels, whereas granules under directional UV illumination have both a highlight aspect and a shadow aspect. However, the UV image analysis procedure provided objective, reproducible measures of a surface morphosculpture that is related to or determined by granulation. The results confirmed significant differences in the areas and Feret's diameters of carapace granules between males and females, with males having larger ROIs than females (Tables 2–3; statistics analyzed in the software Jamovi). The ecological significance of males having larger granules may also lie in their errant behavior which in turn requires a better physical protection and/or camouflage.

No conspicuous differences were found in the external morphology of the genital operculum between males and females; this character is sometimes useful for Iurida. However, we confirmed that genital papillae (which fluoresce under UV light) can be revealed in males by lifting up the genital opercula (Figs. 60–61). Since females do not possess genital papillae, this character can only be used for determining the sex, rather than maturity. Other characters (e. g., ratios) cannot be applied to potentially immature specimens. Based on photos of all the specimens in vivo habitus taken by the second author (as mentioned above, there were more specimens than those finally received by the first author), the new species does not show obvious sexual dimorphism in terms of the relative width of the mesosoma (females are usually wider due to pregnancy, consuming more food to nourish embryos, and carrying offspring, while males do not have such needs but instead require better mobility) given that adult males were very likely to present in a larger sample size. Females may appear bulkier than males, but this could due to the dilation of mesosoma as well as their larger size. This species also does not show sexual dimorphism in the morphology of pedipalp chela (e. g., some adult male scorpions possess a more robust or gracile chela, or they also exhibit an obvious gap between fingers or a proximal lobe on the movable finger with a corresponding notch on the fixed finger) or metasoma (e. g., some adult male scorpions have a much more slender, or on the contrary, a more robust metasoma).

As no structural sexual dimorphism that could clearly indicate maturity was found in the new species, we determined the maturity of males by the presence/ absence of a hemispermatophore and that of females by the presence/ absence of ovaries or eggs or embryos (although it is also possible that a male may had failed to regenerate its hemispermatophores prior to its death). By this method, some small males that were initially identified as juveniles when first examined, were confirmed to be mature (Fig. 60). This result suggests that the new species shows an extreme sexual dimorphism in the body length (size) of adults. However, different size classes of adults exist in other buthids (e. g., Teruel & Turiel, 2022). Although the larger the specimen, the more likely it is mature, measuring the body length does

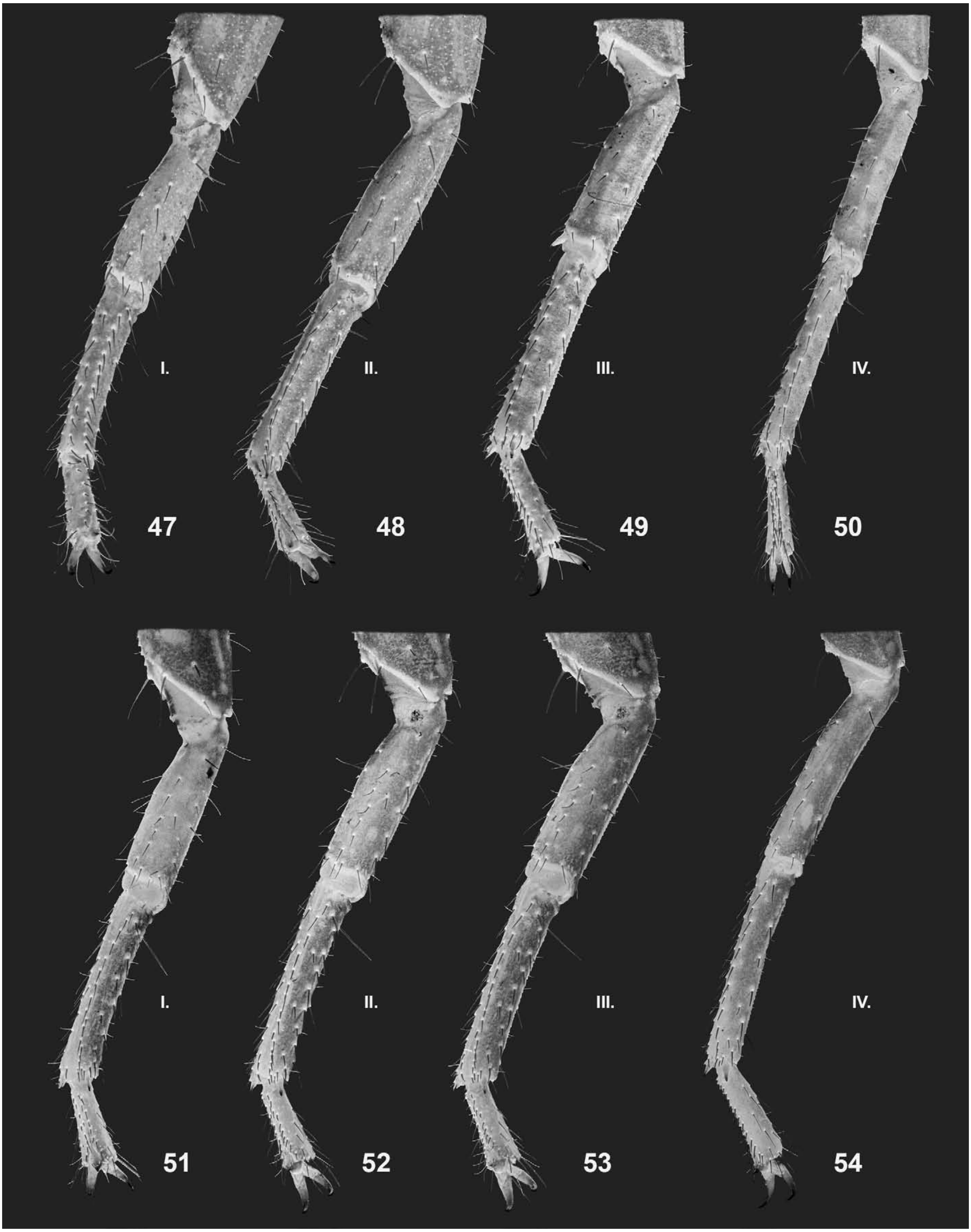

Figures 47–54: *Langxie feti* **gen**. et **sp**. **n**., right legs I–IV of male holotype (47–50) and female paratype (51–54), retrolateral aspect, under UV light.

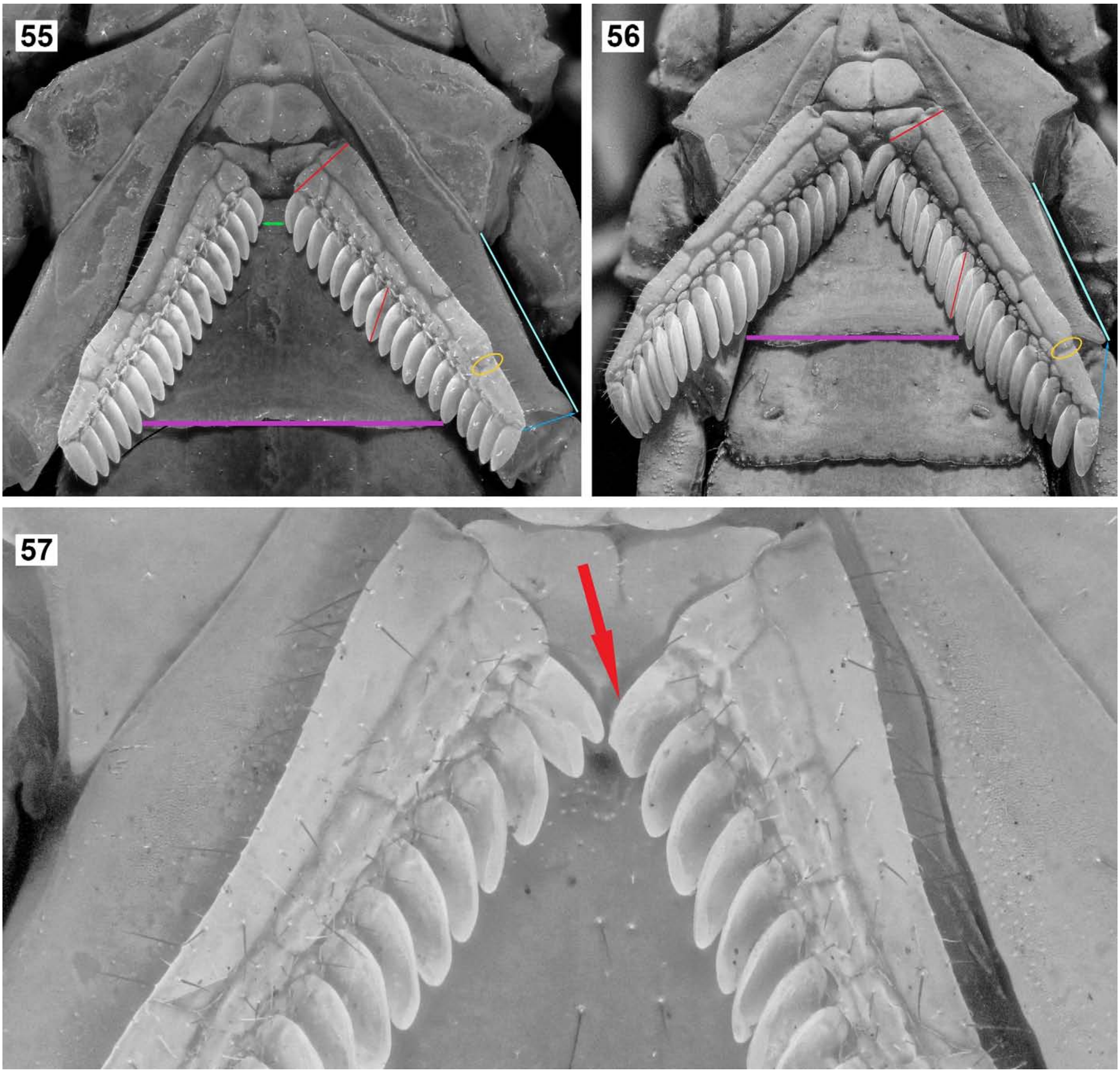

Figures 55–57: *Langxie feti* **gen**. et **sp**. **n**. **Figures 55–56**. Paratypes female (55) and male (56), sternopectinal areas under white light. Explanation of color markings (55–56): green, distance between left and right basal pectinal teeth; purple, posterior margin of sternite; red, comparison between pectinal tooth length and pectinal lamella width; yellow, boundary between 2nd and 3rd marginal lamellae; dark blue, distance between tip of pectine and trochanter-coxa joint; bright blue, external length of coxa. **Figure 57**. Paratype female, a single observed case of a dilated (incompletely separated, see red arrow) pectinal tooth.

not conclusively identify different size classes or distinguish the penultimate instar from the adult. Dissection of genital organs remained a more reliable solution, but is destructive to the specimens (Volschenk et al., 2008). Due to the poor condition of the specimens and the fragility of this species, not all available specimens were dissected to ascertain their maturity; normally, specimens that were already severely damaged were selected as examples. The specimens were allocated into different groups based on sex, coloration, body size, 5th metasomal segment length, size of telson and visually determined coarse ratios of pedipalp chela morphometrics, and only some representatives of each group that appeared to be most feasible were dissected. Other specimens of the same group were then assumed to be of the same instar, but this is not a perfect method as specimens of the same size as other adults (juveniles) could still be juveniles (adults). Hemispermatophores were still retrieved from the smallest male in the group comprising smaller males, and examination of some of the other males suggested that there was no juvenile male in the specimen series. The size of the hemispermatophore varies intraspecifically and is usually correlated with the size of the scorpion. Some males were found with basally connected hemispermatophores, and these might suggest that the male was probably preparing to extrude a spermatophore prior to its death (Alexander, 1959). It was very difficult to reveal the ovariuterus of the female specimens. Long preservation caused condensation of the surrounding tissues and removing them often damaged the fine configuration of the ovarian tubules. A complete and intact ovariuterus could not be exposed, but its existence in certain size groups of this new species was proven (Fig. 61).

A correlation was found between the telson color and maturity: a yellow telson only exists in juveniles; telsons of adults are usually orangish or reddish, but immature specimens may also have an orangish telson. Hence, the color temperature of the telson probably increases with the age of the individual. We also speculate that young adults may also have a coloration of the telson similar to that of elder juveniles (orangish). However, the coloration of long-preserved specimens is only referential, as it may decay with time. Nevertheless, a young juvenile with a yellowish telson was confirmed from the remaining six live specimens. In addition, the color change of metasomal segments of young juveniles is different from the elder instars (see Appendix): in adults, the color gradually becomes lighter from the 5th segment towards the anterior ones (reddish black → reddish brown → brown → yellowish brown); in juveniles, the 4th and 5th segments have prominent brown patterns concentrated posteriorly. We postulate that this color pattern in young juveniles may subsequently develop into a gradually lightening overall trend of color towards the anterior segments by darkening the color of 5th segment, rendering the color difference between the anterior part of 5th segment and the posterior part of 4th segment to be less distinct. Therefore, the telson being yellow and the metasomal segments showing obvious intersegmental color difference are the two absolute indicators for the immaturity of this species, whereas the other extreme of this color spectrum signifies maturity (i.e., telson being reddish brown and metasomal segments showing gradual color change); however, coloration may not distinguish the subadults from adults (i.e., the middle range of color spectrum). The overall coloration in juveniles is lighter than most adults, but this coloration is not correlated with the low color temperature of telson (i.e., light brown mesosoma can be accompanied by a reddish telson, probably a color combination for subadults as they appear to be smaller). Nevertheless, our assumptions and conclusions were mostly based on preserved specimens and a limited sample of live specimens.

The new species warrants special documentation for all the efforts that have been invested in acquiring the material, and our aim here is to make the sacrifice of every individual specimen worthwhile in contributing to knowledge about the morphology. For the record, photographs of the habitus under white light and photographs of the carapace and pectines under UV light with our consideration of sex and maturity for all types are provided in the Appendix, to enable interested readers to evaluate these features by themselves.

Lattice microstructures.

The cuticle of the new genus was found to be scattered with patches of lattice microstructures (i.e., grid-like morphosculpture). These structures were composed of irregularly tessellated hexagonal or pentagonal cells with margins exhibited as small keels rising above the median surface, predominantly found on the carapace, tergites, 7th sternite, pedipalps (patella and femur) and legs, and appearing weaker on the pedipalp chelae and metasoma. A fortuitous comparison with a UV photo of an adult female *Alayotityus sierramaestrae* Armas, 1973 previously sent to the first author by Dr. Graeme Lowe during their personal communication revealed that the latter species and *Langxie feti* **gen**. et **sp**. **n**. show completely reversed configurations of these microstructures relative to the local granular and carinal morphosculpture (cf. Fig. 64 and Fig. 65). In *A. sierramaestrae*, these microstructures occur only on granules and carinae (the former resembling golf balls), while in the new species, they occur only on cuticular surfaces between granules and carinae. Do these phenomena represent any type of physiological or ecological adaptation? Do they have any taxonomic and/or phylogenetic implications?

In the buthid molecular phylogenetic tree constructed by Štundlová et al. (2022), species of *Lychas* and *Janalychas* were placed in a major clade, the "(*Ananteris* + *Isometrus*) group", that was distantly separated from another major clade, the "*Tityus* group", where *Alayotityus* was placed. To explore possible phylogenetic variation of lattice microstructure, we selected representatives of several genera of these divergent lineages for study, including *Lychas*, *Janalychas* and *Isometrus* from the "(*Ananteris* + *Isometrus*) group", and *Tityus*, *Centruroides* and *Heteroctenus* from the "*Tityus* group".

We did not find the same condition as that of *Alayotityus* in other species examined, and this character could be unique to this genus (autapomorphy), but further investigation on a broader scale is required for confirmation. On the contrary, the lattice microstructures are not limited to the new species and were found at least in all the other species examined. However, there is a significant difference in terms of their development. The lattice microstructures are extremely prominent in the new species; the size of each lattice cell is relatively large (Fig. 65). *Janalychas tricarinatus* (Simon, 1884) and *Tityus footei* Chamberlin, 1916 show a smaller scale (Figs. 66, 70), but are nonetheless conspicuous, followed by *Isometrus maculatus* (DeGeer, 1778) (Figs. 76–77). The scale of each grid in *Lychas mucronatus* (less obvious in the female specimen examined; Figs. 68–69), *L. scutilus* (Fig. 67) and *Tityus stigmurus* (Thorell, 1876) (Fig. 71) is even smaller but still detectable. However, this size becomes considerably small and is almost negligible in *Tityus smithii* Pocock, 1893 (Fig. 72), *Heteroctenus garridoi* (Armas, 1974) (Fig. 73), *H. junceus* (Herbst, 1800) (Figs. 74–75), *Centruroides bicolor* Pocock, 1898 (Figs. 79–80), *C. gracilis* (Latreille, 1804) (Fig. 78) and *C. nigrimanus* Pocock, 1898 (Fig. 81). In the taxa that were traditionally placed in Centruroidinae (Esposito et

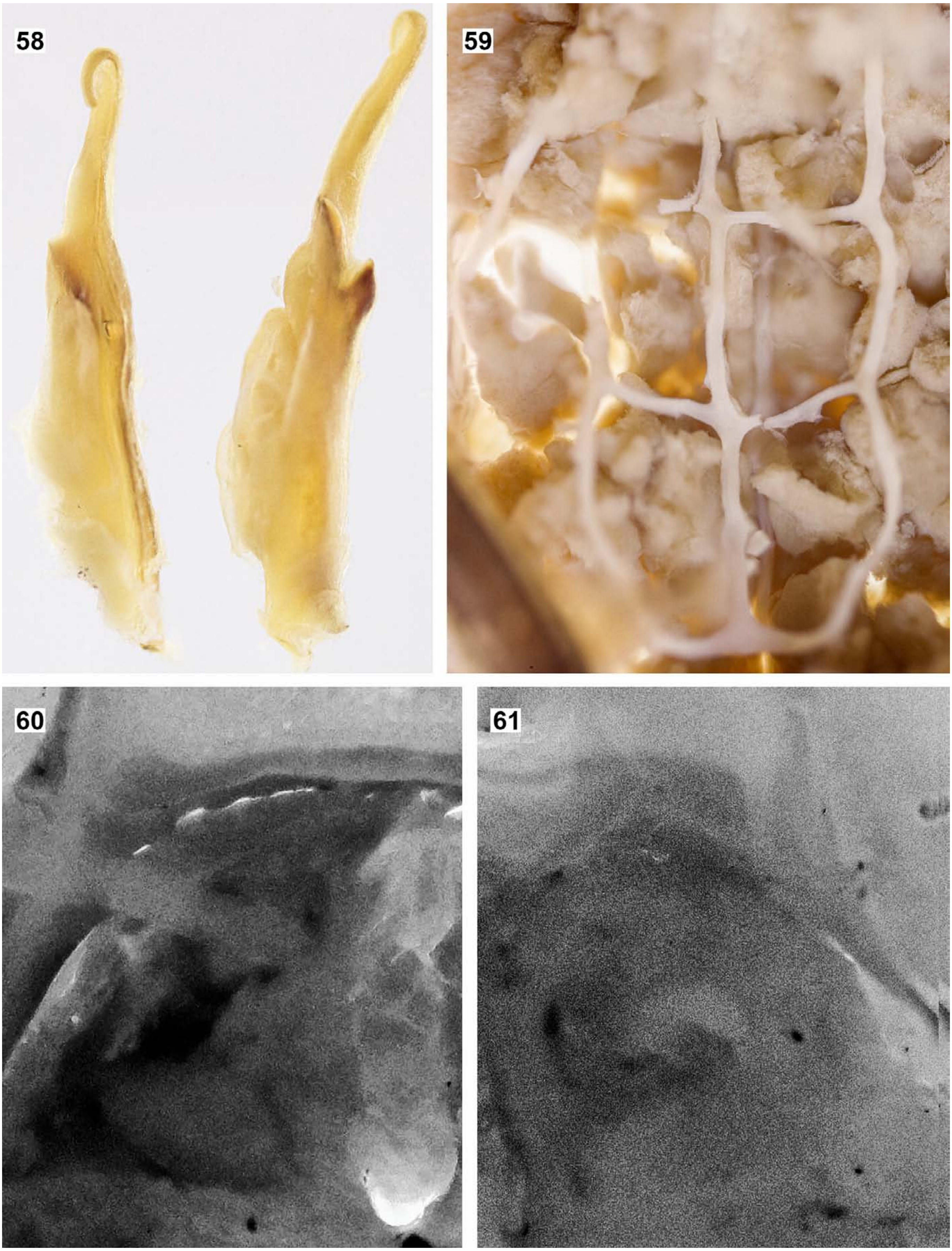

Figures 58–61: Genital organs of *Langxie feti* **gen**. et **sp**. **n**. of under white light. **Figures 58**. Partially damaged hemispermatophores retrieved from an adult male (paratype no. M10). **Figure 59**. Ovariuterus partially revealed from an adult female (paratype no. F35). **Figures 60–61**. Removal of genital opercula of an adult male (60) and an adult female (61) paratypes; left genital papilla of the adult male fluoresces under UV light.

al., 2018), denser granules replace the spaces where these lattice microstructures can occur. The occurrence of the lattice microstructures in the distant clades (i.e., "*Tityus* group") suggests that this character may not be phylogenetically informative with respect to higher level groupings in Buthidae.

The lattice microstructure in scorpions was first reported by Lowe & Kovařík (2022) in their revision of *Teruelius* Lowe & Kovařík, 2019 and *Grosphus* Simon, 1880, two genera belonging to the "(*Charmus* + *Uroplectes*) group" (Štundlová et al., 2022). Similar morphosculpture was subsequently noticed in *Scorpiops tongtongi* Tang, 2022 on its sternites by the first author of our study (Tang, 2022c: fig. 10). Lowe & Kovařík (2022: 8) confirmed its presence on sternite VII in *Grosphus*, as well as in an outgroup taxon, *Lychas mucronatus*, but it was absent on sternite VII in *Teruelius*; those cuticular structures account for the differences in optical reflectance and was considered as a generic character to distinguish *Grosphus* from *Teruelius*. Given the ecological differences between the two genera, the authors hypothesized that those structures function as a crypsis/camouflage for *Grosphus* (Lowe & Kovařík, 2022: 9). These antireflective, matte cuticles extend to many surfaces in *Grosphus*. These forest-dwelling scorpions in epigean habitats may use them to hide themselves from the visual, diurnal predators (e. g., iNaturalist obs. ID = 145577629, 144431705, 144292695, 117693339, 39151303, 17065541). On the contrary, many buthids in more arid regions (including *Teruelius*) have reflective cuticles, but they shelter in burrows to conceal themselves from those predators based on visual detection; a reflective cuticle may also prevent thermal death due to overheat by excessive light absorption.

However, comparing to the other species examined in this study, which are mostly found in forests, *L. feti* **gen**. et **sp**. **n**. inhabits a rockier and drier habitat. We assume that these lattice microstructures may also function in a similar way as the cuticle granules, i.e., enable the scorpions to blend into a rough surface (rocks) of its microhabitat. Perhaps these structures can also capture the dust in the environment, covering them on the cuticle and further reinforcing the camouflage. There is also the possibility of a biomechanical function in which those structures can improve the rigidity of the cuticle, counteracting abrasion against rock surfaces. Additionally, they could be beneficial for gathering water vapor. Animals in more arid regions can obtain water by fog harvesting (Nørgaard, Ebner & Dacke, 2012; Gurera & Bhushan, 2020). Rough surfaces (physical microstructure) are theoretically more hydrophilic and may assist in the dew nucleation process, although the surface hydrophilicity might also be determined by chemical composition of epicuticular lipids (waxes) which can vary between xeric and humid adapted species (Hadley & Jackson, 1977; Toolson & Hadley, 1977). This can potentially explain the reason why the lattice microstructures are less developed in the forest species examined in this study. Interestingly, a more developed condition of this lattice microstructure was found in the pedipalp femur of *Himalayotityobuthus alejandrae* (Lourenço, 2003: fig. 3), which is found along the same mountain range. The effect of this lattice microstructure can be multifaceted, but these hypotheses based on limited species and samples remain to be tested.

Intriguingly, the new species does not have variegated or cryptic vegetation-like color patterns, but instead shows obvious color contrast between its pedipalp and most of the remaining body parts. Although the contrasting color may serve as a distracting or warning signal to visual predators (e. g., some *Parabuthus* species have dark-colored 5th metasoma and/or telson; Kovařík et al., 2019: 32), it is also hypothesized to be advantageous as disruptive patterning for breaking up the body outline in habitats with open vegetation and a heterogeneous substrate (Loria & Prendini, 2021: 120). Along with a potential cryptic role of the lattice microstructure, the coloration may also assist a similar function in the new species.

Langxie feti gen. et sp. n.

(Figures 1–63, 65, 82–155; Tables 1–3)

http://zoobank.org/urn:lsid:zoobank.org:act:02E49E59-799C-4775-8AB1-FF973F28BF5D

Type locality and type repository. **China**, Xizang Autonomous Region (Tibet Autonomous Region), Linzhi (Nyingchi) Prefecture, Chayu (Zayü) County, Gula (Golag) Township (the entire region; 古拉乡 in Chinese), ca. 29°12'91"N 97°57'73"E, ca. 2429 m a. s. l.; VT.

Type material. **China**, Xizang Autonomous Region (Tibet Autonomous Region), Linzhi (Nyingchi) Prefecture, Chayu (Zayü) County, Gula (Golag) Township (the entire region), ca. 29°12'91"N 97°57'73"E, ca. 2429 m a. s. l., 14–16 September 2022, 1♂(holotype) 16♂42♀ 4♀juvs (paratypes), leg. Qingquan Jia. Holotype and most of paratypes are in VT; 1♂1♀(paratypes) are in BMNH; 5♂5♀ (paratypes) are in František Kovařík (FKCP), Graeme Lowe, Ersen Aydın Yağmur and Rolando Teruel personal collections.

Etymology. The specific epithet is a patronym in honor of Victor Fet (Marshall University, USA), who has always been very supportive and encouraging to the first author in all aspects. Chinese equivalent. 费氏狼蝎 (roughly as "Fet's wolf scorpion" in English; see Tang (2022a) for the rules of designation).

Diagnosis. As for the genus.

Description (based on holotype male and paratype female). Photographs of the specimens in Figs. 1–4 were taken under white light. Photographs of the specimen in Figs. 5–57 were taken under UV light so as to depict the surface morphosculpture (granulations and carinae). UV photographs are more informative about the external structural morphology; coloration is referable in Figs. 62–63, 82a–f, 85a–f and Appendix. Due to the lack of live specimens, the holotype and paratype were selected from the specimens preserved in ethanol for about 4 months (see Acknowledgement), thus no in

Figures 62–63: *Langxie feti* **gen**. et **sp**. **n**., intraspecific variation. **Figure 62**. Comparison between the smallest (paratype no. M12) and the largest males (paratype no. M17). **Figure 63**. Comparison between females (paratypes nos. F31, F40, F18, F4, left to right, and bottom); ovariuterus was not subsequently revealed from the bottom female (F4), and it was then presumed to be immature and its value was not considered in the adult size range.

vivo photographs of details under white light were taken. The coloration description was instead based on other photographs taken when specimens were still alive (Figs. 82a–f).

Coloration (*in vivo*) (Figs. 82a–f). General coloration yellowish brown to blackish brown. Dorsal surface of chelicerae brownish and reticulated. Base color of carapace, tergites, metasoma and pedipalp (except for chela) yellowish brown. Pedipalp manus and tip of finger whitish yellow, same color as base of trochanter of pedipalp and leg. Base color of leg darkens gradually towards basitarsus from femur. Dark colors form maculated patterns on carapace, pedipalps (except for chela) and legs (less variegated on trochanter and telotarsus), inconspicuous in dry live specimens. Posterior margin of each tergite generally darker than anterior region, but anterior region still variegated with markings axial symmetrically. Brownish streaks of variable color present along carinae of metasoma and base color darkens towards the fifth segment (gradually changes color from yellowish brown to reddish black from posteriorly). Darkest areas often concentrated in pedipalp chelal finger (base to medial part), pedipalp patella, anterior margin of carapace, median ocular region, and posterior region of the 5th metasomal segment. Femur and patella of each leg sometimes slightly darker than tergites, but anterior carapacial margin and pedipalp patella (and sometimes the fifth metasomal segment) always represent the darkest area. Ventral side of prosoma semi-translucently light brownish yellow, color saturation level of 2nd coxapophyses higher than surrounding area. Pectines, posterior bands of the first four sternites (anterior area almost completely translucent) and book lungs whitish yellow. Telson orange red to reddish brown (may be relevant with age; can be yellowish in juveniles), except for aculeus which is black.

Prosoma (Figs. 5, 7, 9–12). Carapace generally flat, isosceles trapezoidal, slanting laterally with shallow grooves; anterior margin concave (triangularly incised) and thickened (weakly raised) until the posterior end of each lateral ocular carina, with four evenly positioned setae. Dorsal surface highly granulated, granules do not form conspicuous carinae, except for a pair of posterior median carinae weakly to moderately indicated; superciliary carinae weakly present, without granules in between; interocular distance approximates or is greater than diameter of one median ocellus. Intergranular surfaces either smooth or scrobiculate (present as lattice microstructures, never on granules/carinae), but both types of areas scattered axial symmetrically throughout the entire dorsal surface. Five pairs of lateral eyes, three major ocelli, two minor ocelli; PDMi posterior to PLMa, ADMi smaller and above PLMa (posterior to lateral ocular carina); posterior area of each group of lateral eyes on dorsal surface of carapace shallowly depressed and smooth. Ventral surface of prosoma smooth. Sternum type 1, sub-triangular in shape. Genital operculum medially separated with two macrosetae on each half near the posterior margin. Pectines with three marginal lamellae equipped with moderate length setae laterally, 1st (basal) lamella conspicuously longer than the other two, 2nd (medial) and 3rd (distal) lamellae similar in length; one small piece presents between basal and medial marginal lamella; median lamellae subdivided into usually 7–9 pieces, scattered with short setae; pectinal fulcra strongly developed, scattered with short setae; pectinal teeth number 20–19 in holotype male and 18–18 in paratype female; sensorial area located anteriorly on each tooth, slender in male.

Mesosoma (Figs. 6, 8, 13–14). Tergites highly granulated, with size of granules and intensity increasing successively. One median carina composed of relatively small granules, flanked with a pair of shallow, smooth, oval depressions anteriorly, starting from the 2nd tergite. Boundary between pretergite and posttergite pleated and undulate. 7th tergite with additional two pairs of strongly developed carinae connected to the posterior margin; median carina on this tergite fades out medially. Ventral surface of mesosoma smooth, except for sternite VII with four carinae (the two in middle more prominent) and moderately granulated. Previous sternites glossy with posterior margins undulate; lateral margins of sternites to V–VII serrated. Spiracles located near the posterior corner of sternites; small, slit-like, posterior area with lattice microstructures.

Chelicerae (Figs. 23–26). Chelicerae with typical buthid dentition, basal and median denticle forming a bicuspid on fixed finger which is armed with one enlarged accessory denticle ventrally; movable finger with dorsal distal, subdistal, median and basal (bicuspid) denticles dorsally, one ventral distal denticle and 2–3 ventral accessory denticles ventrally. Fixed finger with long, fine, curved (appearing soft) setae ventrally, manus with few, fine, sublinear setae on fixed finger dorsally and long, fine, sublinear setae ventrally, concentrated on the area beneath fixed finger; internal margin of manus equipped with numerous long, thick, dark, nearly straight setae ventrally but fine, short setae dorsally; ventral surface with single accessory denticle.

Metasoma and telson (Figs. 15–22). Entire metasoma and telson glabrous but granular. Metasomal segments slender and increase in length posteriorly; I–II with 10 carinae (dorsosubmedian, dorsolateral, median lateral, ventrolateral and ventrosubmedian, all in pairs), III–IV with 8 carinae (dorsosubmedian, dorsolateral, ventrolateral and ventrosubmedian, all in pairs), V with 5 carinae (dorsolateral and ventrolateral in pairs, and one single ventromedian); all carinae strongly developed and costate-granular, becoming more granular towards dorsal surface and more costate towards ventral surface. Median lateral carina on metasomal segment II become vestigial proximally; this carina is replaced by scattered series of granules that do not form distinct carinae on subsequent metasomal segments. Dorsosubmedian and dorsolateral carinae of metasomal segments I–III terminate in a tooth which is relatively enlarged. Granule density of ventral surface higher than that of lateral surface which is higher than that of dorsal surface. Granule intensity of dorsal surface between dorsosubmedian carinae decreases from metasomal segment I to III. Dorsal surface of metasomal segment IV shows two inconspicuous series of granules between

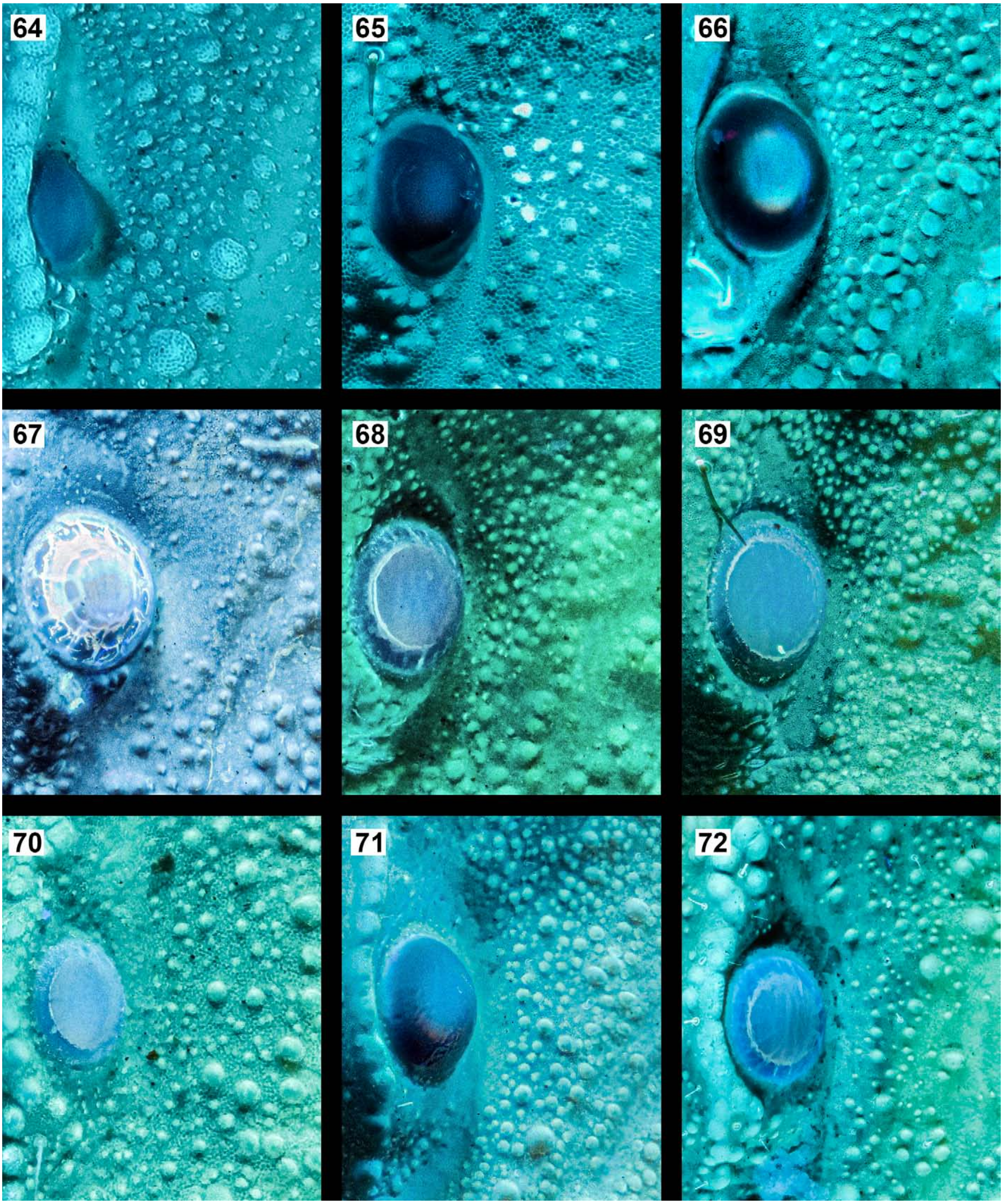

Figures 64–72. Lattice microstructure comparison among *Alayotityus sierramaestrae* Armas, 1973 (female, 64; photograph by G. Lowe), *Langxie feti* **gen**. et **sp**. **n**. (female, paratype, 65), *Janalychas tricarinatus* (Simon, 1884) (female, 66), *Lychas scutilus* C. L. Koch, 1845 (juvenile, 67), *Lychas mucronatus* (Fabricius, 1798) (female, 68, and male, 69), *Tityus footei* Chamberlin, 1916 (male, 70), *Tityus stigmurus* (Thorell, 1876) (female, 71) and *Tityus smithii* Pocock, 1893 (female, 72).

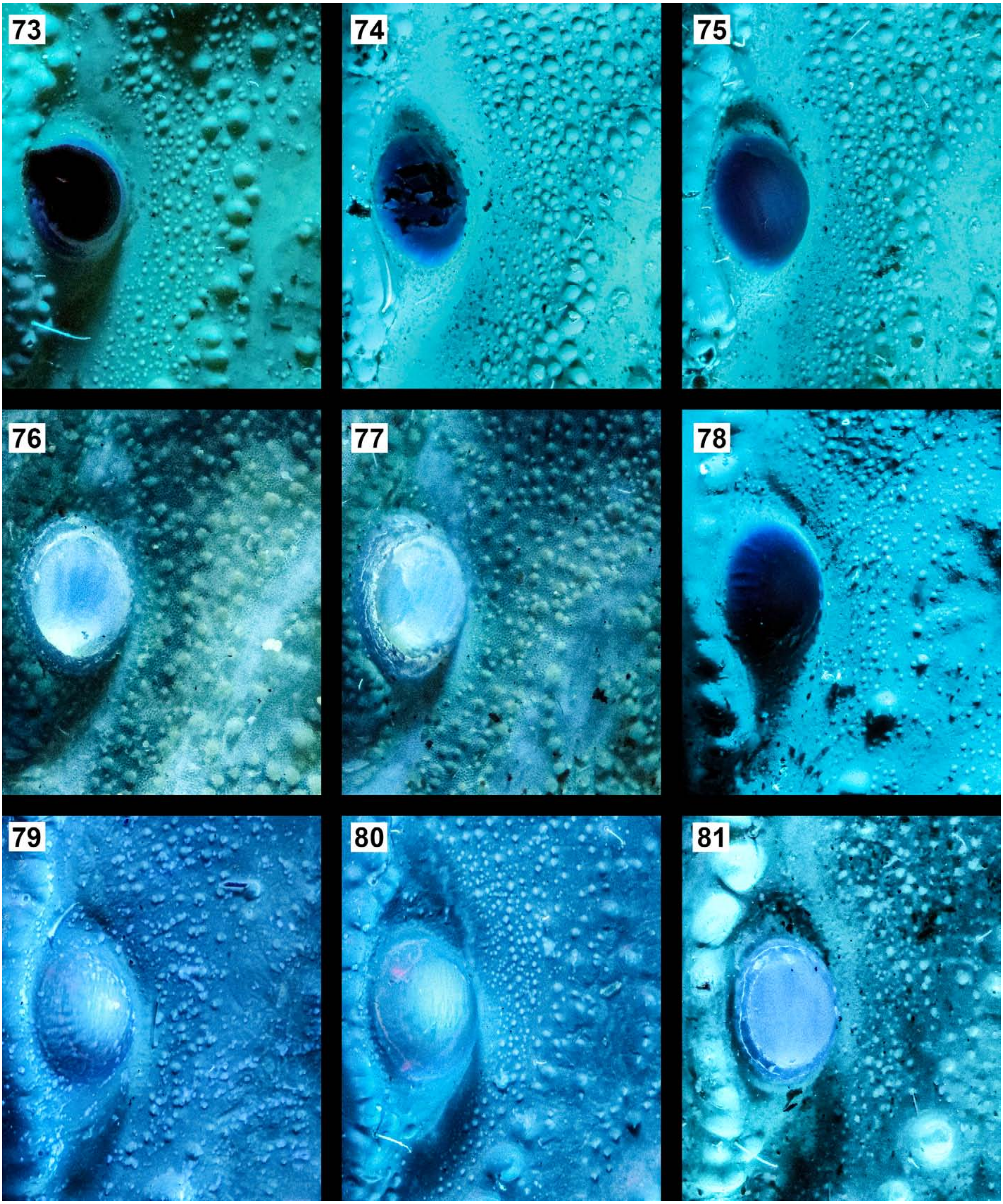

Figures 73–81. Lattice microstructure comparison among *Heteroctenus garridoi* (Armas, 1974) (female, 73), *Heteroctenus junceus* (Herbst, 1800) (female, 74, and male, 75), *Isometrus maculatus* (DeGeer, 1778) (female, 76, and male, 77), *Centruroides gracilis* (Latreille, 1804) (male, 78), *Centruroides bicolor* Pocock, 1898 (female, 79, and male, 80) and *Centruroides nigrimanus* Pocock, 1898 (male, 81).

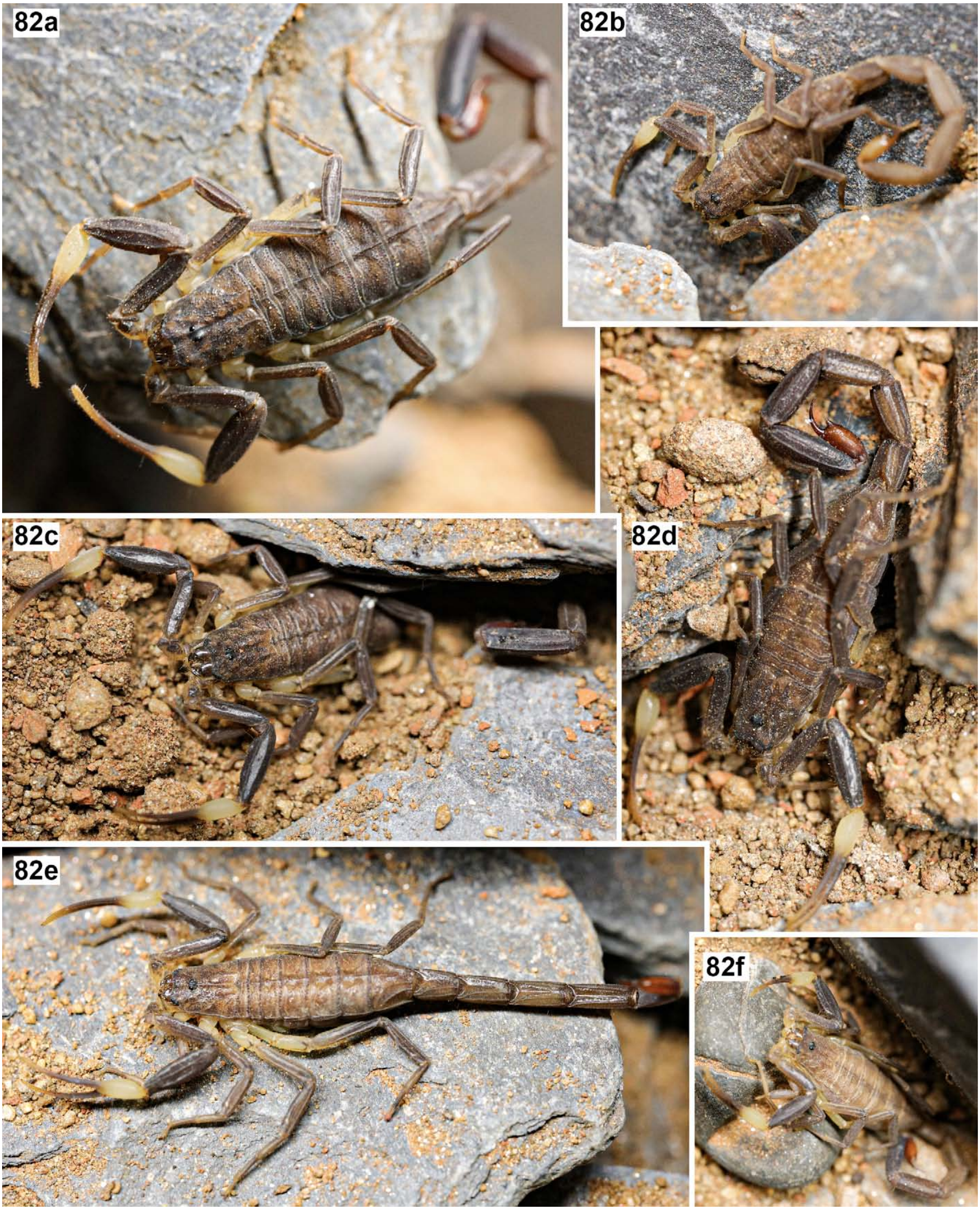

Figures 82a–**f**. *Langxie feti* **gen**. et **sp**. **n**., *in vivo*, live paratypes females (82 a, c, d, e) and males (probably subadult, 82b and 82f).

Figures 83a–**f**. Gula Township, type locality of *Langxie feti* **gen**. et **sp**. **n**.

dorsosubmedian carinae; similar series pair also exists on dorsal surface of metasomal segment V. Anal arch without prominent lobes; ventral margin of anal arch nearly straight, equipped with four evenly spaced setae. Telson weakly granulated, elongate, ellipsoidal in shape, bilaterally with shallow sulci and one carina comprised of small granules. Subaculear tooth distinct, triangular, sometimes with a secondary tubercle on dorsal surface. Ventral surface of telson and subaculear tooth with fluorescent setae, moderate in length; dorsal surface with short, fluorescent setae; few additional non-fluorescent macrosetae present on subaculear tooth, middle range and proximal end of ventral surface. Aculeus moderately curved and long, approximating the length of vesicle.

Pedipalps (Figs. 27–46). Pedipalps slender and glabrous; short, fluorescent setae dominate, but longer, non-fluorescent setae also present; patella wider and relatively longer than femur. Orthobothriotaxic, type Aβ, femur trichobothrium d_2 prolateral to prodorsal carina, close to $i_{1\text{-}4}$ series, patella d_3 between retrodorsal and dorsomedian carina, close to latter; periphery of each trichobothrium on femur and patella locally appearing brighter in fluorescence intensity under UV light. Femur with five granulated carinae, intercarinal surfaces with small granules and lattice microstructures; proventral carinae weakest, prodorsal and retrodorsal carinae well developed with fine granules, promedian and retromedian carinae indicated by larger granules. Patella with seven weaker carinae, intercarinal surfaces with lattice microstructures; promedian carinae formed by moderate granules, prodorsal and dorsomedian carinae formed by fine granules, other carinae smooth. Pedipalp chela slender, with smooth carinae which may be discernible throughout the length of the fixed finger; chelal finger conspicuously longer than manus (ca. 2 times), weakly curved inwardly and upwardly. Fixed finger with 7 oblique rows of MDs; row 1 to 5 gradually increase in length proximally and slightly curve externally when approaching the final MD; row 6 and 7 similar in length and together form a linear arrangement; one IAD proximally flanks row 1 to 6 respectively, EAD absent from all rows. Movable finger comprises 6 oblique rows of MDs that successively increase in length proximally; row 1 to 5 end in a moderately enlarged MD proximally which is flanked by an IAD but lacks an EAD; row 6 obviously longer than previous rows, without EAD along its length and is not flanked by an IAD, apical row anterior to the 1st row very short, composed of less than 5 subterminal denticles, distal end flanked by one or two terminal denticles.

Legs (Figs. 47–54). Weak, smooth carinae comprised of small granules present from femur to basitarsus. Tibial spurs of leg III and IV similar in length and shape, both short and reduced. Femur and patella with only a few setae; setal density increases from tibia to telotarsus retrolaterally and ventrally; tibia and tarsus without bristle combs, most setae

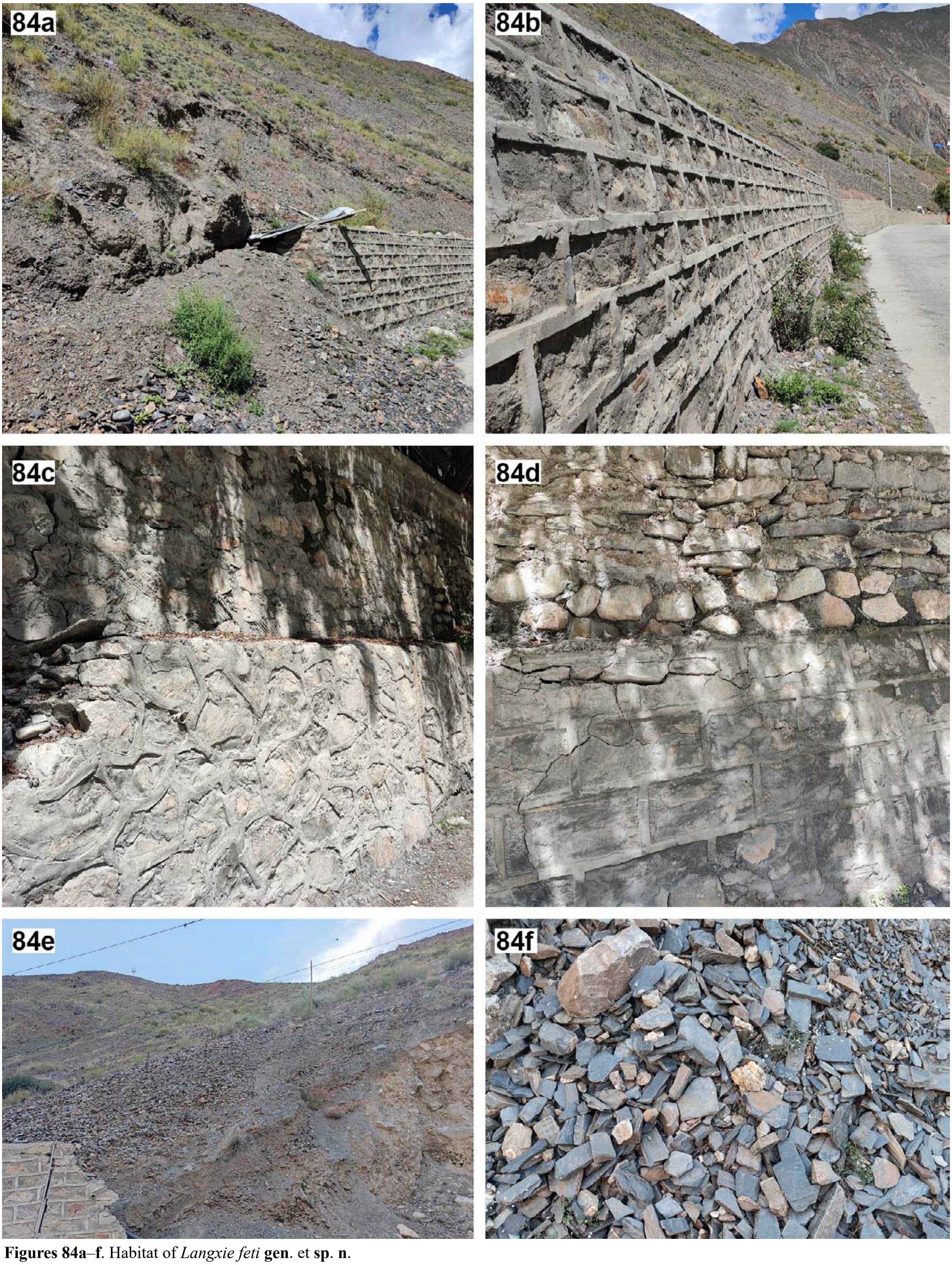

Figures 84a–**f**. Habitat of *Langxie feti* **gen**. et **sp**. **n**.

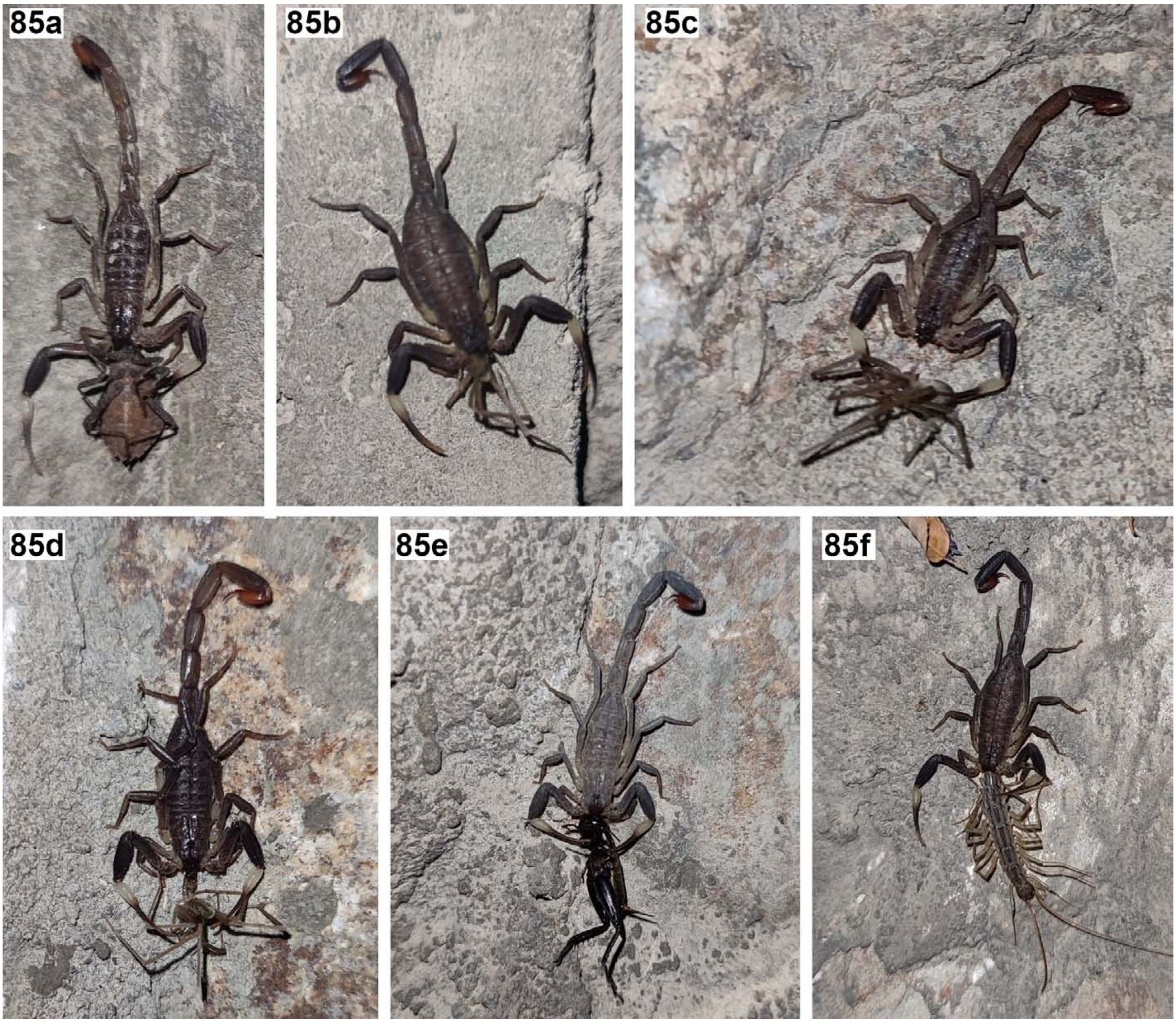

Figures 85a–f. Topotypes of *Langxie feti* **gen**. et **sp**. **n**. observed feeding on different preys in the wild at night.

on tibia similar in length, retrolateral setae relatively longer than ventral setae on basitarsus, distal setae conspicuously longer than ventral setae on telotarsus; basitarsus and telotarsus with two rows of ventral setae. Tarsal ungues curved and stout; two pedal spurs and one dactyl on each leg, short and stout.

Measurements. See Table 1.

Variation (see Appendix, Figs. 90–155). As mentioned above, there is variation among different individuals in both the overall coloration and the coloration of telson. Some individuals, presumably older, are blackish brown with dark red telson, while others are yellowish brown, especially their tergites. For PTC, among the 109 pectines enumerated, 33 belong to male specimens. In these male specimens, 2 pectines were recorded with 18 teeth, 11 with 19, 14 with 20 and 6 with 21. In the remaining female specimens, 9 pectines were recorded with 16 teeth, 21 with 17, 35 with 18, 10 with 19 and 1 with 20. In one female specimen, a basal tooth was found to be dilated and appeared to be a result of incomplete partition (Fig. 57). Granulation and carination on the carapace may vary, but neither of them was found to be consistently related to certain development stages. There is also a variation regarding the relative slenderness of the pedipalp chela finger, and the relative width and length of the pedipalp chela manus with respect to the fingers, but no consistent positive correlations with other features (e. g., body size, 5th metasoma, telson) were found. Variation in body size was found in both adult males and adult females (Figs. 62–63). It is interesting to note that although two different adult female specimens were similar in terms of the telson size, the relative ratio of their 5th metasoma sizes can be different; usually, larger females have more slender 5th metasoma.

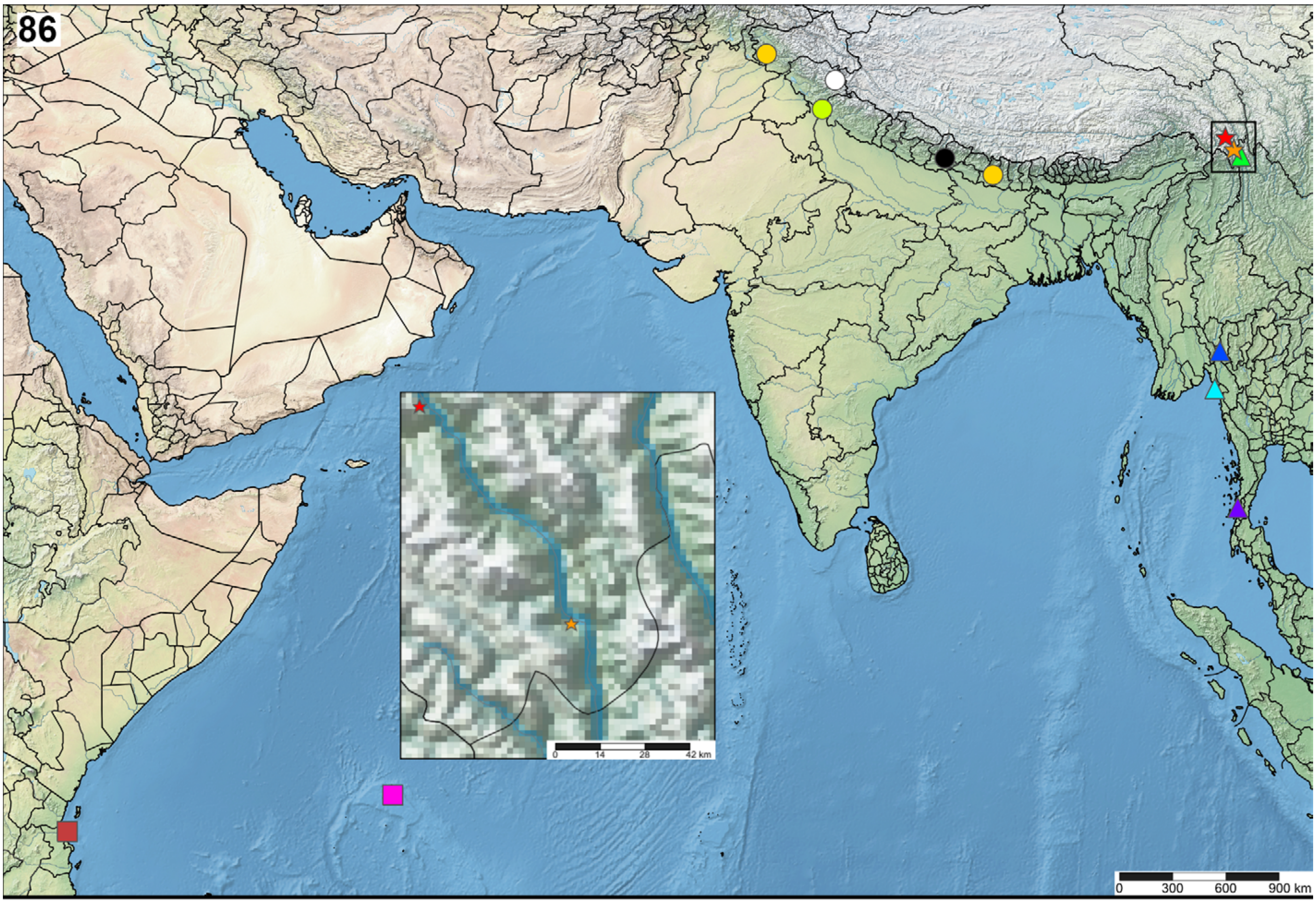

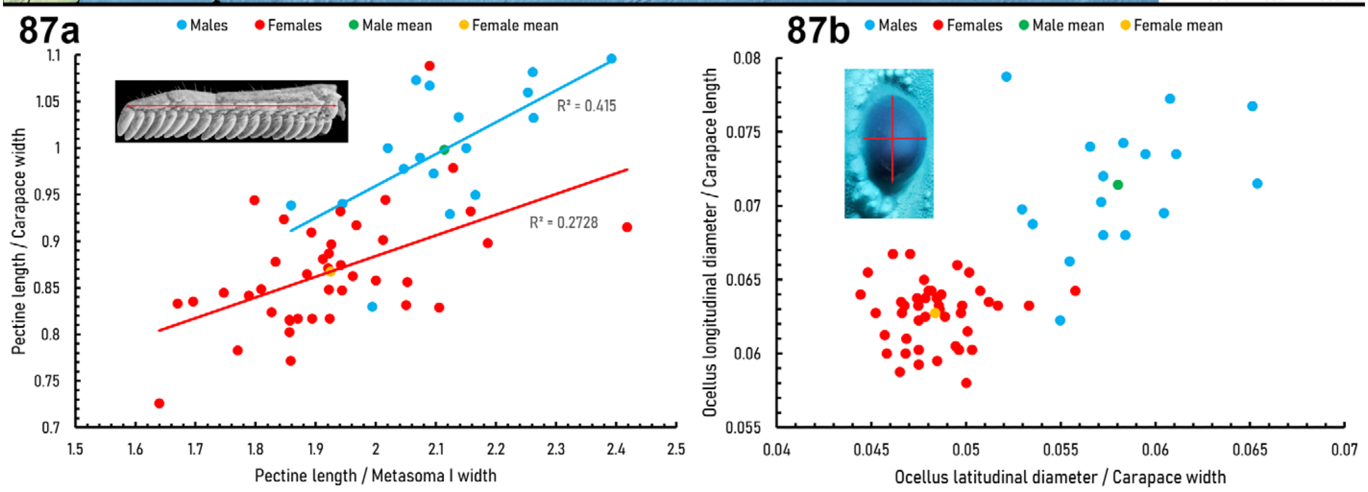

Figures 86–87: **Figure 86**. Map showing the representative localities of the discussed species. *Langxie feti* **gen**. et **sp**. **n**. (★, Gula (Golag) Township, type locality in Tibet Autonomous Region, China), *Langxie* cf. *feti* **gen**. et **sp**. **n**. (★, Chawalong (Cawarong or Tsawarong) Township, locality in Tibet Autonomous Region, China); *Lychas mucronatus* (▲, the north-most record in Deqin County of Yunnan Province, China; for other localities, see Tang 2022c); *L. brehieri* (▲, "Saddan Sin Gu" Cave, type locality in Myanmar); *L. gravelyi* (▲, Mawlamyine ("Moulmein"), type locality in Myanmar); *L. scutilus* (▲, Maliwan Village, the only known locality in Myanmar); *Afrolychas braueri* (■, Praslin Island, type locality in Seychelles); *A. burdoi* (■, Zanzibar, type locality in Tanzania); *Himalayotityobuthus alejandrae* (●, north of Saharanpur, type locality in India, approximated from fig. 16 in Lourenço (2003)); *H. martensi* (●, Tangmarg (left), type locality in India, and locality ("Tribani Ghat", Lourenço, 1997) in Nepal, approximated from fig. 16 in Lourenço (2003); it appears that "Tribani Ghat" should instead be "Triveni Ghat" (○) in India or "Tribeni" in Nepal (●)). **Figures 87a–b**: Morphometric analyses of potential sexual dimorphisms among all the adult females and males (one injured adult female excluded; paratype, no. F8). **Figure 87a**. Bivariate scatter plot comparing ratiometrics regarding pectine length/ metasoma I width (abscissa) vs. pectine length/carapace width (ordinate). Only one pectine of each specimen was examined (the most ideal one, i.e., less deformed). The manual measurement upon these tiny structures can easily arouse errors and deformation of specimens may cause anomalies, thus this result is only referential for the general trend. **Figure 87b**. Bivariate scatter plot comparing ratiometrics regarding longitudinal diameter of median ocelli/carapace length (abscissa) vs. latitudinal diameter of median ocelli/carapace width (ordinate); normalized in pixels (another female paratype, no. F17 with obvious carapace deformation was excluded).

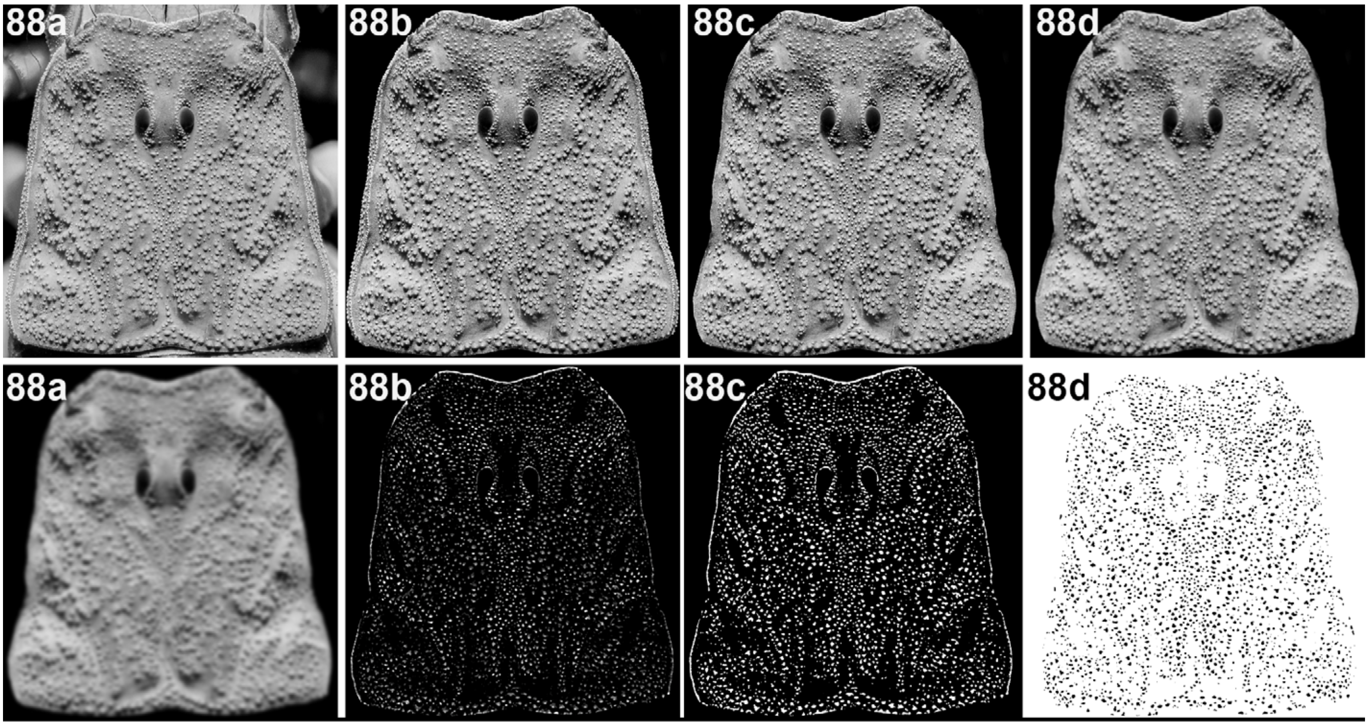

Figures 88–89: **Figures 88a–h**: Exemplary procedures of granulometric analysis using ImageJ on a full resolution image of a single carapace. The results of automated computer analysis differ from those obtained by human recognition and delimitation of granule shapes, but are sufficient to resolve sexual dimorphism. **Figure 88a**. Original carapace image acquired under UV fluorescence. **Figure 88b**. Carapace surface manually cropped from original image, with brightness and contrast adjusted. **Figure 88c**. Carapacial margins manually erased to exclude marginal granulation. **Figure 88d**. Image filtered with a low-pixel Gaussian blur (6-pixel radius) acting as a low-pass filter to suppress digital image noise and minute surface textures (e.g., lattice microstructures) (this step is unnecessary for Fig. 91 which already has a lower resolution). **Figure 88e**. Image filtered again with a higher-pixel Gaussian blur (20-pixel radius), acting as a low pass filter to suppress granules. **Figure 88f**. Image obtained by subtracting the second filtered image (88e) from the first (88d) to emphasize the granules by removing larger scale background intensity trends; brightness and contrast adjusted. **Figure 88g**. Result of applying an automatic thresholding algorithm (Yen method). **Figure 88h**. Particles detected in the thresholded image, under the criteria: area = 7–2,000 pixel^2, circularity = 0.50–1.00. **Figure 89**. Comparison of ROIs retrieved by automatic detection method (left) and manually generated granule profiles estimated by human visual perception and interpretation of the UV fluorescence image (right).

Table 2. Mann-Whitney U test		
	Statistic	**p-value**
ROI area	7.33e+8	< 0.001
ROI Feret's diameter	7.37e+8	< 0.001
Note . H_a μ Female < μ Male		

Table 3. Group Descriptives						
	Group	**N**	**Mean**	**Median**	**SD**	**SE**
ROI area	F	67516	39.56	28.00	36.77	0.1415
	M	24424	47.45	34.00	44.99	0.2879
ROI Feret's diameter	F	67516	8.92	8.06	3.88	0.0149
	M	24424	9.72	8.60	4.39	0.0281

Tables 2–3. Results of statistical analysis of female ROI vs. male ROI. **Table 2**. Results of Mann-Whitney U test. A non-parametric test was applied because frequency histograms showed that ROI area and Feret's diameter distributions were heavily right-skewed, showing that the variables did not obey a normal distribution. **Table 3**. Values of descriptive statistics (N = number, SD = standard deviation, SE = standard error).

DISTRIBUTION (Fig. 86). Known only from the southeast region of the Tibet Autonomous Region in China, and at least had been recorded in two townships, Chawalong (Cawarong or Tsawarong) and Gula (Golag), both close to the border between Xizang and Yunnan Provinces.

ECOLOGY. The new species is extremely abundant in the region (Gula Township; Figs. 83a–f) and nearly 400 specimens were discovered on three nights (14–16 September; no early instar individuals were found at this period of time). Most of the specimens were found hiding in rock crevices or wandering on walls of the flood embankment slope, as well as in the nearby rocky grassland (Figs. 84a–f). The elongation and slenderization of appendages and metasoma are probably an adaptation to the crevice microhabitat. The habitat and habitus of the new species are consistent with the lapidicolous ecomorphotype (*sensu* Prendini, 2001), or the lithophilous ecomorph (*sensu* Coelho et al., 2022). Scorpions became active after 21:00 pm, and they were found to be feeding on a variety of prey, including crickets, spiders, scutigerids, and hemipterans, clinging on the stone wall and facing downwards (Figs. 85a–f). The new species also exhibited a rapid escape response with high velocity of locomotion. Regarding the surrounding environment, a river (presumably a tributary of the Nu River) flows through the Gula Township and dense vegetation is found on both of the river banks. This may have provided sufficient humidity to the region to make it a favorable habitat for this scorpion. Under captive environments, this species demonstrates high tolerance towards other conspecifics when kept in a community. It exhibits positive thigmotaxis and an escape response can be easily evoked by a single tactile stimulation or a flipping of shelter. It is observed that this species will quickly seek narrow shelters once they find themselves exposed to bright light.

Conservation status. Only two scorpion species are regionally protected in China: *Mesobuthus thersites* (C. L. Koch, 1839) and *Olivierus martensii* (Karsch, 1879). Little is known about the authentic distribution range of the new genus, therefore the evaluation for its conservation status is undecided. Scorpions recorded in the adjacent region belong to the genus *Scorpiops* and it seems that those scorpions have been negatively affected by anthropic activities as few species had been found since their initial description (Zhiyong Di, pers. comm.). However, the errant species of Buthidae are not soil-dependent and they may show a higher level of dispersal ability. Furthermore, the current study discovered an extremely high density of this species within a small region, and the geography of Tibet Autonomous Region can prevent the excessive hunting targeted at this species (entry is difficult). Local residents also showed great respect to those animals due to their religious beliefs. The Tibetan people do not kill animals unless necessary, and they also protect them, living in harmony with those wild species in nature. The protection of this species is nonetheless recommended until its population is fully studied.

Acknowledgements

Our gratitude goes to various anonymous people, including lawyers, government officers and personnel, local authorities and chairmen of international enterprises, who helped us by negotiating with local public security in Chayu County (of Linzhi City). The second author (collector) was reported to the local police by the local residence for being suspicious as he was searching around for scorpions. Several local forest rangers and agents of the National Security Agency were also involved, they investigated him thoroughly by inspecting his phone and his chat history with the first author, and questioned his motivation. They surmised him to be a spy and intended to disturb the national unity. The second author repeatedly stated that he was only searching for scorpions for scientific research, but these officers rejected to believe him merely because they themselves had no interest in scorpions. However, even after the second author had clarified that he had previously contacted the Forestry Bureau of Linzhi and confirmed that the scorpion collection was permitted, these rangers and police refused to accept the fact and continued to deceive themselves by adhering to their absurd assumption. They professed that publishing papers of scorpiology that contain geographical information (maps) could leak important natural information to the scheming people, which would imperil the national security. However, no one would endeavor themselves to search and read a research paper just for acquiring the ecological information of a certain place, and many open websites like Wikipedia, contain much more detailed information than a scorpiology paper does. After they had recorded all the information, they executed a temporary control on the second author, forbidding him from collecting scorpions in Chayu and deprived his future rights of entering this county. All these ridiculous actions caused adverse emotional influence in both authors, jeopardized the schedule and incurred extravagant financial costs. The current study was once presumed to be a waste of all the labor. But thanks to those kind people, all these unreasonable penalties and restrictions were abolished, allowing the second author to fulfil his mission. However, due to the tedious and so-called "scientific" policy against the pandemic in China, the second author had no choice but to postpone his collection until 14 September (arrived in Gula on 11 August) as the static management (forbidding personal outdoor activities and conducting the DNA test) was repeatedly implemented in Chayu. These chaotic policies continually frustrated the two authors, sabotaged all the subsequent schedules as dominoes, compromised the second author on suspending his departure from Xizang until 12th October on account of the unremitting cancellations of flight, rendering a retention therein for two months, along with huge daily consumptions. The deferment of second author's return from Xizang due to the policy of pandemic prevention hindered the first author from obtaining the specimens prior to her trip to England, which subsequently caused a series of obstacles in receiving the specimens due to both the Chinese policy against COVID and their nonacceptance of IATA (International Air Transport Association) regulations for transporting dangerous goods (e. g., animal specimens preserved in ethanol) by the Chinese international delivery service; dozens of live specimens died and decomposed. It was not until 25th January 2023 that the first author finally received the specimens, of which only six were still alive. Nevertheless, we are grateful to all the people who spared no effort to contribute to our collection of the new species, although they were powerless against all these policies. Without their help, collecting the new species would be impossible in the first place. We also extend our gratitude to three anonymous reviewers for their valuable comments on the taxonomic position of the new species and two people who had helped us in delivering the specimens: Jiaming Sun (孙嘉明) and Maxwell Wang. The second author would also like to thank his girlfriend, Bei Hong (洪蓓), for her support.

References

ALEXANDER, A. J. 1959. Courtship and mating in the buthid scorpions. *Proceedings of the Zoological Society of London*, 133 (1): 145–169.

CAIN, S., E. GEFEN & L. PRENDINI. 2021. Systematic revision of the sand scorpions, genus *Buthacus* Birula, 1908 (Buthidae C. L. Koch, 1837) of the Levant, with redescription of *Buthacus arenicola* (Simon, 1885) from Algeria and Tunisia. *Bulletin of the American Museum of Natural History*, 450: 134 pp.

COELHO, P., A. KALIONTZOPOULOU, P. SOUSA, M. STOCKMANN & A. MEIJDEN. 2022. Reevaluating scorpion ecomorphs using a naïve approach. *BMC Ecology and Evolution*, 22 (17): 1−10.

DI, Z.-Y., Z.-J. CAO, Y.-L. WU, L. ZHU, H. LIU & W.-X. LI. 2013a. The scorpions of Hainan Island, China (Arachnida: Scorpiones). *Euscorpius*, 153: 1–24.

DUPRÉ, G. 2016. Dictionary of scientific scorpion names. *Arachnides*, 78: 1–68.

ESPOSITO, L. A., H. Y. YAMAGUTI, R. PINTO-DA-ROCHA & L. PRENDINI. 2018. Plucking with the plectrum: phylogeny of the New World buthid scorpion subfamily Centruroidinae Kraus, 1955 (Scorpiones: Buthidae) reveals evolution of three pecten-sternite stridulation organs. *Arthropod Systematics & Phylogeny*, 76 (1): 87–122.

FARZANPAY, R. & M. VACHON. 1979. Contribution à l'étude des caractères sexuels secondaires chez les scorpions Buthidae (Arachnida). *Revue Arachnologique* 2 (4): 137–142.

FET, V. 1997. Notes on the taxonomy of some old-world scorpions (Scorpiones: Buthidae, Chactidae, Ischnuridae, Scorpionidae). *The Journal of Arachnology*, 25: 245–250.

FET, V., W. D. SISSOM, G. LOWE & M. E. BRAUNWALDER (eds.). 2000. *Catalog of the Scorpions of the World (1758–1998).* New York: The New York Entomological Society.

FET, V., M. E. SOLEGLAD & G. LOWE. 2005. A new trichobothrial character for the high-level systematics of Buthoidea (Scorpiones: Buthida). *Euscorpius*, 23: 1–40.

FOX, G. A., A. M. COOPER & W. K. HAYES. 2015. The dilemma of choosing a reference character for measuring sexual size dimorphism, sexual body component dimorphism, and character scaling: cryptic dimorphism and allometry in the scorpion *Hadrurus arizonensis*. *PLoS ONE*, 10(3): e0120392. https://doi:10.1371/journal.pone.0120392

FRANCKE, O. F. 1985. Conspectus genericus scorpionorum 1758–1982 (Arachnida: Scorpiones). *Occasional Papers of the Museum, Texas Tech University*, 98: 1–32.

GURERA, D. & B. BHUSHAN. 2020. Passive water harvesting by desert plants and animals: lessons from nature. *Philosophical Transactions of the Royal Society A*, 378: 20190444. http://doi.org/10.1098/rsta.2019.0444

HADLEY, N. F. & L. L. JACKSON. 1977. Chemical composition of the epicuticular lipids of the scorpion, *Paruroctonus mesaensis*. *Insect Biochemistry*, 7: 85–89.

HEWITT, J. 1913. The Percy Sladen memorial expedition to Great Namaqualand, 1912-1913. Records and descriptions of the Arachnida of the collection. *Annals of the Transvaal Museum*, 4: 146-159.

KOCH, L. E. 1977. The taxonomy, geographic distribution and evolutionary radiation of Australo-Papuan scorpions. *Records of the Western Australian Museum*, 5(2): 83–367.

KOVAŘÍK, F. 1995. Review of Scorpionida from Thailand with descriptions of *Thaicharmus mahunkai* gen. et sp. n. and *Lychas krali* sp. n. (Buthidae). *Acta Societatis Zoologicae Bohemicae*, 59: 187–207.

KOVAŘÍK, F. 1997. Revision of the genera *Lychas* and *Hemilychas*, with descriptions of six new species (Scorpiones, Buthidae). *Acta Societatis Zoologicae Bohemicae*, 61: 311-371.

KOVAŘÍK, F. 2009. *Illustrated catalog of scorpions. Part I. Introductory remarks; keys to families and genera; subfamily Scorpioninae with keys to* Heterometrus *and* Pandinus *species*. Prague: Clairon Production, 170 pp.

KOVAŘÍK, F. 2004. *Parabuthus cimrmani* sp. nov. from Somalia (Scorpiones, Buthidae). *Acta Societas Zoologicae Bohemicae*, 68 (1): 15–19.

KOVAŘÍK, F. 2019. Taxonomic reassessment of the genera *Lychas*, *Mesobuthus*, and *Olivierus*, with descriptions of four new genera (Scorpiones: Buthidae). *Euscorpius*, 288: 1–27.

KOVAŘÍK, F. 2023. *Lychas jakli* sp. n. (Scorpiones: Buthidae) from Indonesia. *Euscorpius*, 367: 1–8.

KOVAŘÍK, F., V. FET & E. A. YAĞMUR. 2020. Further review of *Orthochirus* Karsch, 1892 (Scorpiones: Buthidae) from Asia: taxonomic position of *O. melanurus*, *O. persa*, *O. scrobiculosus*, and description of six new species. *Euscorpius*, 318: 1–73

KOVAŘÍK, F. & G. LOWE. 2022. Scorpions of the Horn of Africa (Arachnida, Scorpiones). Part XXVIII. Scorpions of Djibouti. *Euscorpius*, 357: 1−31.

KOVAŘÍK, F., G. LOWE, H. S. A. ELMI & F. ŠŤÁHLAVSKÝ. 2019. Scorpions of the Horn of Africa (Arachnida: Scorpiones). Part XXI. *Parabuthus* (Buthidae) (Part II), with description of five new species from Somaliland and Ethiopia. *Euscorpius*, 290: 1−63.

KOVAŘÍK, F., G. LOWE, K. B. RANAWANA, D. HOFEREK, V. A. S. JAYARATHNE, J. PLÍŠKOVÁ & F. ŠŤÁHLAVSKÝ. 2016. Scorpions of Sri Lanka (Scorpiones: Buthidae, Chaerilidae, Scorpionidae) with description of four new species of the genera *Charmus* Karsch, 1879 and *Reddyanus* Vachon, 1972, stat. n.. *Euscorpius*, 220: 1–133

KOVAŘÍK, F., G. LOWE & F. ŠŤÁHLAVSKÝ. 2018. Review of the genus *Babycurus* Karsch, 1886 (Arachnida, Scorpiones, Buthidae), with descriptions of *Barbaracurus* gen. n. and two new species from Oman and Yemen. *Euscorpius*, 267: 1−41.

KOVAŘÍK, F. & S. WHITMAN. 2005. Cataloghi del Museo di Storia Naturale dell'Università di Firenze - Sezione di Zoologia «La Specola». XXII. Arachnida scorpiones. Tipi. Addenda (1988–2004) e checklist della collezione (Euscorpiinae esclusi). *Atti della Società Toscana di Scienze Naturali, Memorie*, serie B, 111 (2004): 103–119.

KRAEPELIN, K. 1891. Revision der Skorpione. I. Die Familie des Androctonidae. *Jahrbuch der Hamburgischen Wissenschaftlichen Anstalten*, 8(1890): 144–286 (1–144).

LEVY, G. & AMITAI, P. 1980. *Scorpiones. Fauna Palaestina. Arachnida* I. The Israel Academy of Sciences and Humanities. Jerusalem, 1980.

LORIA, S. F. & L. PRENDINI. 2021. Burrowing into the forest: phylogeny of the Asian forest scorpions (Scorpionidae: Heterometrinae) and the evolution of ecomorphotypes. *Cladistics*, 37: 109–161.

LOURENÇO, W. R. 1997. Description of a new genus and new species of Buthidae scorpion from the Himalayas of India and Nepal, with some new biogeographic implications. *Entomologische Mitteilungen aus dem Zoologischen Museum Hamburg*, 13 (161): 133–138.

LOURENÇO, W. R. 2003. Description of a new species of scorpion belonging to the genus *Himalayotityobuthus* Lourenço (Scorpiones, Buthidae). *Revista Ibérica de Aracnologia*, 7: 225–229.

LOURENÇO, W.R. 2006. Further considerations on the genus *Buthacus* Birula, 1908 (Scorpiones: Buthidae), with a description of one new species and two new subspecies. *Boletín de la Sociedad Entomológica Aragonesa*, 38: 59–70.

LOURENÇO, W. R. & S. E. SADINE. 2014. A new species of the rare buthid scorpion genus *Lissothus* Vachon, 1948 from Central Algeria (Scorpiones, Buthidae). *Comptes Rendus Biologies*, 337(6): 416–422.

LOWE, G. 2018. The genera *Butheolus* Simon, 1882 and *Xenobuthus* gen. nov. (Scorpiones: Buthidae) in Oman. *Euscorpius*, 261: 1–73.

LOWE, G. & F. KOVAŘÍK. 2022. Reanalysis of *Teruelius* and *Grosphus* (Scorpiones: Buthidae) with descriptions of two new species. *Euscorpius*, 356: 1–105.

LOWE, G., E. A. YAĞMUR & F. KOVAŘÍK. 2014. A review of the genus *Leiurus* Ehrenberg, 1828 (Scorpiones: Buthidae) with description of four new species from the Arabian Peninsula. *Euscorpius*, 191: 1–129.

LV, H.-Y & Z.-Y DI. 2022. *Scorpiops lourencoi* sp. nov., the revalidation of *Scorpiops atomatus* Qi, Zhu & Lourenço, 2005, and the redescription of *Scorpiops tibetanus* Hirst, 1911 (Scorpiones, Scorpiopidae) from China. *ZooKeys*, 1132: 189–214.

MNHN-RS-RS8236. *Himalayotityobuthus martensi* Lourenço, 1997. Allotype. *Muséum National d'Histoire Naturelle, Paris, France* (accessed 28. II. 2023). https://science.mnhn.fr/institution/mnhn/collection/rs/item/rs8236?lang=en_US

NØRGAARD, T., M. EBNER & M. DACKE. 2012. Animal or plant: Which is the better fog water collector? *PLoS ONE*, 7(4): e34603. https://doi.org/10.1371/journal.pone.0034603

POCOCK, R. I. 1900. Arachnida. *The Fauna of British India, Including Ceylon and Burma*. Published under the authority of the Secretary of State for India in Council. London: W. T. Blandford, xii, 279 pp.

PRENDINI, L. 2001. Substratum specialization and speciation in southern African scorpions: the Effect Hypothesis revisited. Pp. 113–138 *in:* Fet, V. & P.A. Selden (editors), *Scorpions 2001: In Memoriam Gary A. Polis*. Burnham Beeches, Bucks, U.K.: British Arachnological Society.

PRENDINI, L. 2004. Revision of *Karasbergia* Hewitt (Scorpiones: Buthidae), a monotypic genus endemic to southern Africa. *Journal of Afrotropical Zoology*, 1: 77–93.

PRENDINI, L., V. L. EHRENTHAL & S. F. LORIA. 2021. Systematics of the relictual Asian scorpion family Pseudochactidae Gromov, 1998, with a review of cavernicolous, troglobitic, and troglomorphic scorpions. *Bulletin of the American Museum of Natural History*, 453: 1–149.

SCHNEIDER, C. A., W. S. RASBAND & K. W. ELICEIRI. 2012. NIH Image to ImageJ: 25 years of image analysis. *Nature Methods*, 9(7): 671–675.

SISSOM, W. D. 1990. Systematics, biogeography, and paleontology. Pp. 163–223. *In*: Polis, G. A. (ed.) *The Biology of Scorpions*. Stanford University Press, Stanford.

SOLEGLAD, M. E. & V. FET. 2003. The scorpion sternum: structure and phylogeny (Scorpiones: Orthosterni). *Euscorpius*, 5: 1–34.

SOLEGLAD, M. E. & W. D. SISSOM, 2001. Phylogeny of the family Euscorpiidae Laurie, 1896: a major revision. Pp. 25–111 *in* Fet, V. & P.A. Selden (eds). *Scorpions 2001. In memoriam Gary A. Polis*. Burnham Beeches, Bucks: British Arachnological Society.

STAHNKE, H. L. 1971. Scorpion nomenclature and mensuration. *Entomological News*, 81(12): 297–316.

STATHI, I. & W. R. LOURENÇO. 2003. Description of a new scorpion species of the genus *Birulatus* Vachon, 1974 (Scorpiones, Buthidae) from Syria. *Zoology in the Middle East*, 30: 105–110.

STOCKWELL, S. A. 1989. *Revision of the Phylogeny and Higher Classification of Scorpions (Chelicerata)*. Ph.D. Dissertation, University of Berkeley, Berkeley, California. 319 pp. (unpublished). University Microfilms International, Ann Arbor, Michigan.

ŠTUNDLOVÁ, J., F. ŠŤÁHLAVSKÝ, V. OPATOVÁ, J. ŠTUNDL, F. KOVAŘÍK, P. DOLEJŠ & J. ŠMÍD. 2022. Molecular data do not support the traditional morphology-based groupings in the scorpion family Buthidae (Arachnida: Scorpiones). *Molecular Phylogenetics and Evolution*, 173(2022) 107511: 1–5 and Supplementary Information. https://www.sciencedirect.com/science/article/pii/S1055790322001245

TANG, V. 2022a. A standardized list of scorpion names in Chinese, with an etymological approach. *Euscorpius*, 350: 1–91.

TANG, V. 2022b. Scorpions of China: an updated checklist with comments on some taxonomic issues (Arachnida: Scorpiones). *Euscorpius*, 355: 1–18.

TANG, V. 2022c. A new species of *Scorpiops* Peters, 1861 from Yunnan Province, China, with a preliminary review of its congeners in Yunnan (Scorpiones: Scorpiopidae). *Euscorpius*, No. 360: 1–45.

TANG, V. 2022d. Reanalysis of the Yunnan population of *Scorpiops kubani* (Kovařík, 2004) with a description of a new species, *Scorpiops lowei* sp. n. (Scorpiones: Scorpiopidae). *Euscorpius*, 361: 1–22.

TERUEL, R. F. KOVAŘÍK & V. FET. 2018. Revision of the Central Asian scorpion genus *Anomalobuthus* Kraepelin, 1900, with descriptions of three new species and a generic synonymy (Scorpiones: Buthidae). *Euscorpius*, 270: 1–45.

TERUEL, R. & C. TURIEL. 2022. The genus *Buthus* Leach, 1815 (Scorpiones: Buthidae) in the Iberian Peninsula. Part 5: a new psammophile species from northern Spain, a synonymy and first albinism record in the genus. *Revista Ibérica de Aracnología*, 41: 15–36.

TIKADER, B. K. & D. B. BASTAWADE. 1983. Scorpions (Scorpionida: Arachnida). In *The Fauna of India*, Vol. 3. (Edited by the Director). Calcutta: Zoological Survey of India, 671 pp.

TOOLSON, E. C. & N. F. HADLEY. 1977. Cuticular permeability and epicuticular lipid composition in two Arizona vejovid scorpions. *Physiological Zoology*, 50 (4): 323–330.

VACHON, M. 1952. *Études sur les Scorpions*. Institut Pasteur d´Algérie, Alger, 482 pp. (published 1948–1951 in *Archives de l´Institut Pasteur d´Algérie*, 1948, 26: 25–90, 162–208, 288–316, 441–481. 1949, 27: 66–100, 134–169, 281–288, 334–396. 1950, 28: 152–216, 383–413. 1951, 29: 46–104).

VACHON, M. 1958. A propos de *Liobuthus kessleri* Birula, scorpion psammophile nouveau pour la faune iranienne. *Bulletin du Muséum National d' Histoire Naturelle*, 30 (5): 422–426.

VACHON, M. 1974. Etude des caractères utilisés pour classer les familles et les genres de Scorpions (Arachnides). 1. La trichobothriotaxie en Arachnologie. Sigles trichobothriaux et types de trichobothriotaxie chez les scorpions. *Bulletin du Muséum National d'Histoire Naturelle, Paris*, (3), 140 (Zool. 104), mai-juin 1973: 857–958.

VACHON, M. 1986. Étude de la denture des doigts des pédipalpes chez les scorpions du genre *Lychas*. *Bulletin du Muséum National d'Histoire Naturelle, Paris*, 8: 835–850.

VOLSCHENK, E. S., C. I. MATTONI & L. PRENDINI. 2008. Comparative anatomy of the mesosomal organs of scorpions (Chelicerata, Scorpiones), with implications for the phylogeny of the order. *Zoological Journal of the Linnean Society*, 154 (4): 651–675.

YEN, J.-C., F.-J. CHANG & S. CHANG. 1995. A new criterion for automatic multilevel thresholding. *IEEE Transactions on Image Processing*, 4(3): 370–378.

YTHIER, E. & W. R. LOURENÇO. 2022. A new species of *Lychas* C. L. Koch, 1845 from Thailand (Scorpiones: Buthidae). *Faunitaxys*, 10 (26): 1–7.

Appendix.

Figures of all examined type specimens (dorsal habitus under white light, carapace and pectines under UV light)

Angles at which the specimens were placed on the examination board can induce different visual effects of shadows and thus that of carinae and granulation. The contraction due to dehydration, or on the contrary, edema-like inflation of the specimens may also render the same effect to the carapace shape. We provided photographs of all the type specimens to reduce the unfavorable biases caused by these variables.

The individual habitus photos were taken when the specimens were not completely dried as vibrations may occur during the photography procedure. The adhesive property of the water allows the specimens to be more stable during this process. Water can also reveal the authentic coloration/patterns of the type specimens, although it incurs reflection on the specimens.

Scale: scale of grid = 1 square inch; scale bar in each specimen photo = 1 cm.

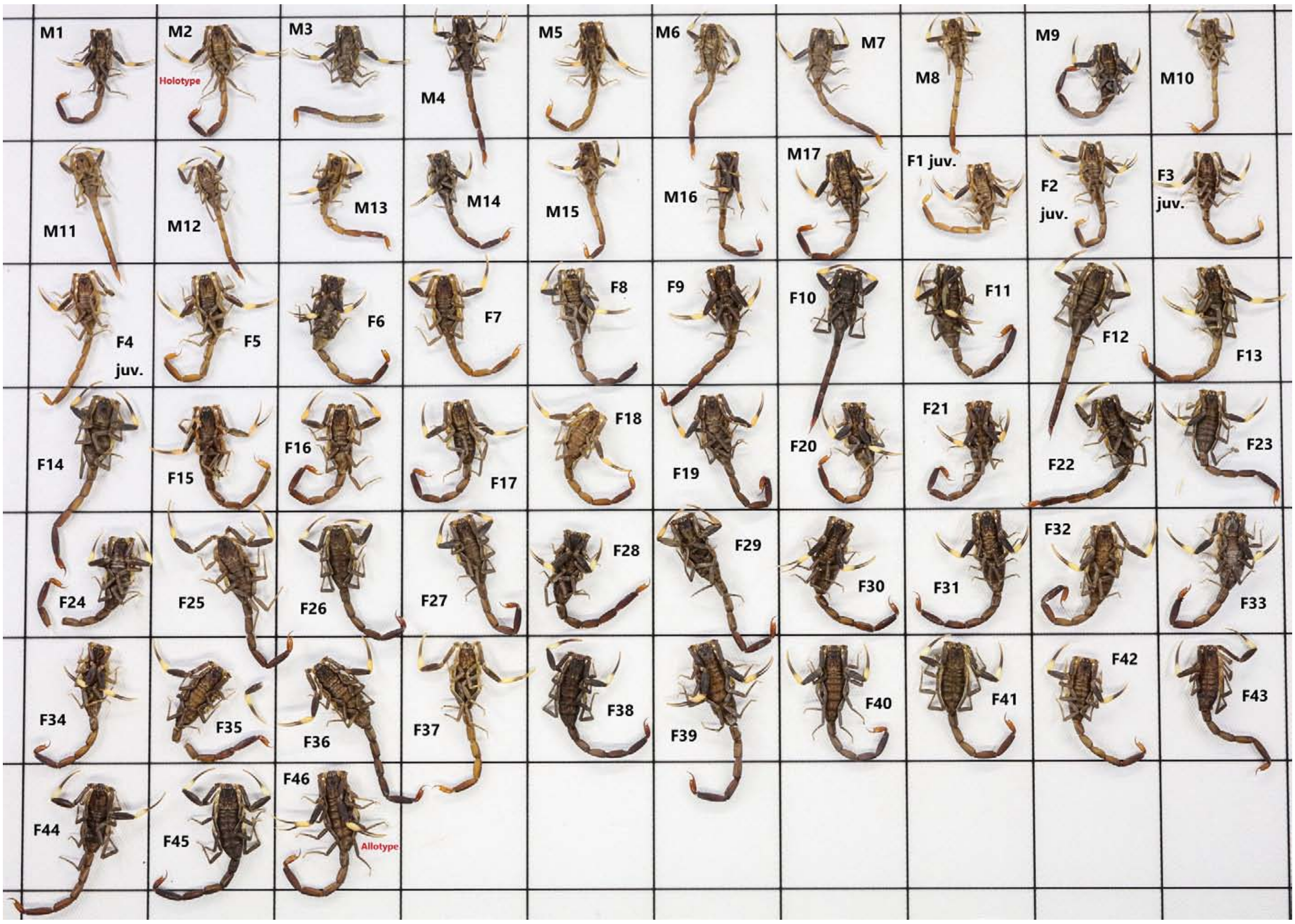

Figure 90. Habitus of all the type specimens of *Langxie feti* **gen**. et **sp**. **n**.; specimens are placed in the same sequence as the subsequent order of each specimen (start from above to below and left to right (same for all rows of specimens)).

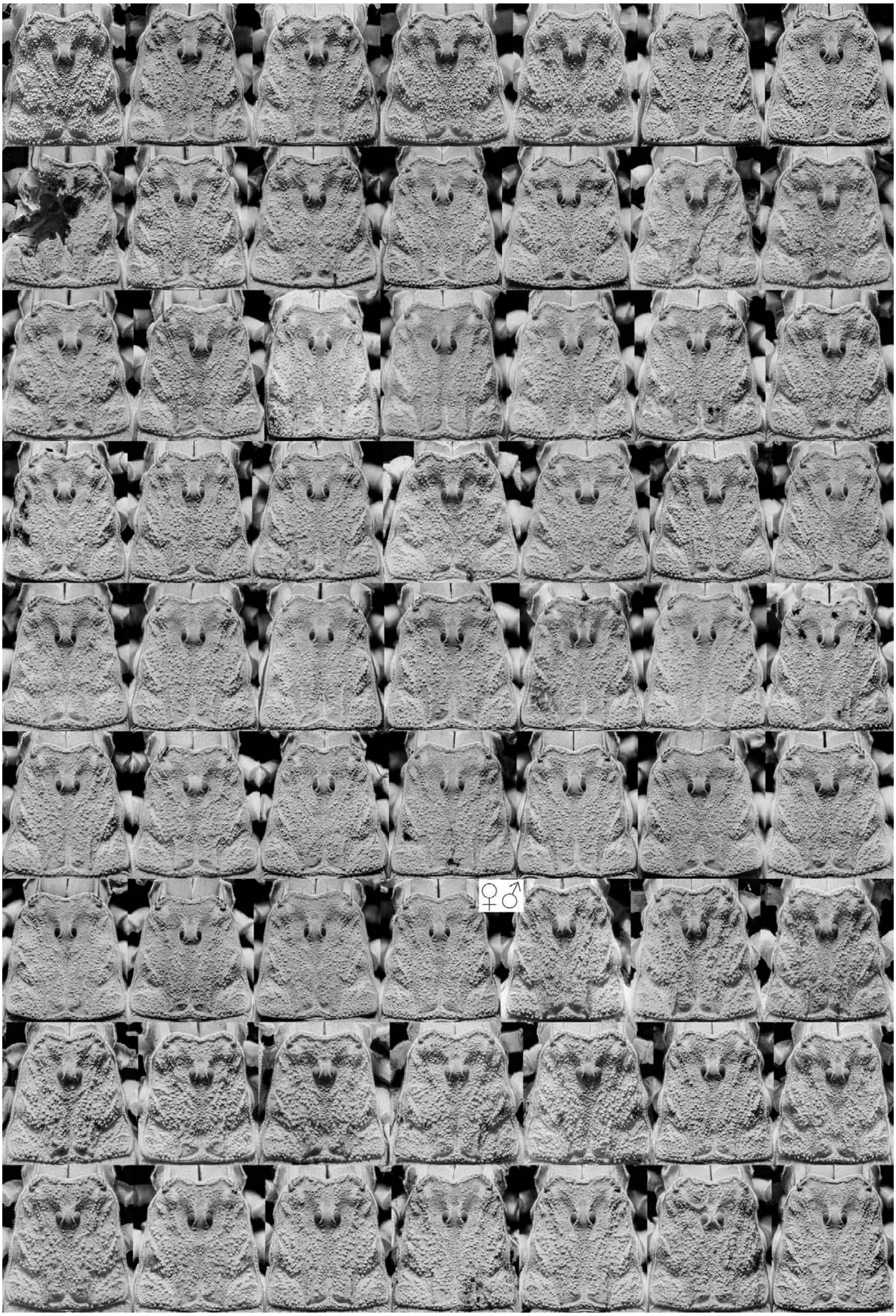

Figure 91. Compilation of carapace morphology of all the types of *Langxie feti* **gen**. et **sp**. **n**. (first four are juveniles, others are females and last 17 are males).

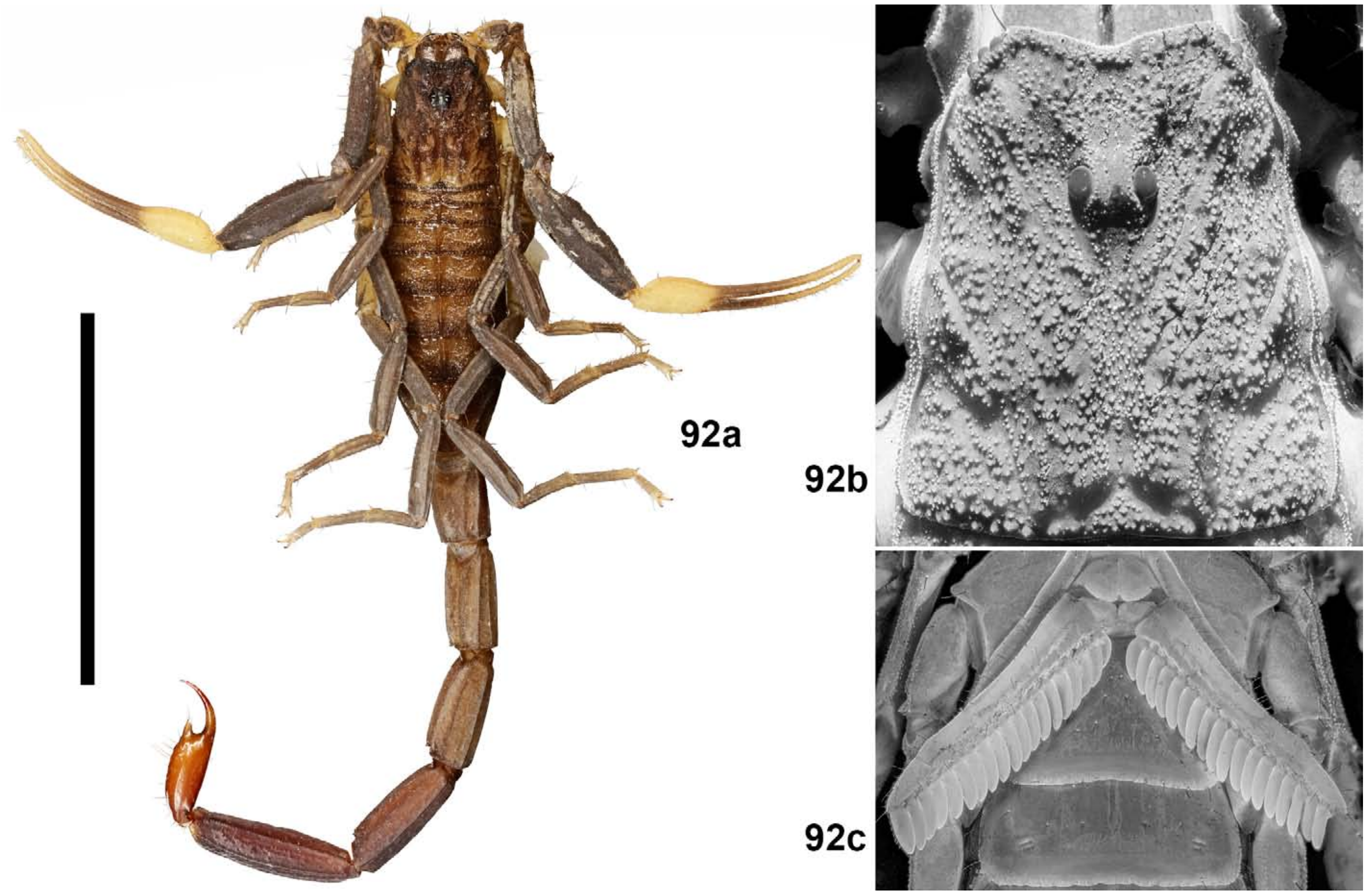

Figures 92a–**c**. *Langxie feti* **gen**. et **sp**. **n**., male paratype no. M1, habitus (92a), carapace (92b) and sternopectinal area (92c). Scale bar = 10 mm (92a).

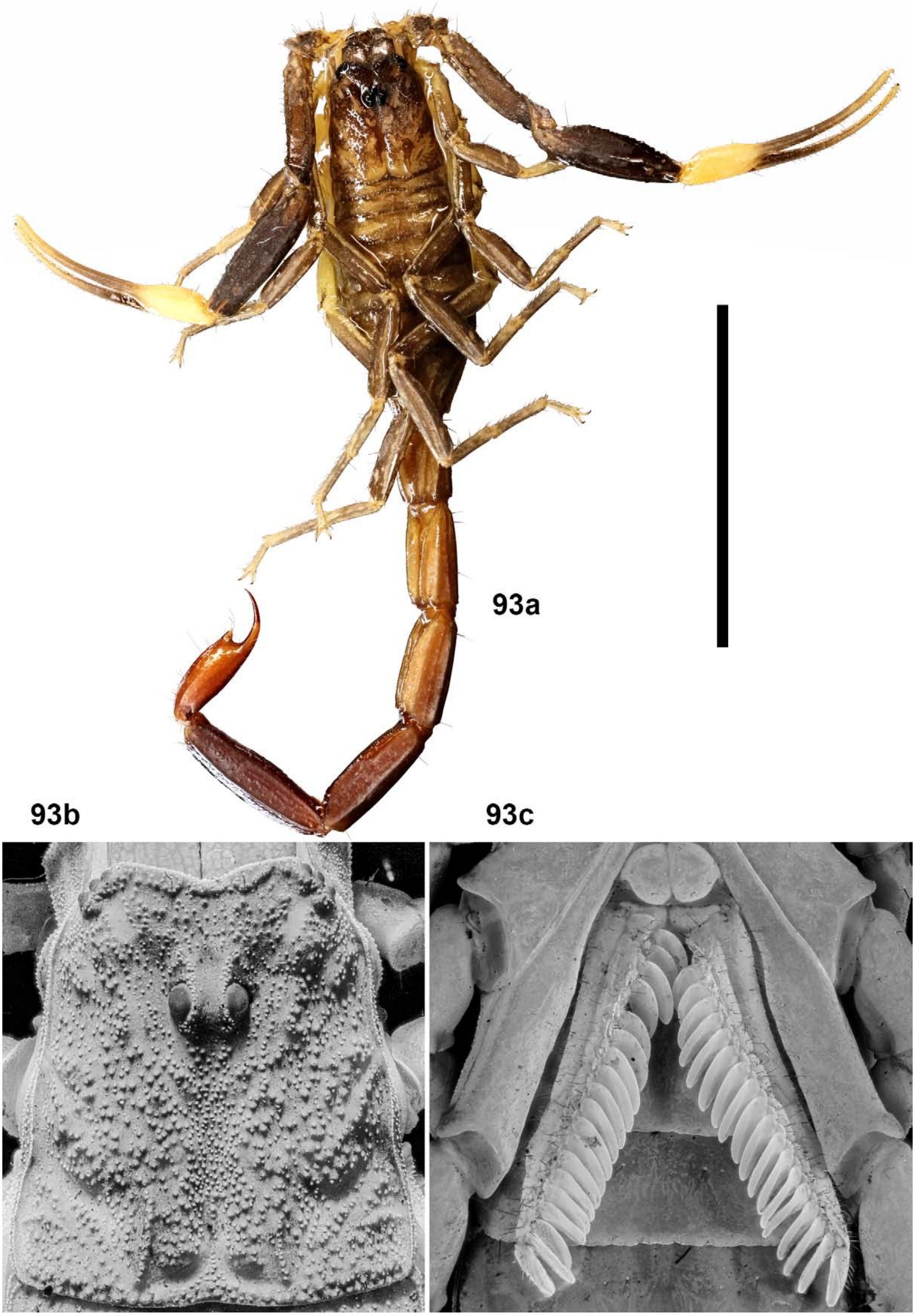

Figures 93a–c. *Langxie feti* **gen**. et **sp**. **n**., male holotype, habitus (93a), carapace (93b) and sternopectinal area (93c). Scale bar = 10 mm (93a).

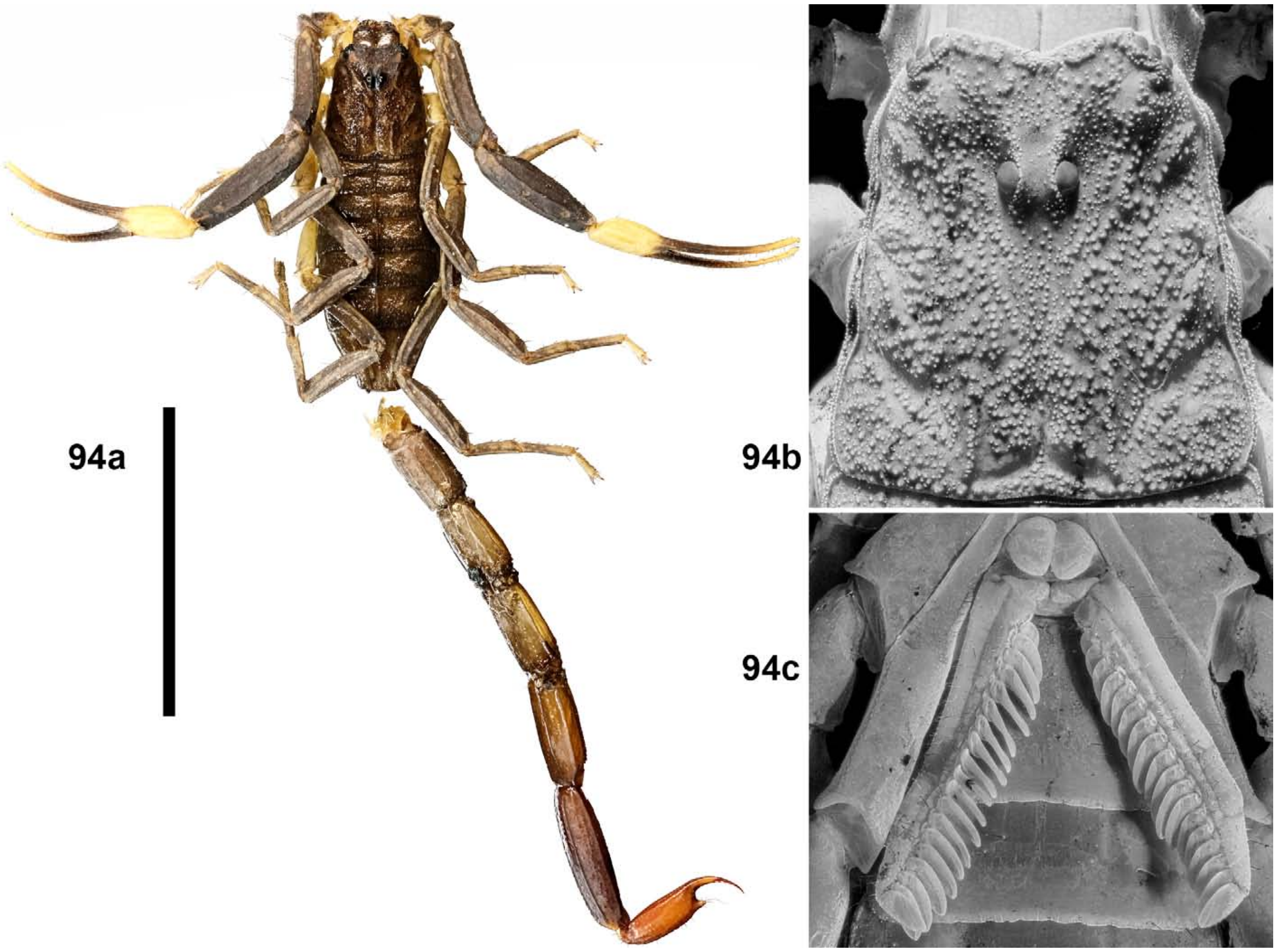

Figures 94a–**c**. *Langxie feti* **gen**. et **sp**. **n**., male paratype no. M3, habitus (94a), carapace (94b) and sternopectinal area (94c). Scale bar = 10 mm (94a).

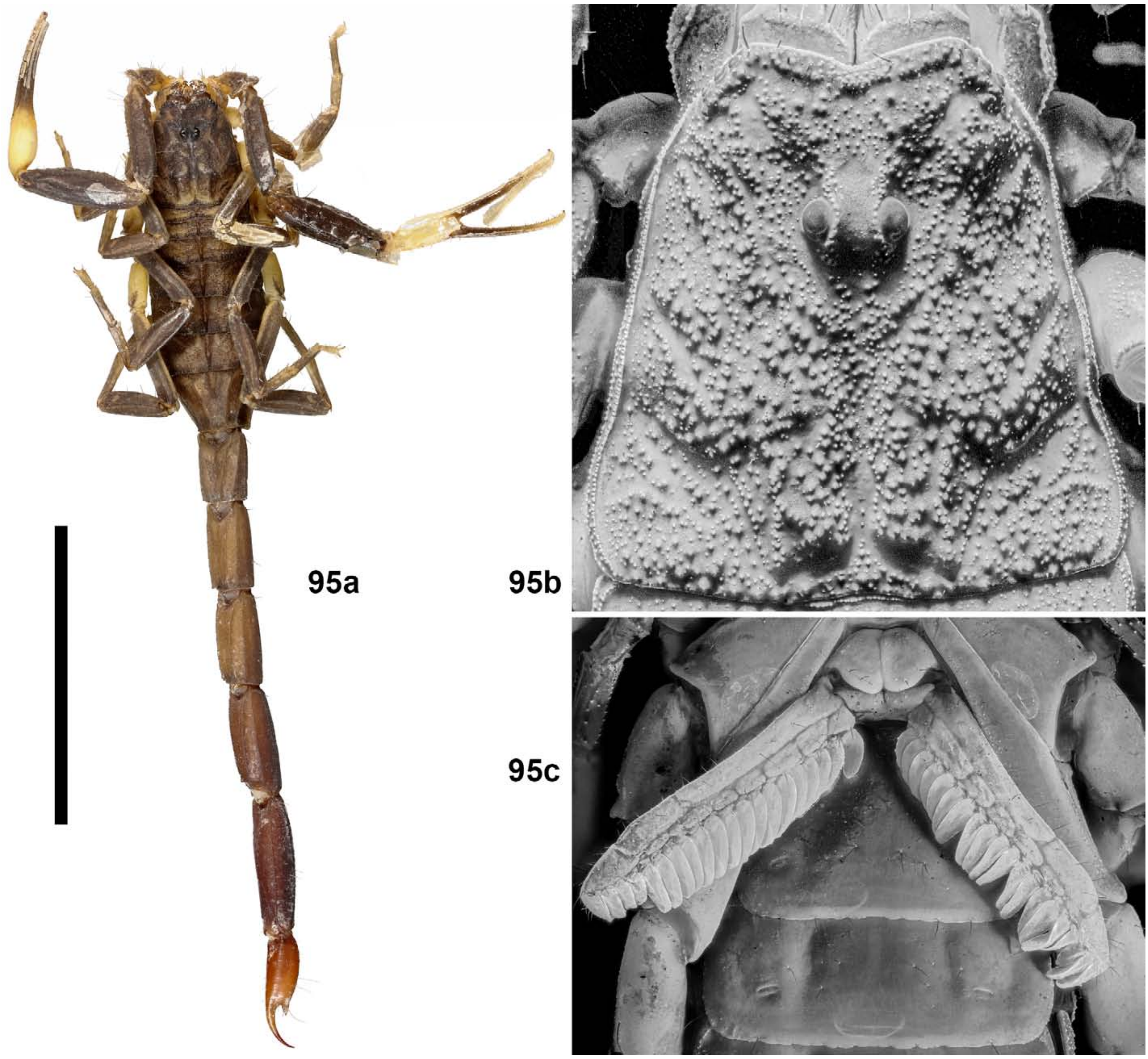

Figures 95a–c. *Langxie feti* **gen**. et **sp**. **n**., male paratype no. M4, habitus (95a), carapace (95b) and sternopectinal area (95c). Scale bar = 10 mm (95a).

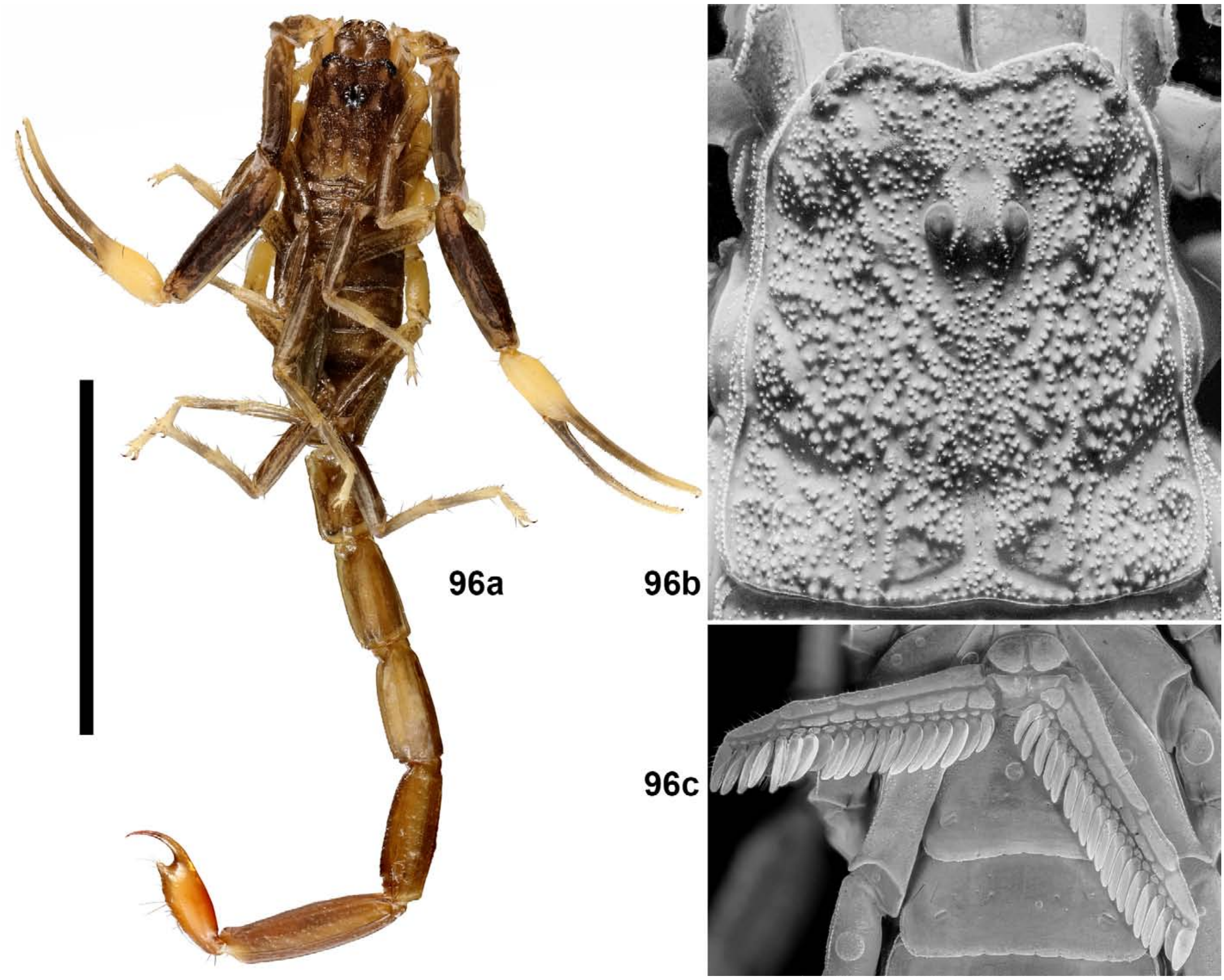

Figures 96a–**c**. *Langxie feti* **gen**. et **sp**. **n**., male paratype no. M5, habitus (96a), carapace (96b) and sternopectinal area (96c). Scale bar = 10 mm (96a).

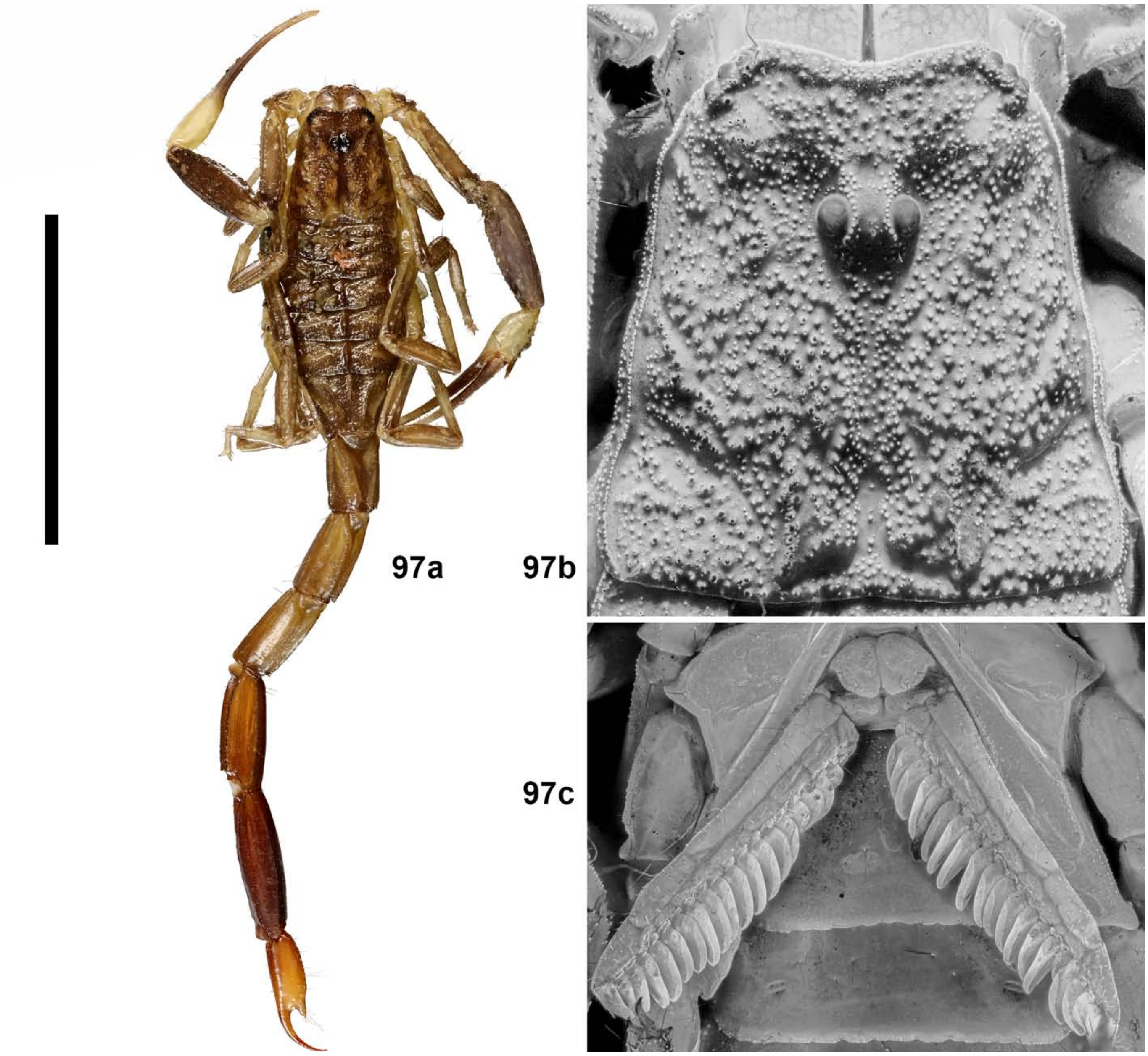

97a 97b 97c

Figures 97a–**c**. *Langxie feti* **gen**. et **sp**. **n**., male paratype no. M6, habitus (97a), carapace (97b) and sternopectinal area (97c). Scale bar = 10 mm (97a).

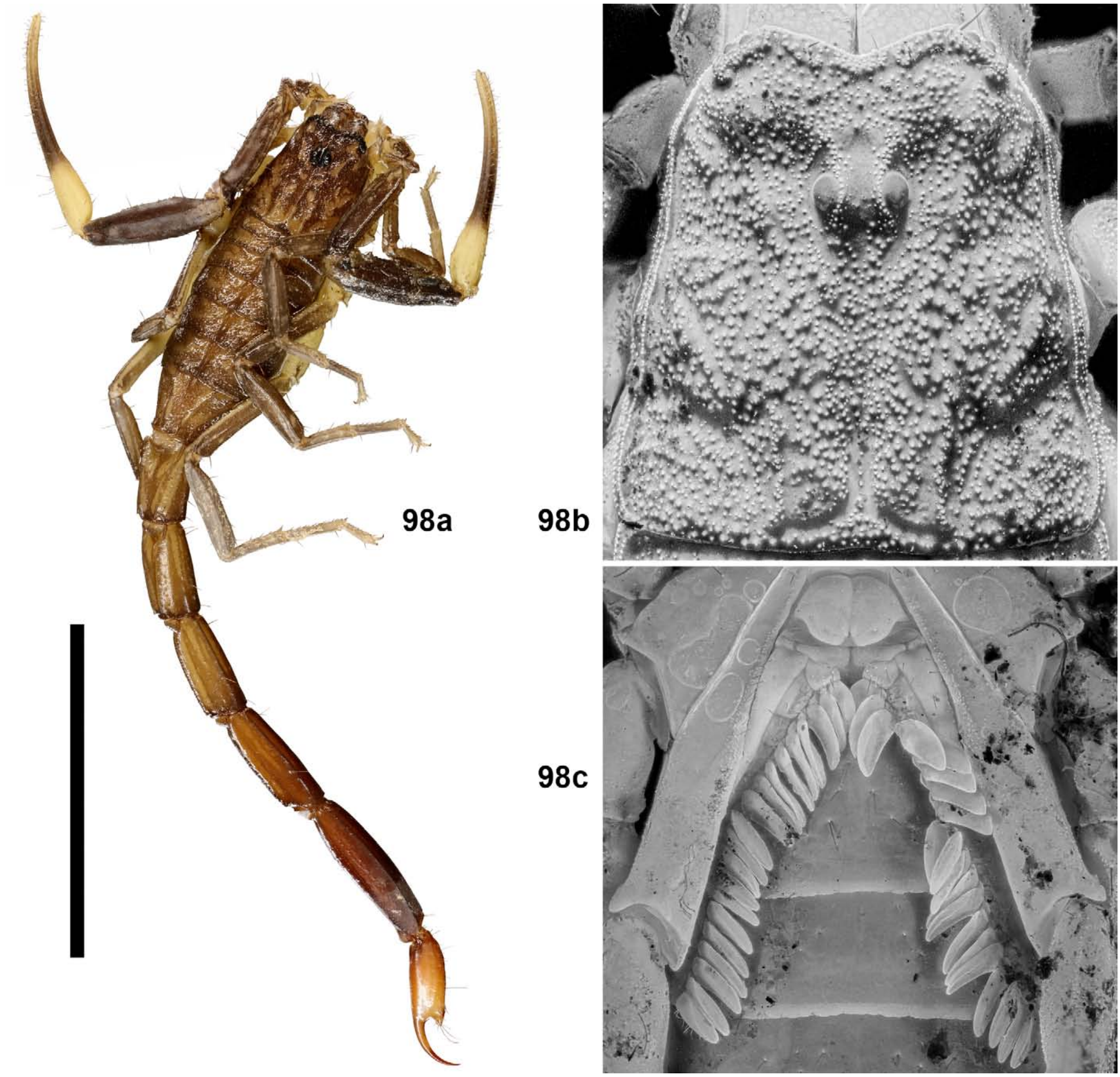

Figures 98a–c. *Langxie feti* **gen**. et **sp**. **n**., male paratype no. M7, habitus (98a), carapace (98b) and sternopectinal area (98c). Scale bar = 10 mm (98a).

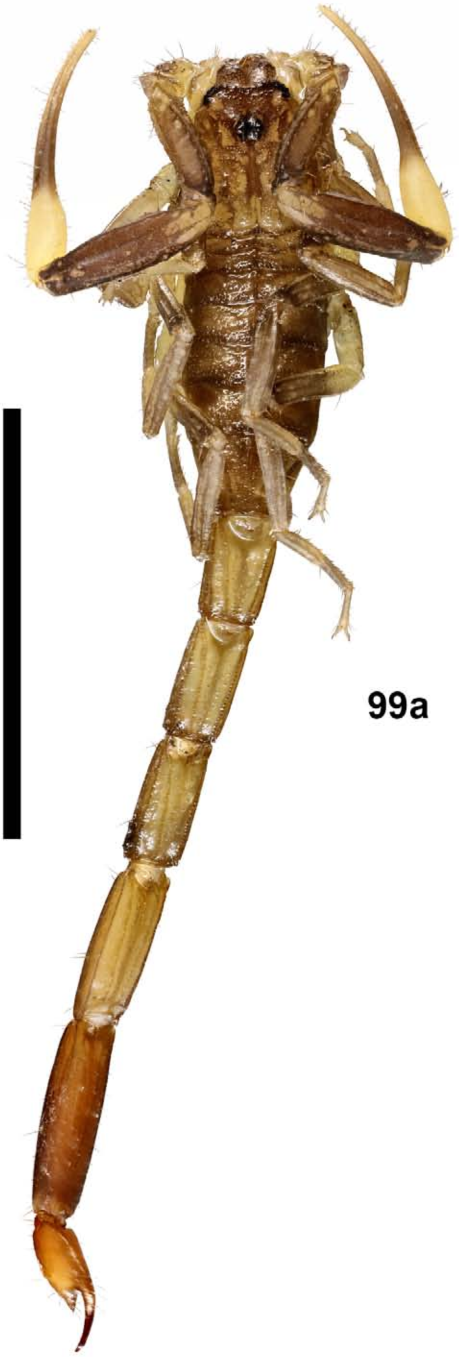

99a

99b

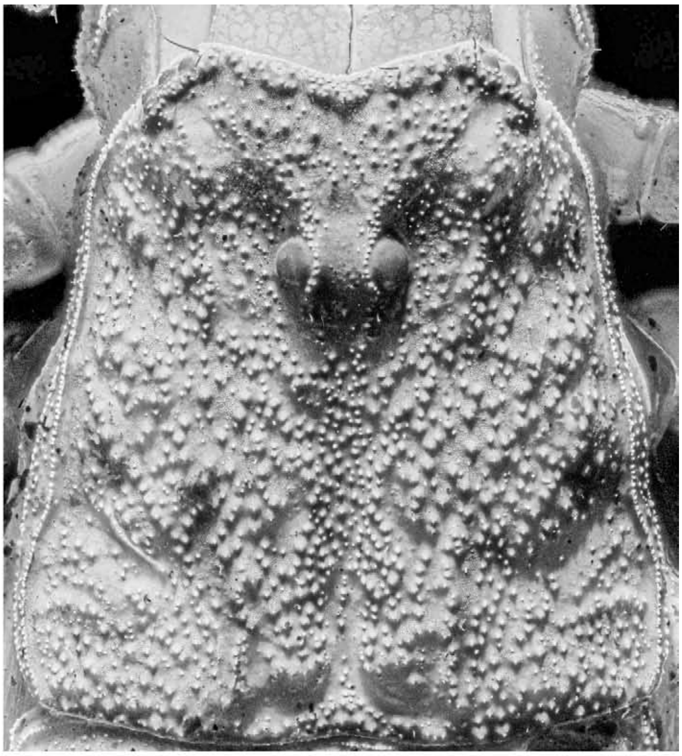

99c

Figures 99a–c. *Langxie feti* **gen**. et **sp**. **n**., male paratype no. M8, habitus (99a), carapace (99b) and sternopectinal area (99c). Scale bar = 10 mm (99a).

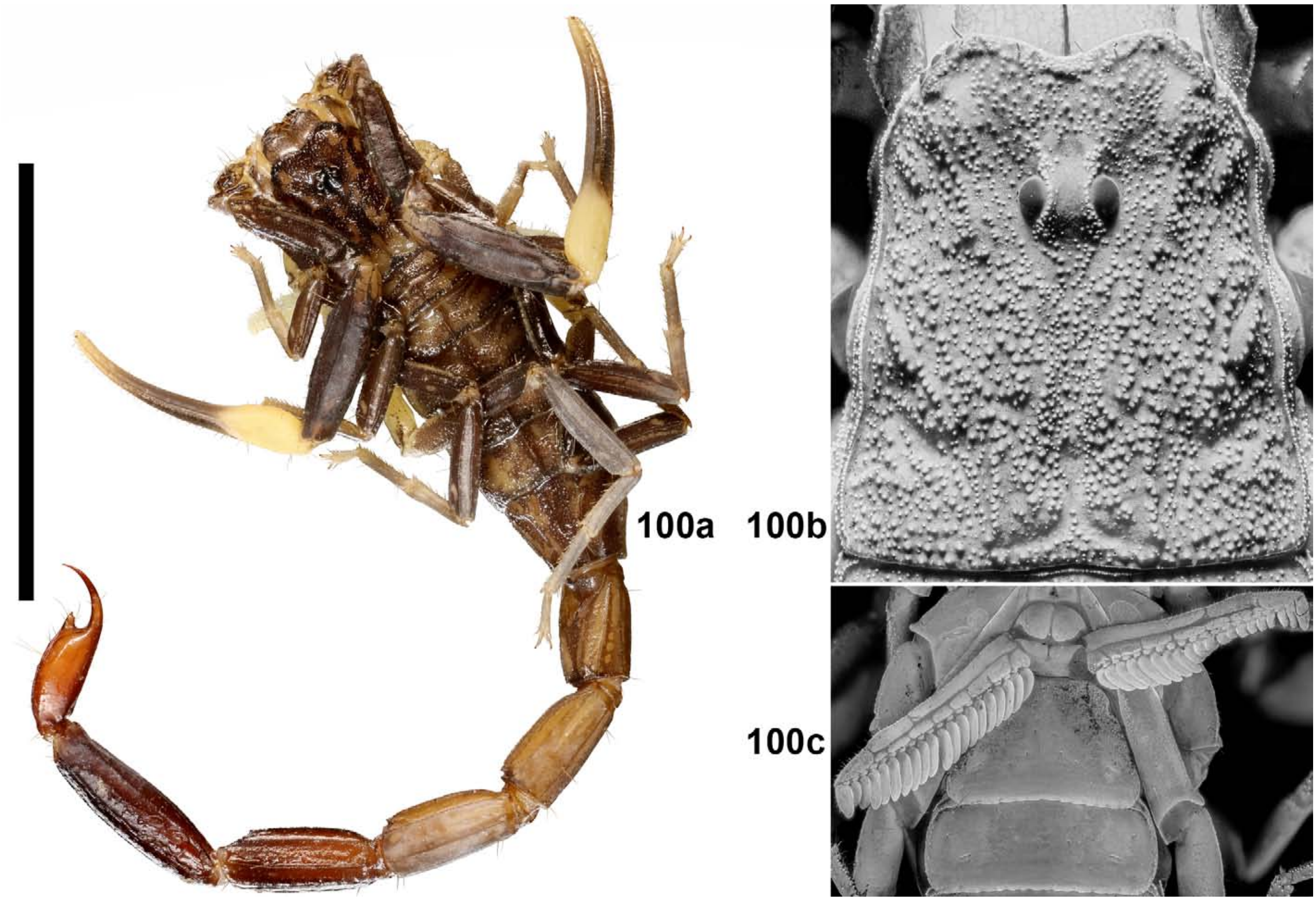

Figures 100a–**c**. *Langxie feti* **gen**. et **sp**. **n**., male paratype no. M9, habitus (100a), carapace (100b) and sternopectinal area (100c). Scale bar = 10 mm (100a).

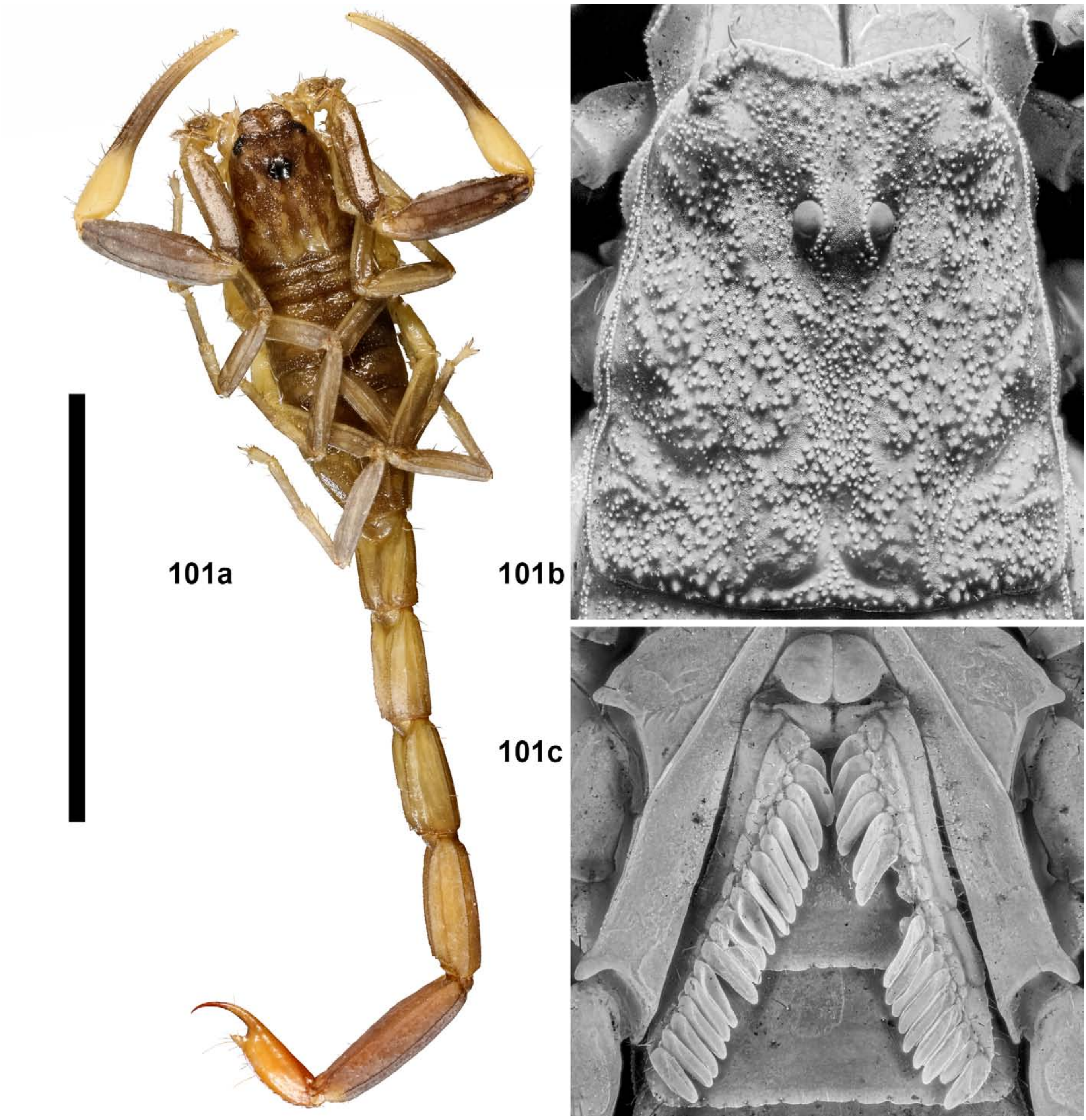

Figures 101a–**c**. *Langxie feti* **gen**. et **sp**. **n**., male paratype no. M10, habitus (101a), carapace (101b) and sternopectinal area (101c). Scale bar = 10 mm (101a).

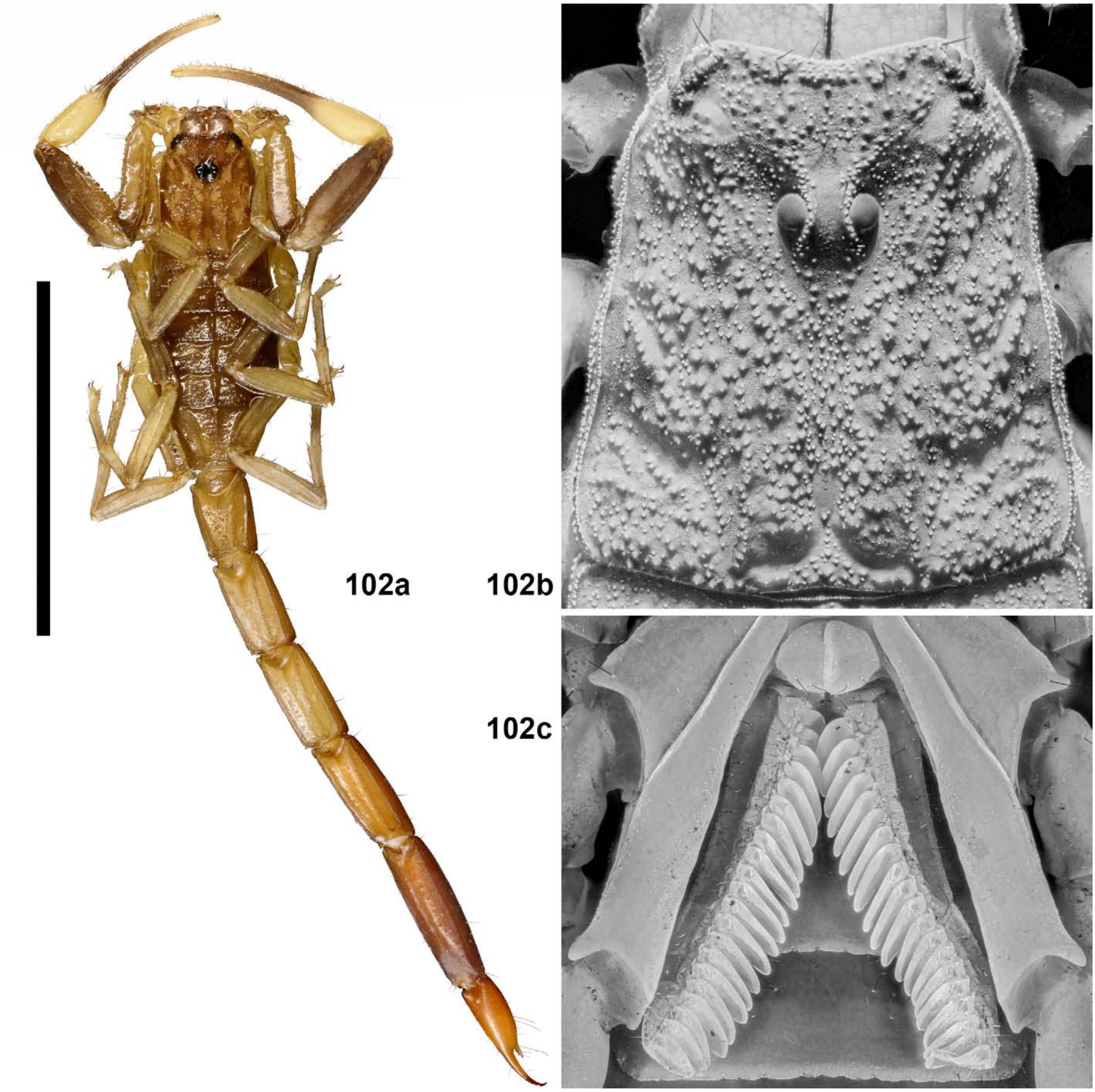

Figures 102a–**c**. *Langxie feti* **gen**. et **sp**. **n**., male paratype no. M11, habitus (102a), carapace (102b) and sternopectinal area (102c). Scale bar = 10 mm (102a).

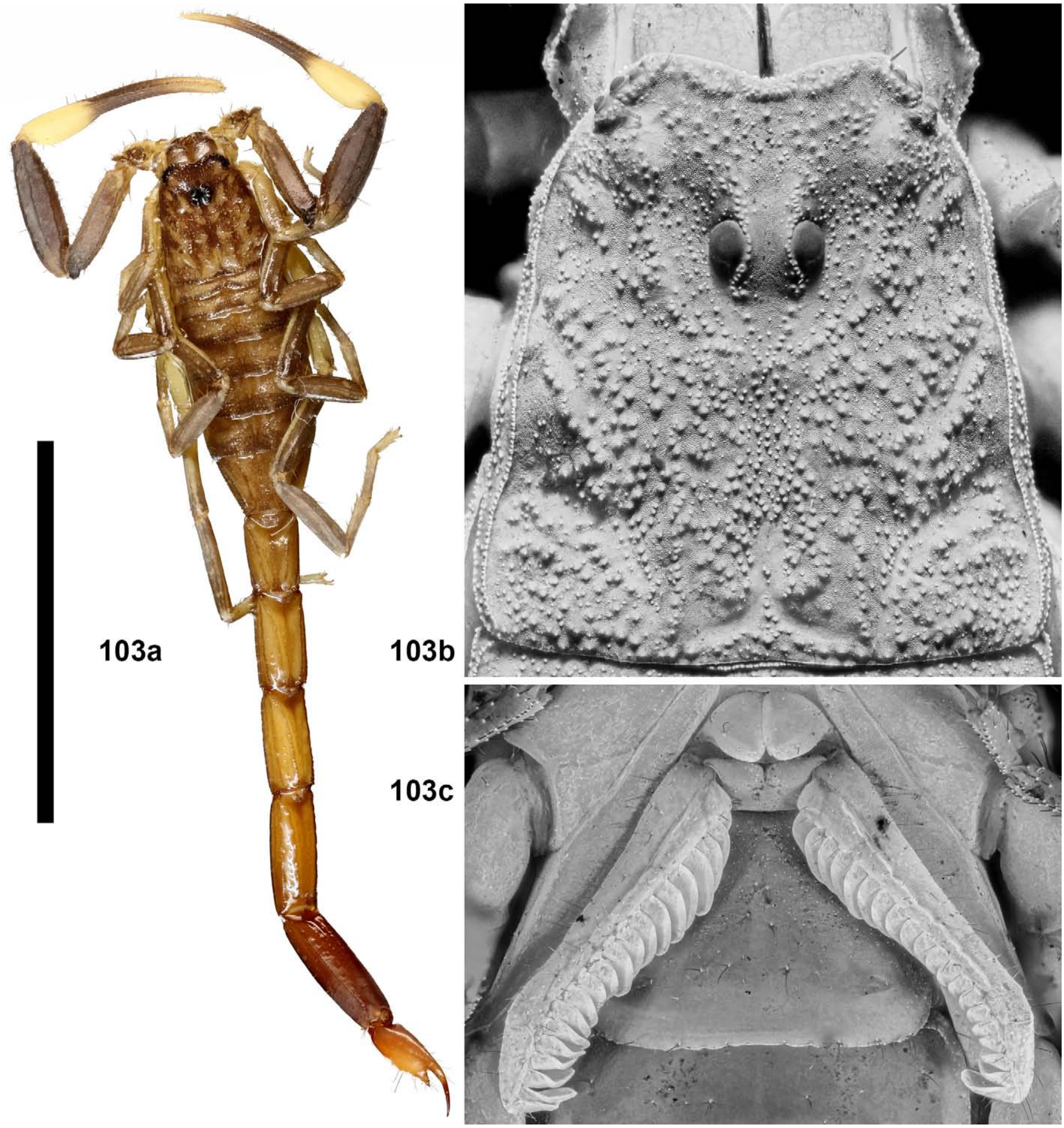

Figures 103a–**c**. *Langxie feti* **gen**. et **sp**. **n**., male paratype no. M12, habitus (103a), carapace (103b) and sternopectinal area (103c). Scale bar = 10 mm (103a).

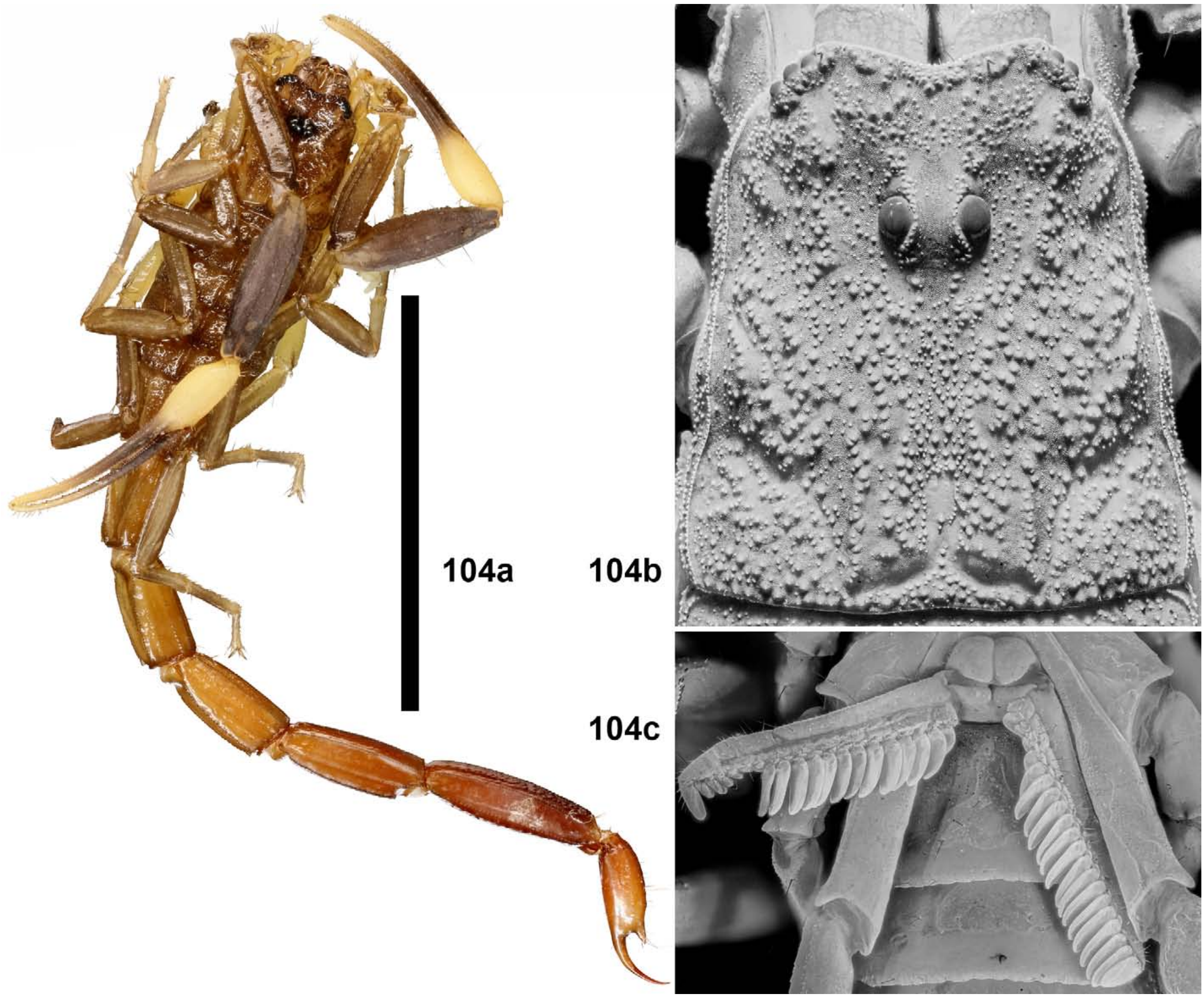

Figures 104a–c. *Langxie feti* **gen**. et **sp**. **n**., male paratype no. M13, habitus (104a), carapace (104b) and sternopectinal area (104c). Scale bar = 10 mm (104a).

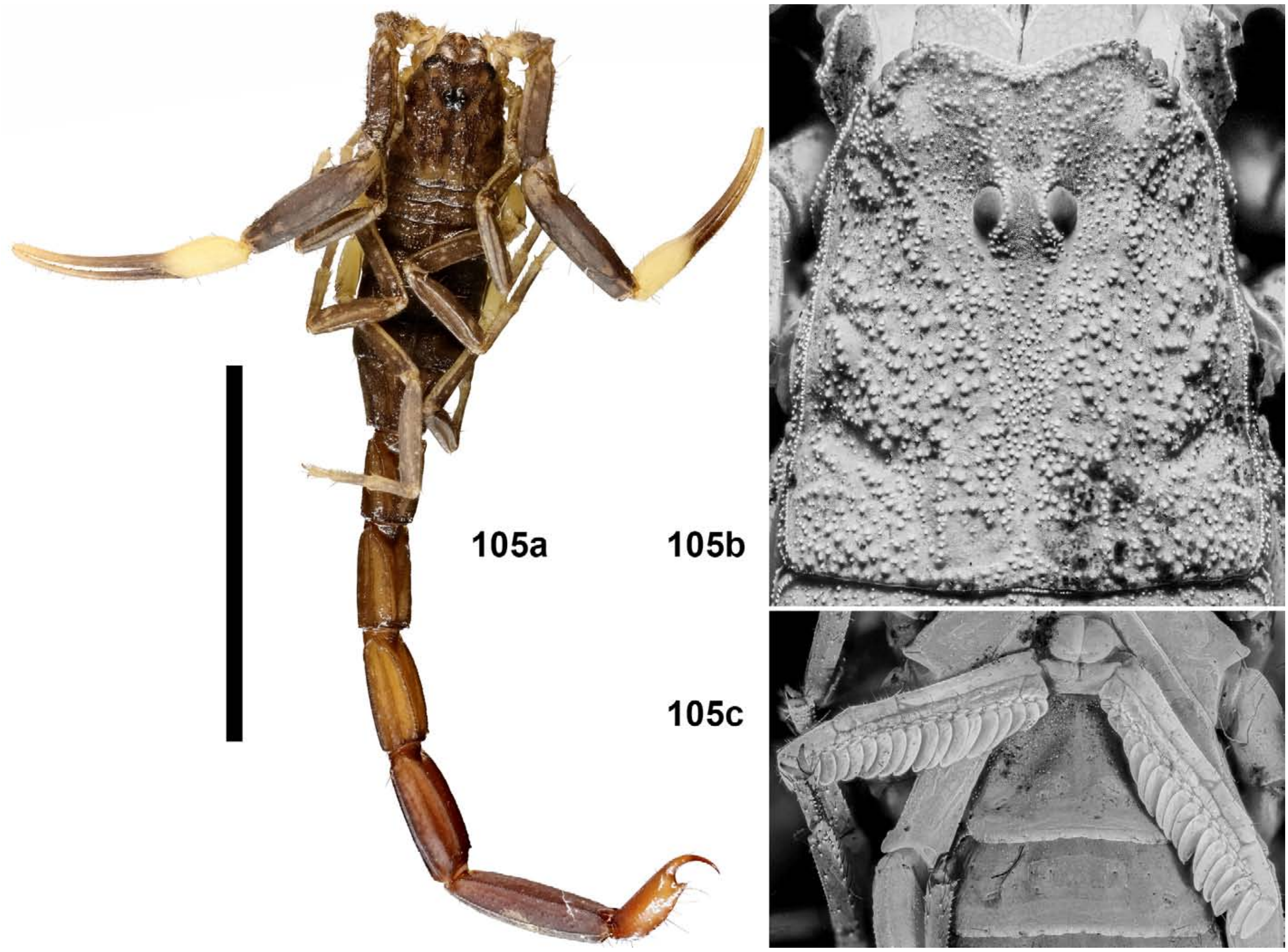

Figures 105a–**c**. *Langxie feti* **gen**. et **sp**. **n**., male paratype no. M14, habitus (105a), carapace (105b) and sternopectinal area (105c). Scale bar = 10 mm (105a).

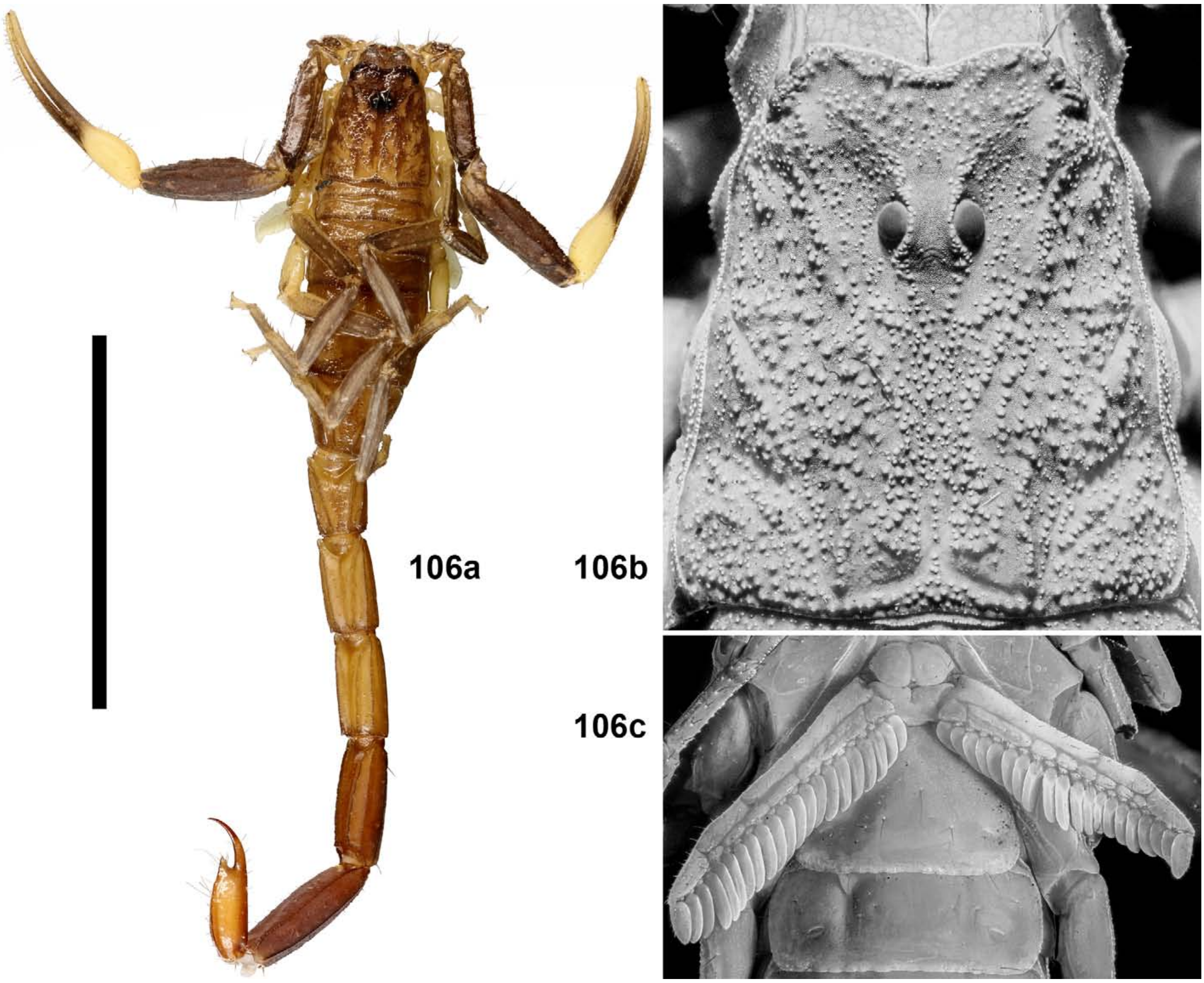

Figures 106a–c. *Langxie feti* **gen**. et **sp**. **n**., male paratype no. M15, habitus (106a), carapace (106b) and sternopectinal area (106c). Scale bar = 10 mm (106a).

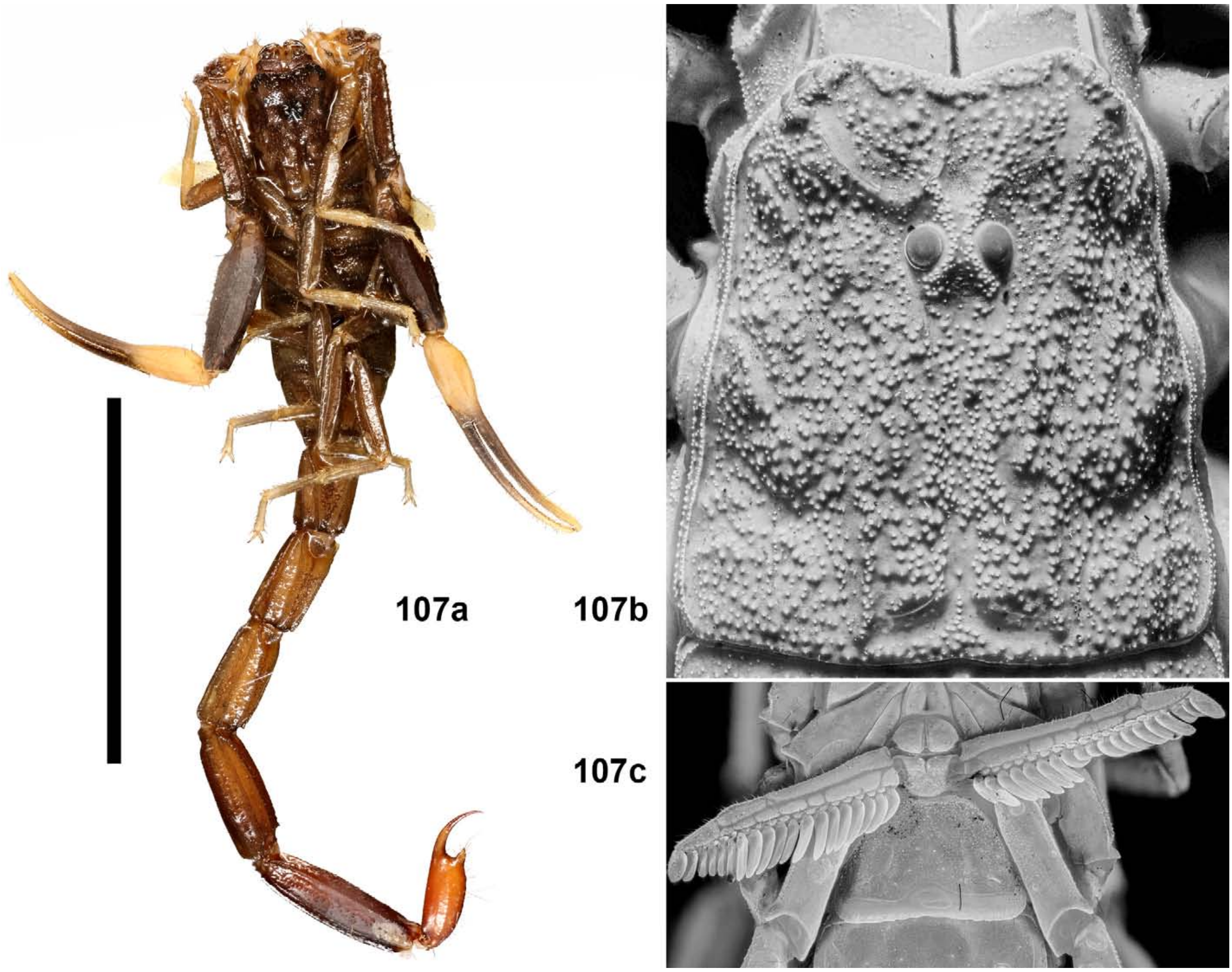

Figures 107a–**c**. *Langxie feti* **gen**. et **sp**. **n**., male paratype no. M16, habitus (107a), carapace (107b) and sternopectinal area (107c). Scale bar = 10 mm (107a).

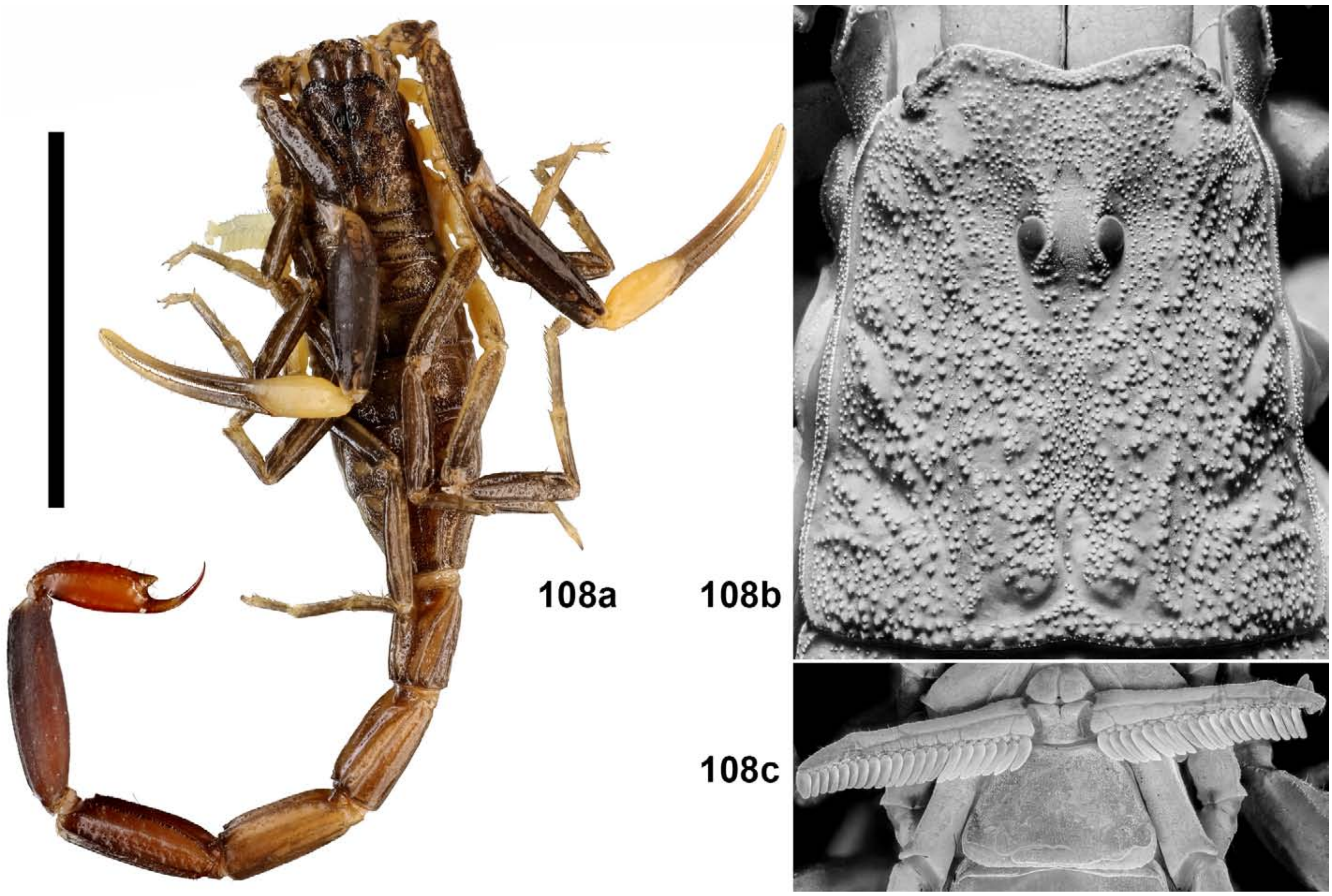

Figures 108a–c. *Langxie feti* **gen**. et **sp**. **n**., male paratype no. M17, habitus (108a), carapace (108b) and sternopectinal area (108c). Scale bar = 10 mm (108a).

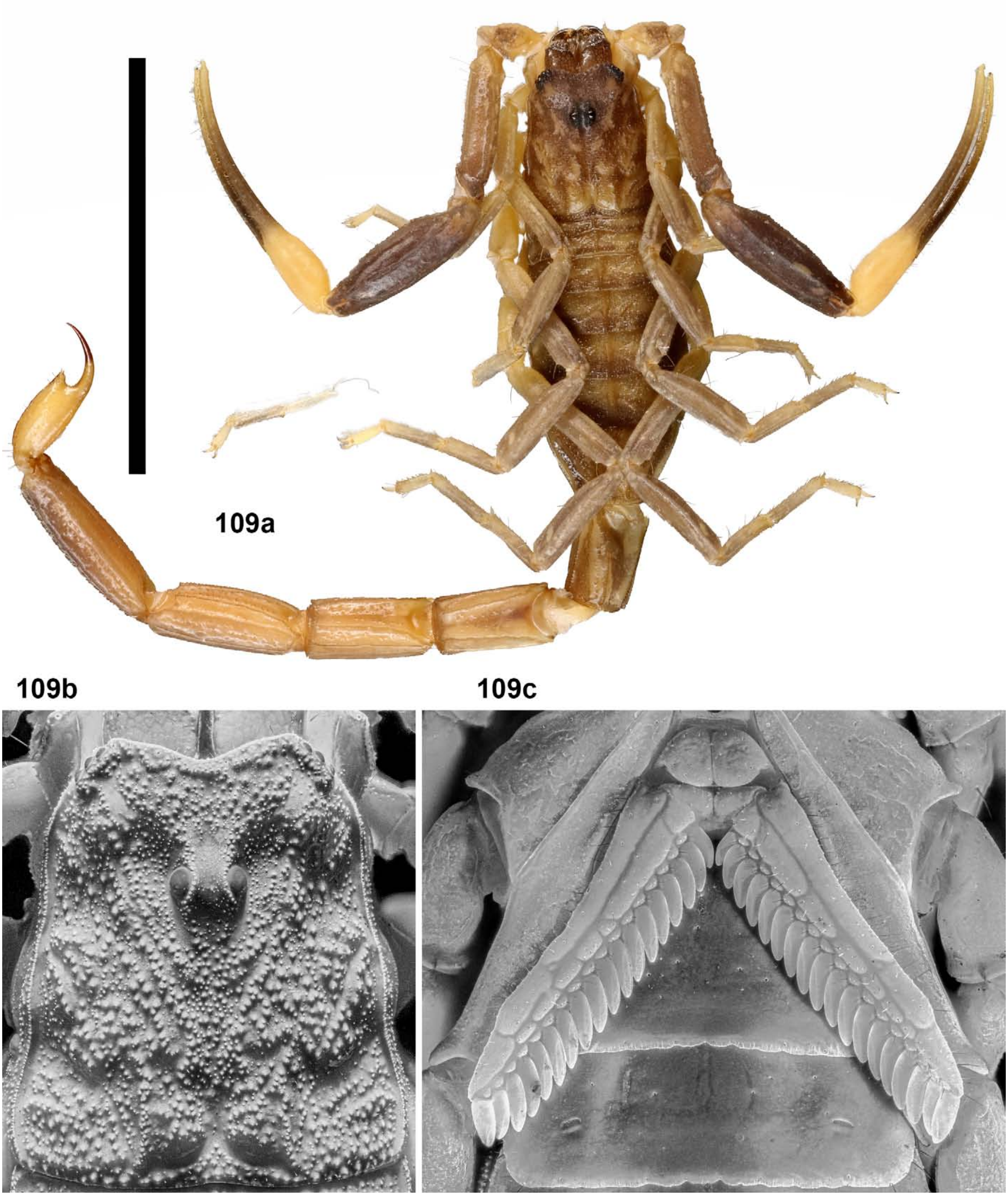

Figures 109a–c. *Langxie feti* **gen**. et **sp**. **n**., female juvenile paratype no. F1, habitus (109a), carapace (109b) and sternopectinal area (109c). Scale bar = 10 mm (109a).

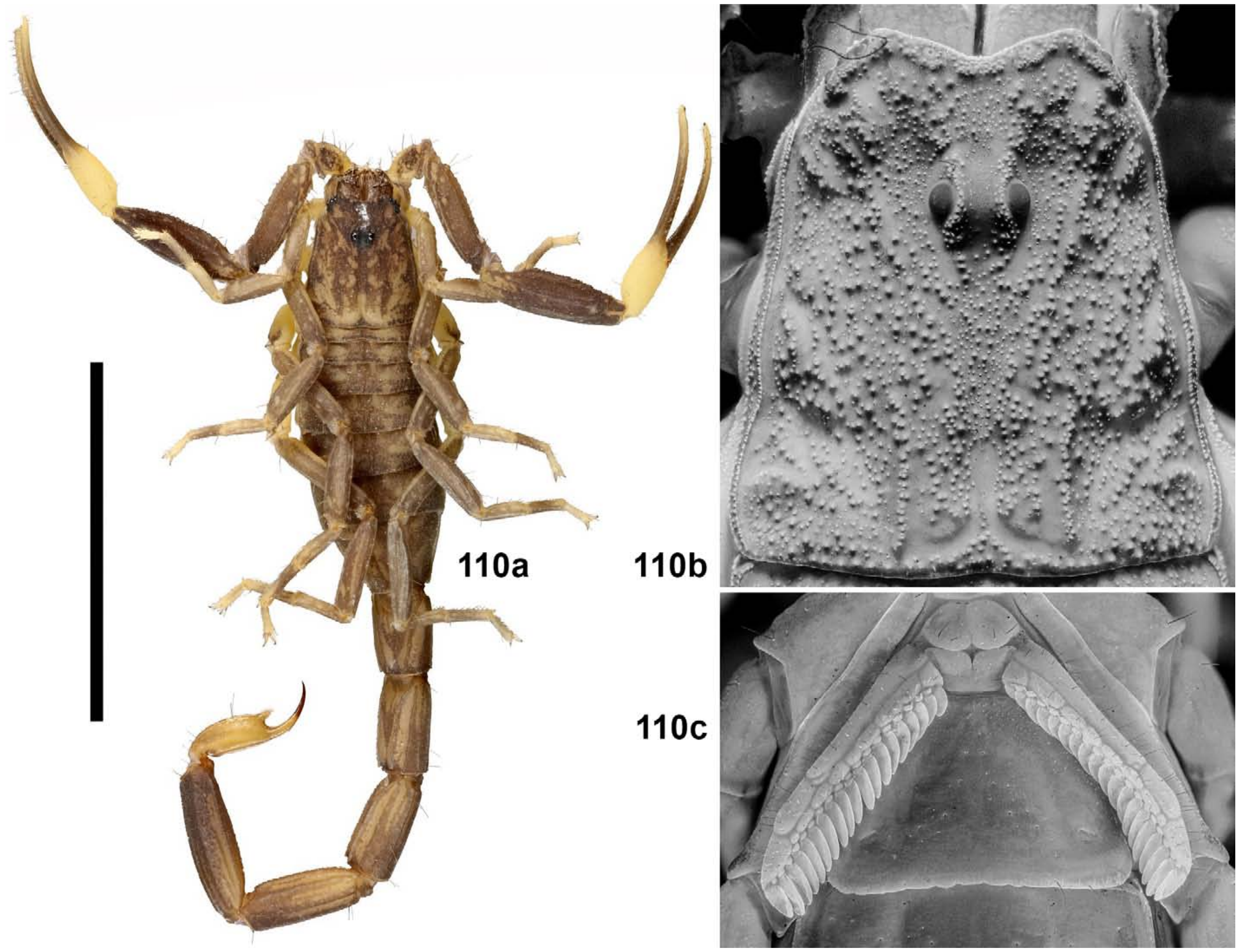

Figures 110a–c. *Langxie feti* **gen**. et **sp**. **n**., female juvenile paratype no. F2, habitus (110a), carapace (110b) and sternopectinal area (110c). Scale bar = 10 mm (110a).

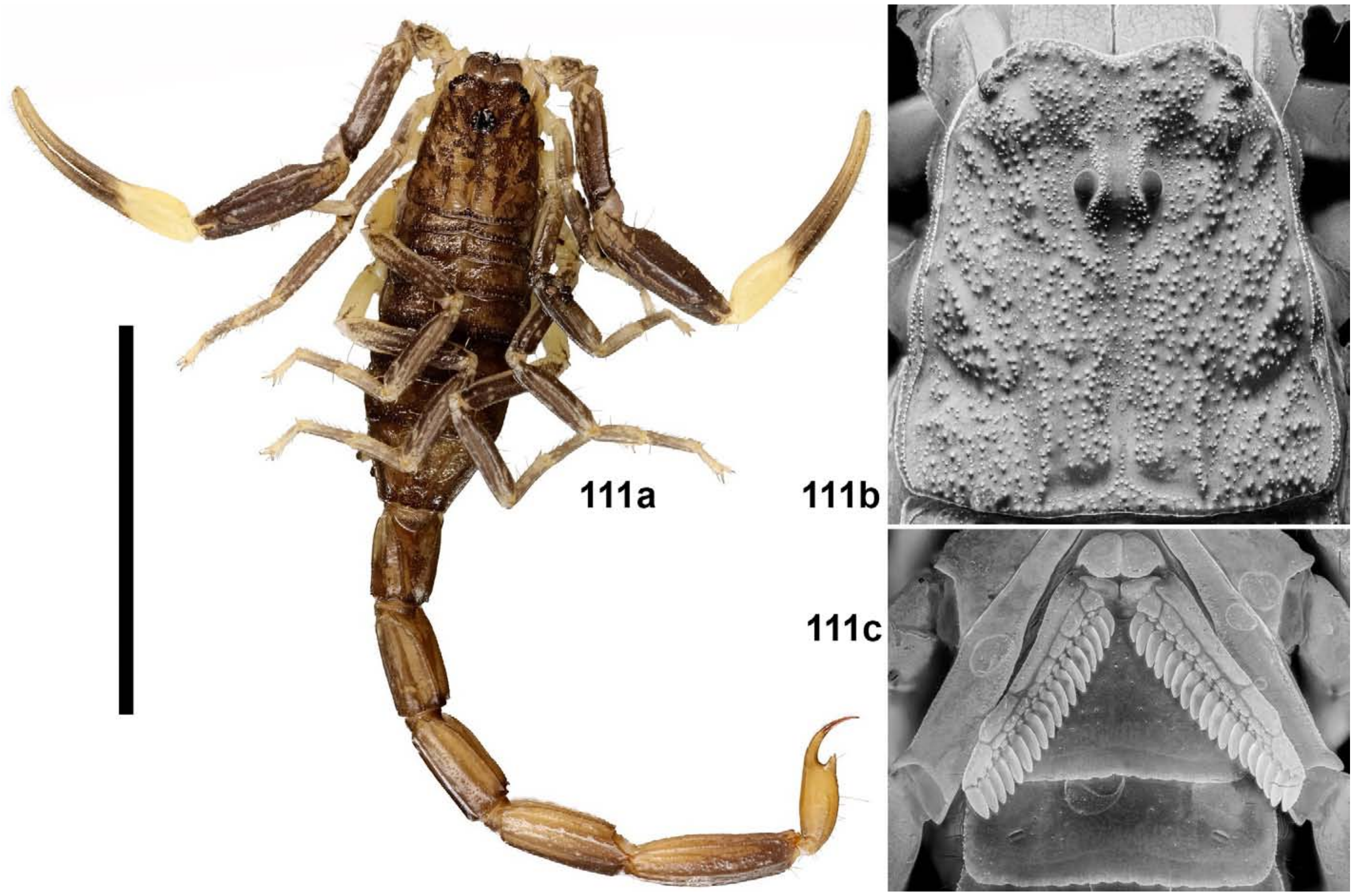

Figures 111a–c. *Langxie feti* **gen**. et **sp**. **n**., female juvenile paratype no. F3, habitus (111a), carapace (111b) and sternopectinal area (111c). Scale bar = 10 mm (111a).

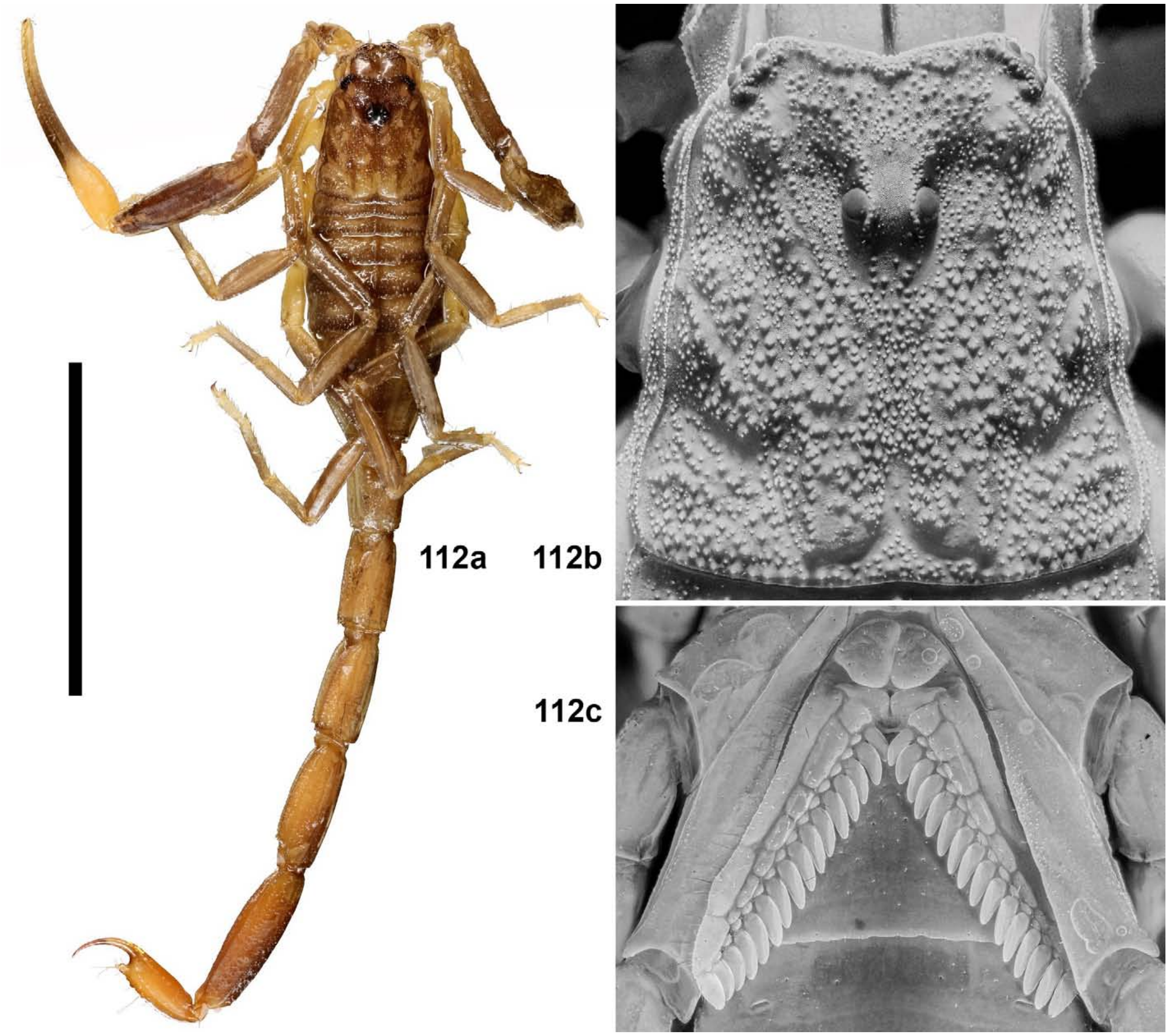

Figures 112a–**c**. *Langxie feti* **gen**. et **sp**. **n**., female juvenile paratype no. F4, habitus (112a), carapace (112b) and sternopectinal area (112c). Scale bar = 10 mm (112a).

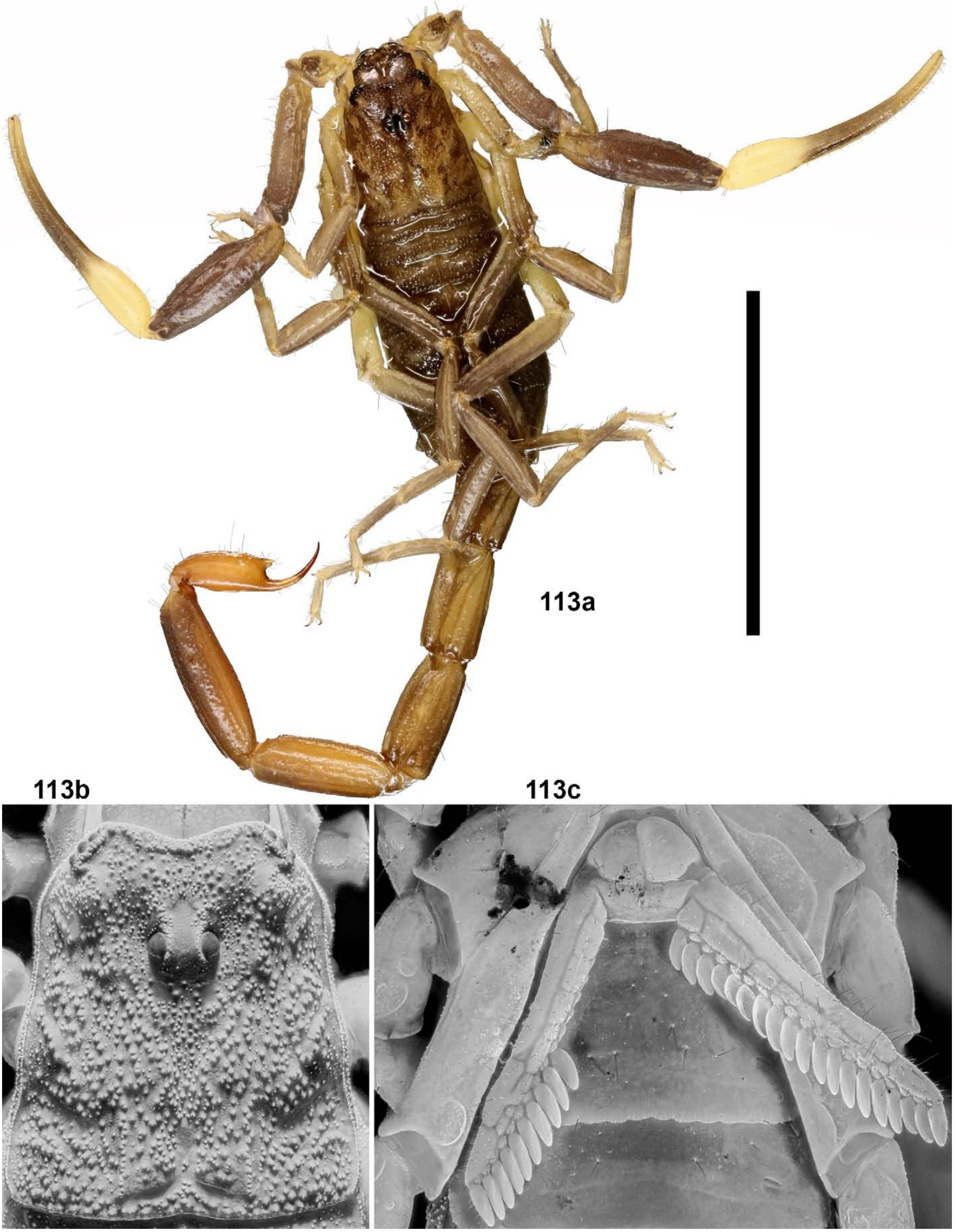

Figures 113a–c. *Langxie feti* **gen**. et **sp**. **n**., female paratype no. F5, habitus (113a), carapace (113b) and sternopectinal area (113c). Scale bar = 10 mm (113a).

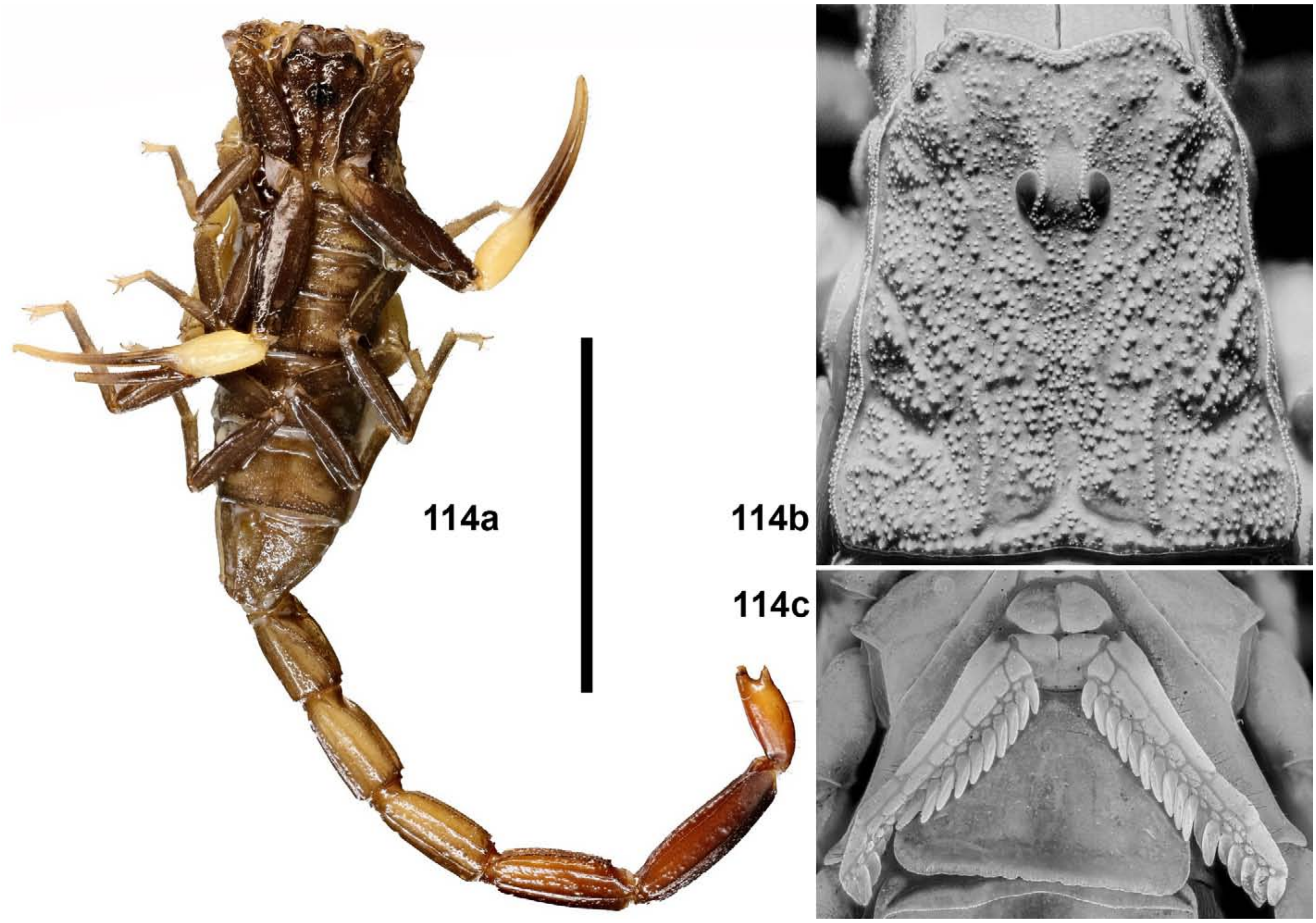

Figures 114a–**c**. *Langxie feti* **gen**. et **sp**. **n**., female paratype no. F6, habitus (114a), carapace (114b) and sternopectinal area (114c). Scale bar = 10 mm (114a).

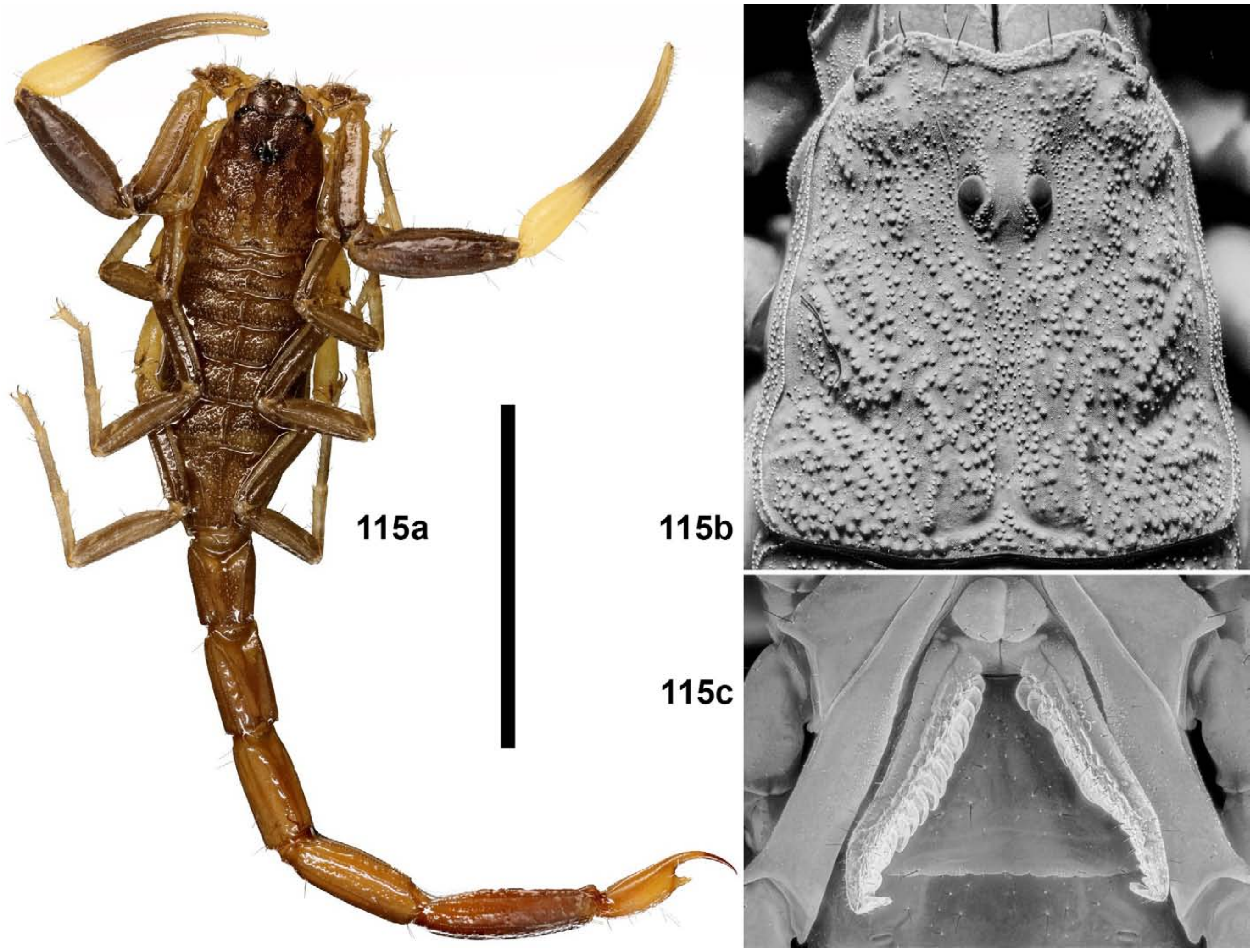

Figures 115a–**c**. *Langxie feti* **gen**. et **sp**. **n**., female paratype no. F7, habitus (115a), carapace (115b) and sternopectinal area (115c). Scale bar = 10 mm (115a).

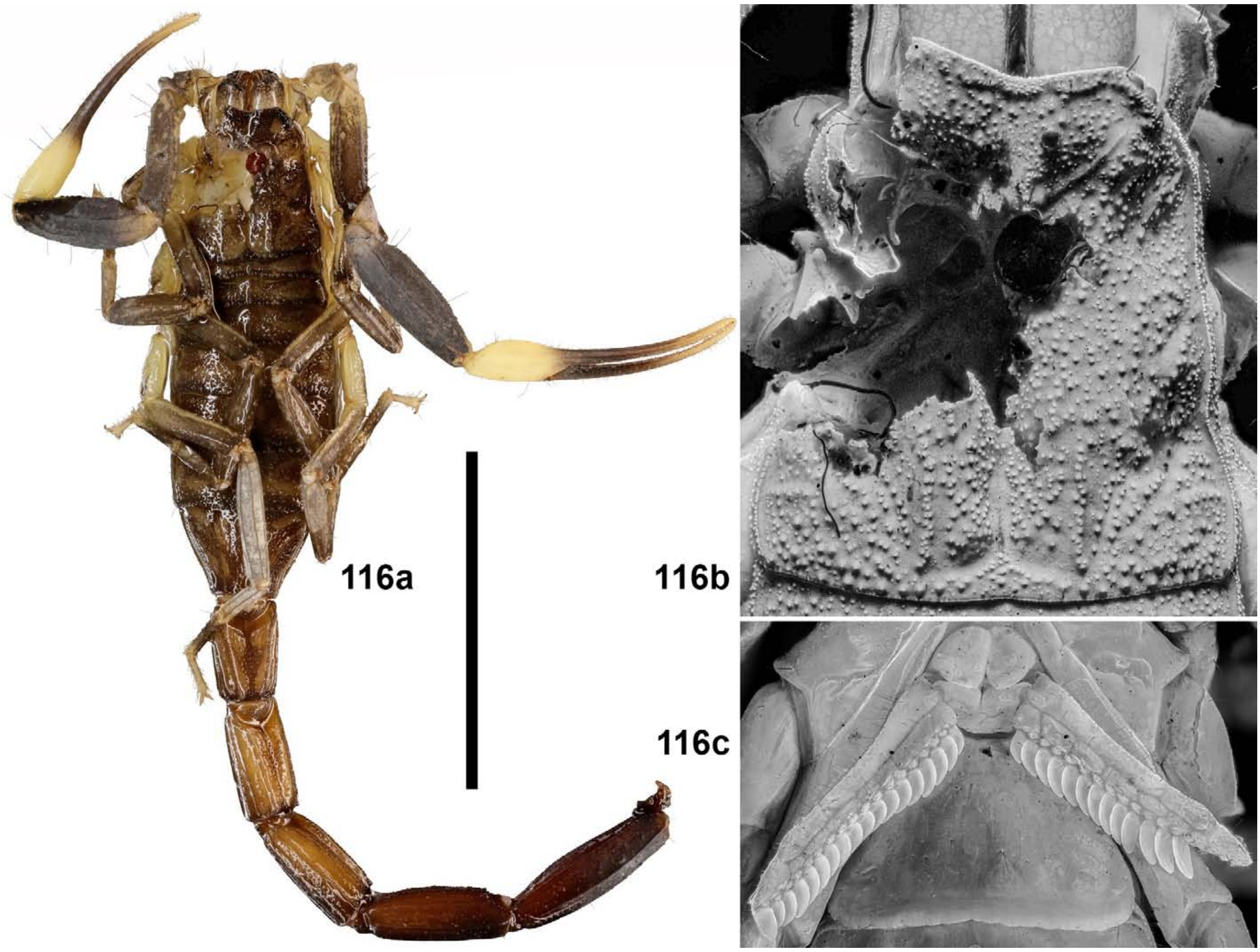

Figures 116a–**c**. *Langxie feti* **gen**. et **sp**. **n**., female paratype no. F8, habitus (116a), carapace (116b) and sternopectinal area (116c). Scale bar = 10 mm (116a).

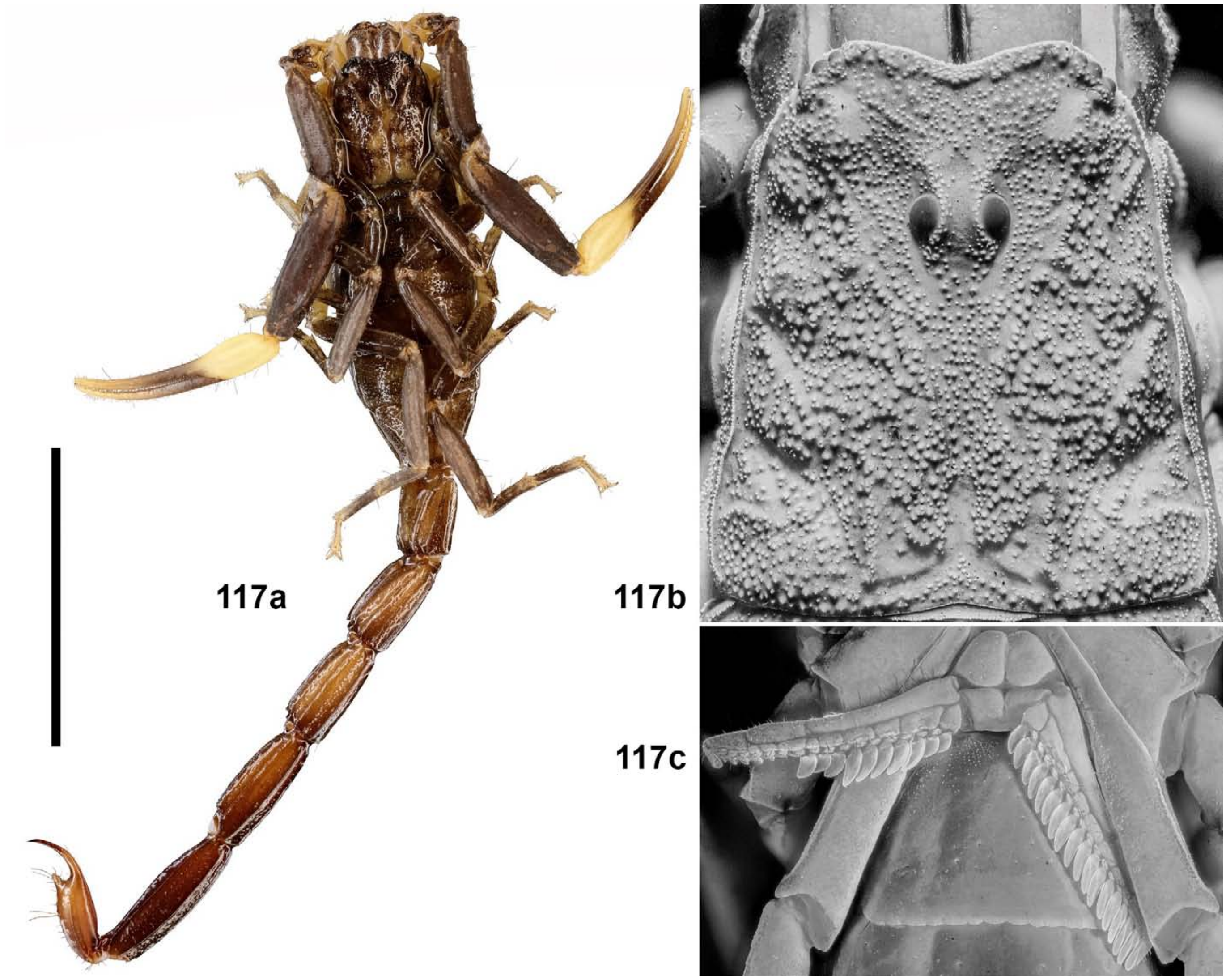

Figures 117a–**c**. *Langxie feti* **gen**. et **sp**. **n**., female paratype no. F9, habitus (117a), carapace (117b) and sternopectinal area (117c). Scale bar = 10 mm (117a).

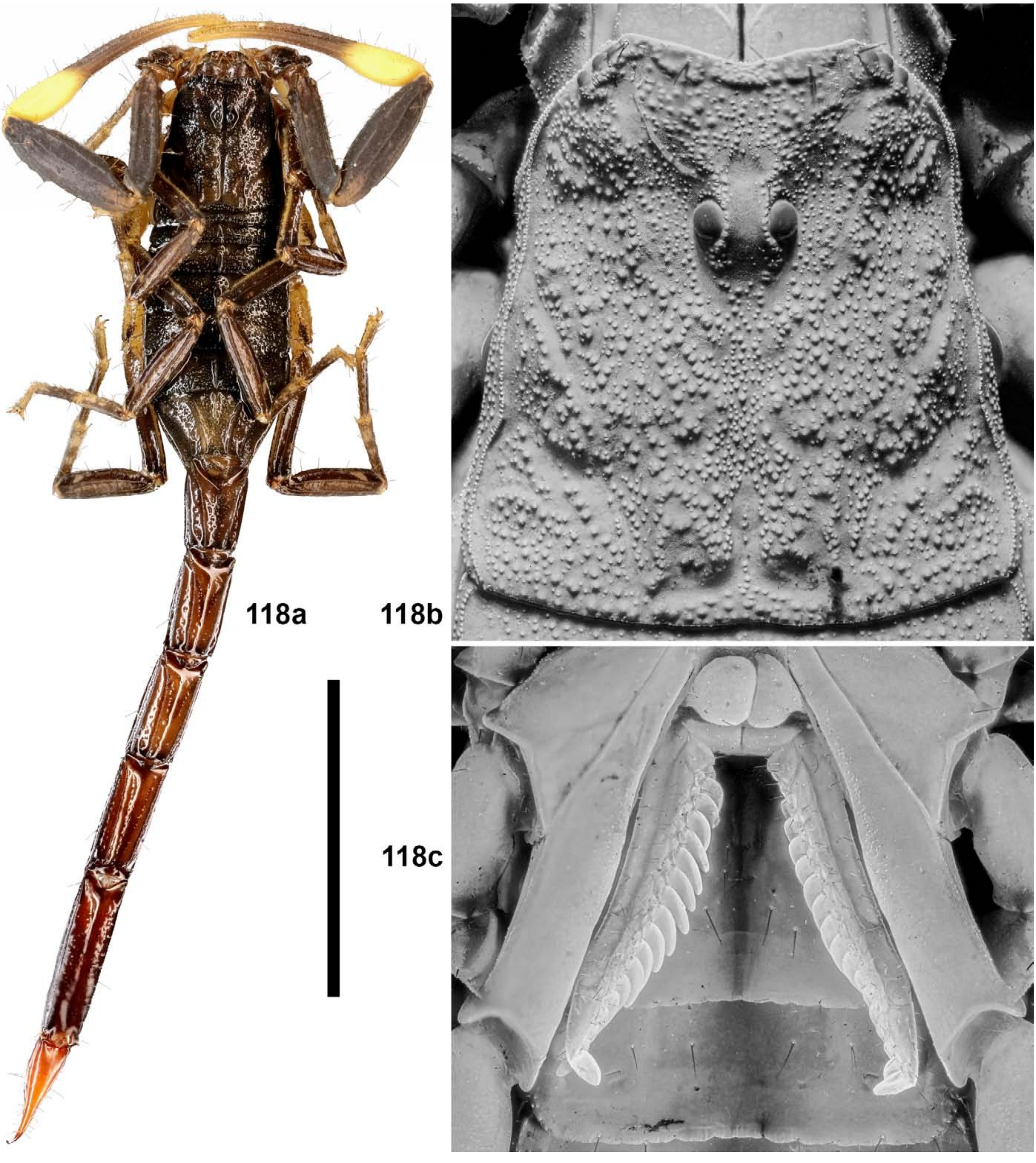

Figures 118a–c. *Langxie feti* **gen**. et **sp**. **n**., female paratype no. F10, habitus (118a), carapace (118b) and sternopectinal area (118c). Scale bar = 10 mm (118a).

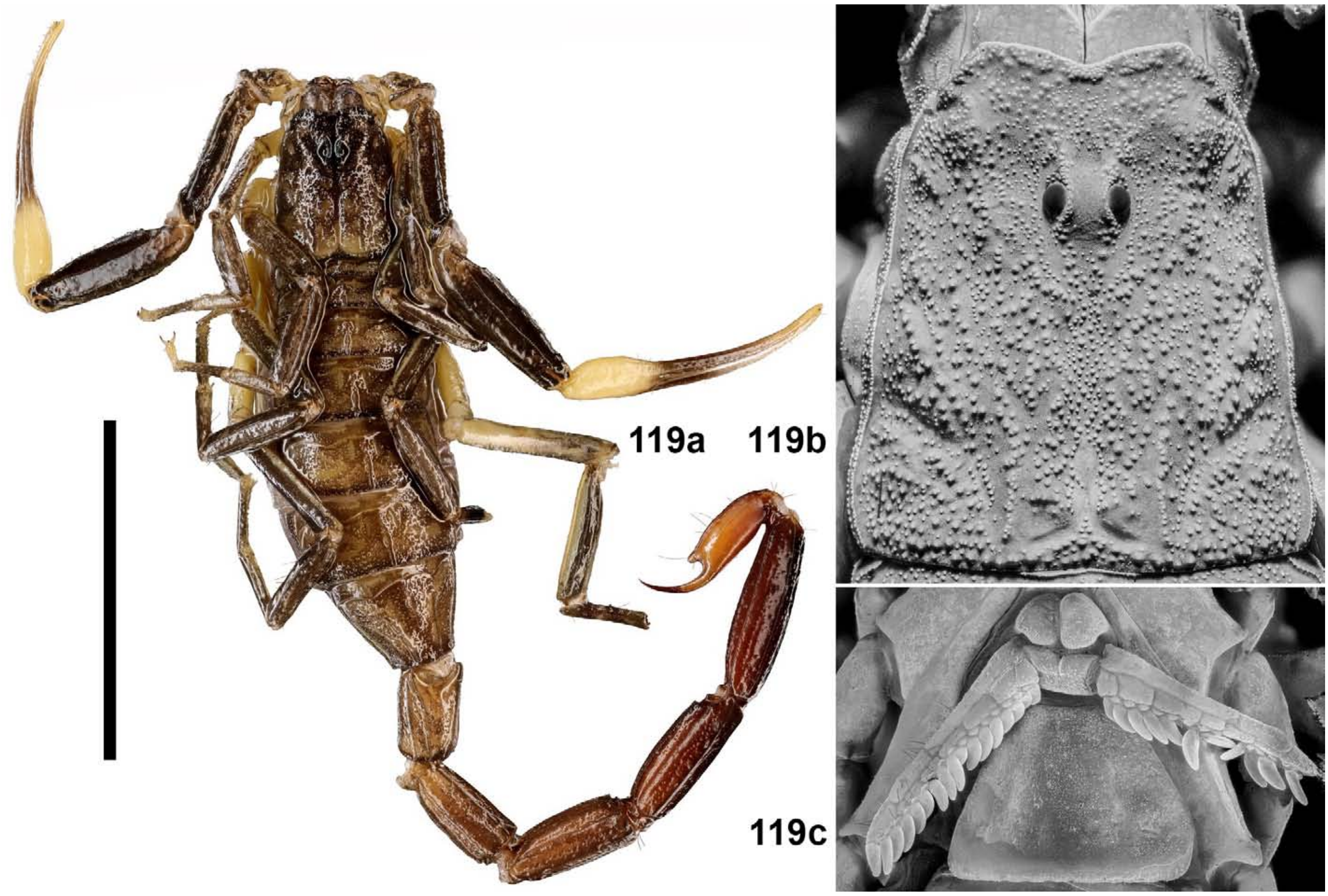

Figures 119a–**c**. *Langxie feti* **gen**. et **sp**. **n**., female paratype no. F11, habitus (119a), carapace (119b) and sternopectinal area (119c). Scale bar = 10 mm (119a).

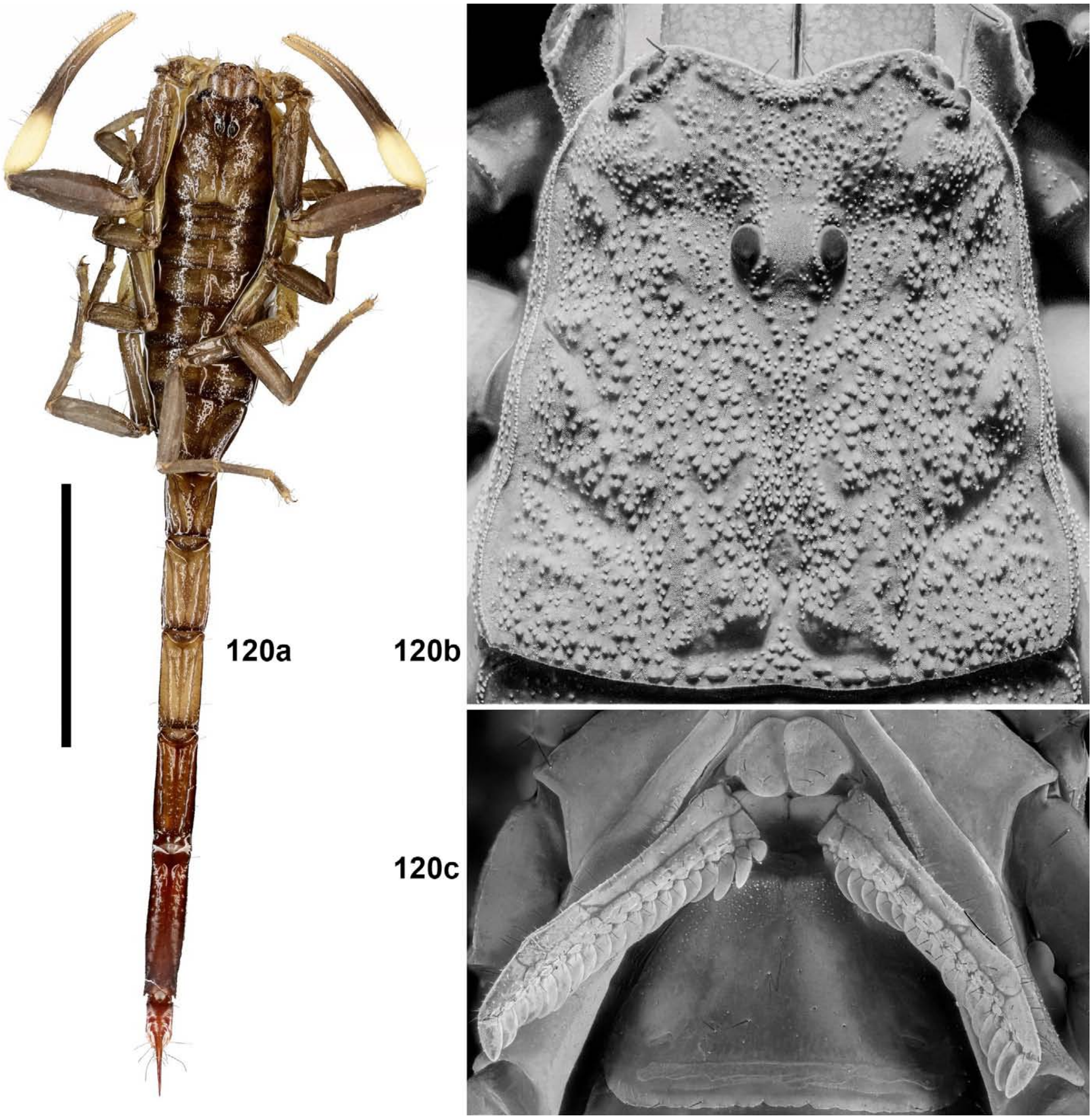

Figures 120a–**c**. *Langxie feti* **gen**. et **sp**. **n**., female paratype no. F12, habitus (120a), carapace (120b) and sternopectinal area (120c). Scale bar = 10 mm (120a).

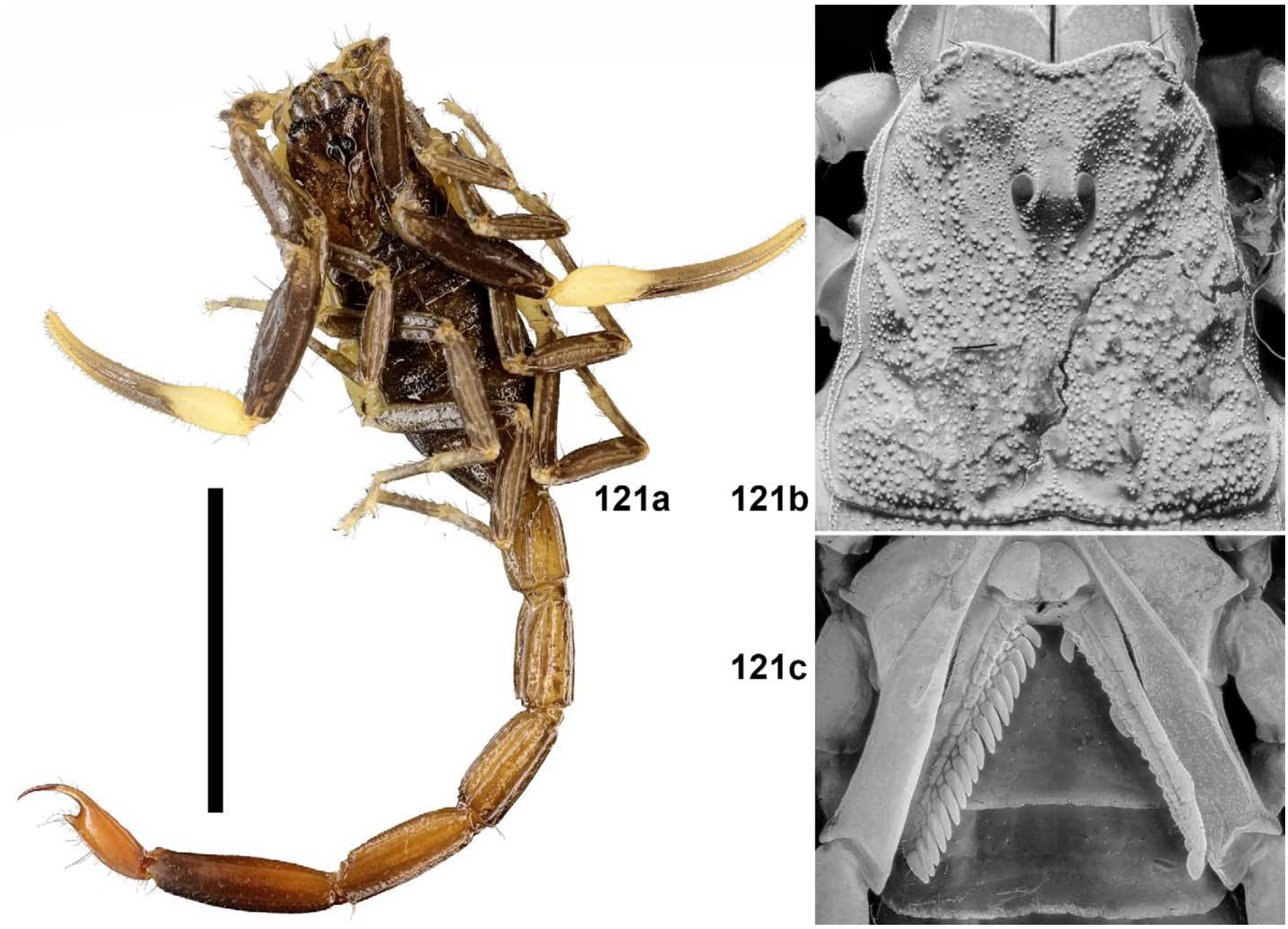

Figures 121a–**c**. *Langxie feti* **gen**. et **sp**. **n**., female paratype no. F13, habitus (121a), carapace (121b) and sternopectinal area (121c). Scale bar = 10 mm (121a).

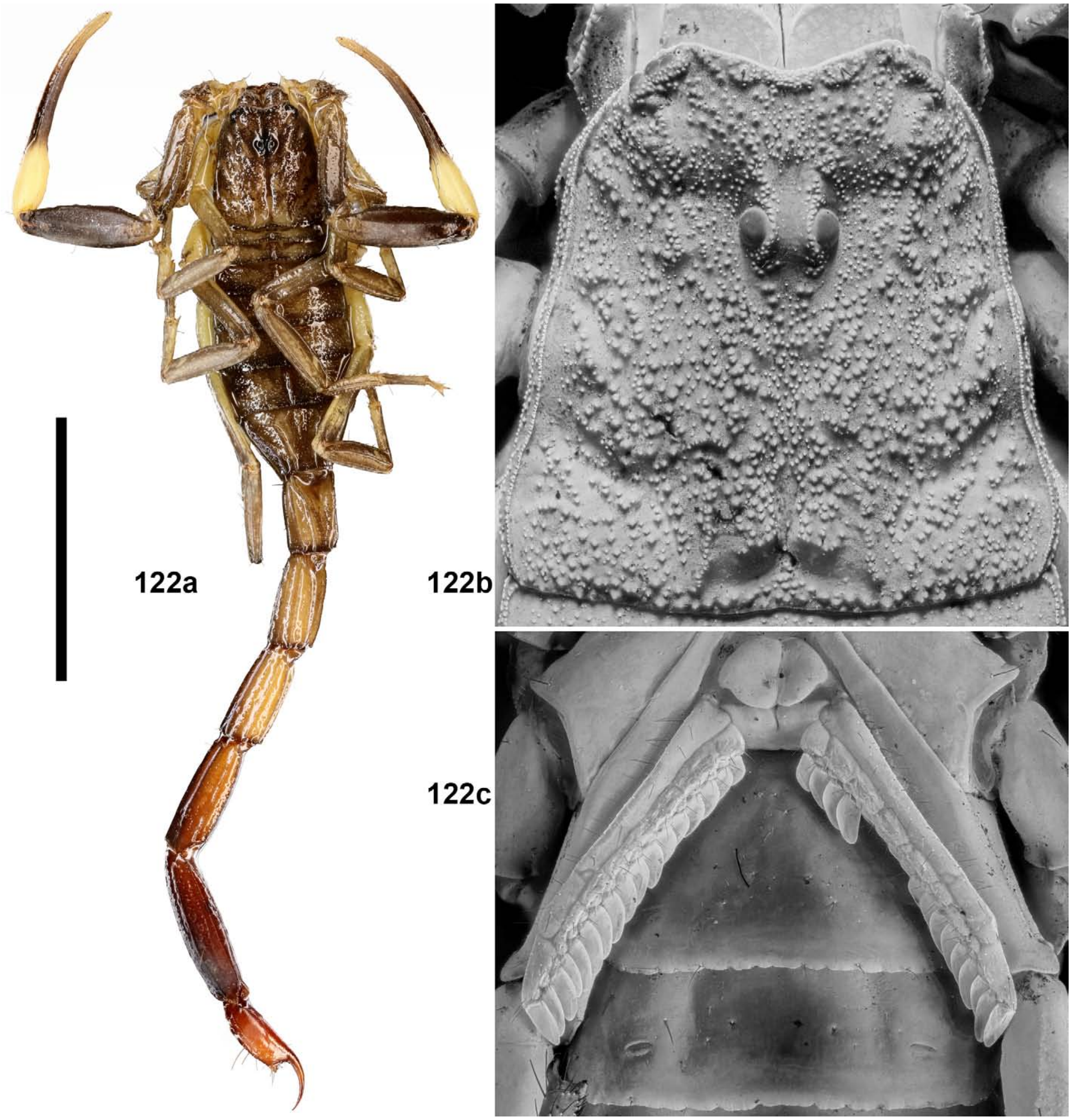

Figures 122a–**c**. *Langxie feti* **gen**. et **sp**. **n**., female paratype no. F14, habitus (122a), carapace (122b) and sternopectinal area (122c). Scale bar = 10 mm (122a).

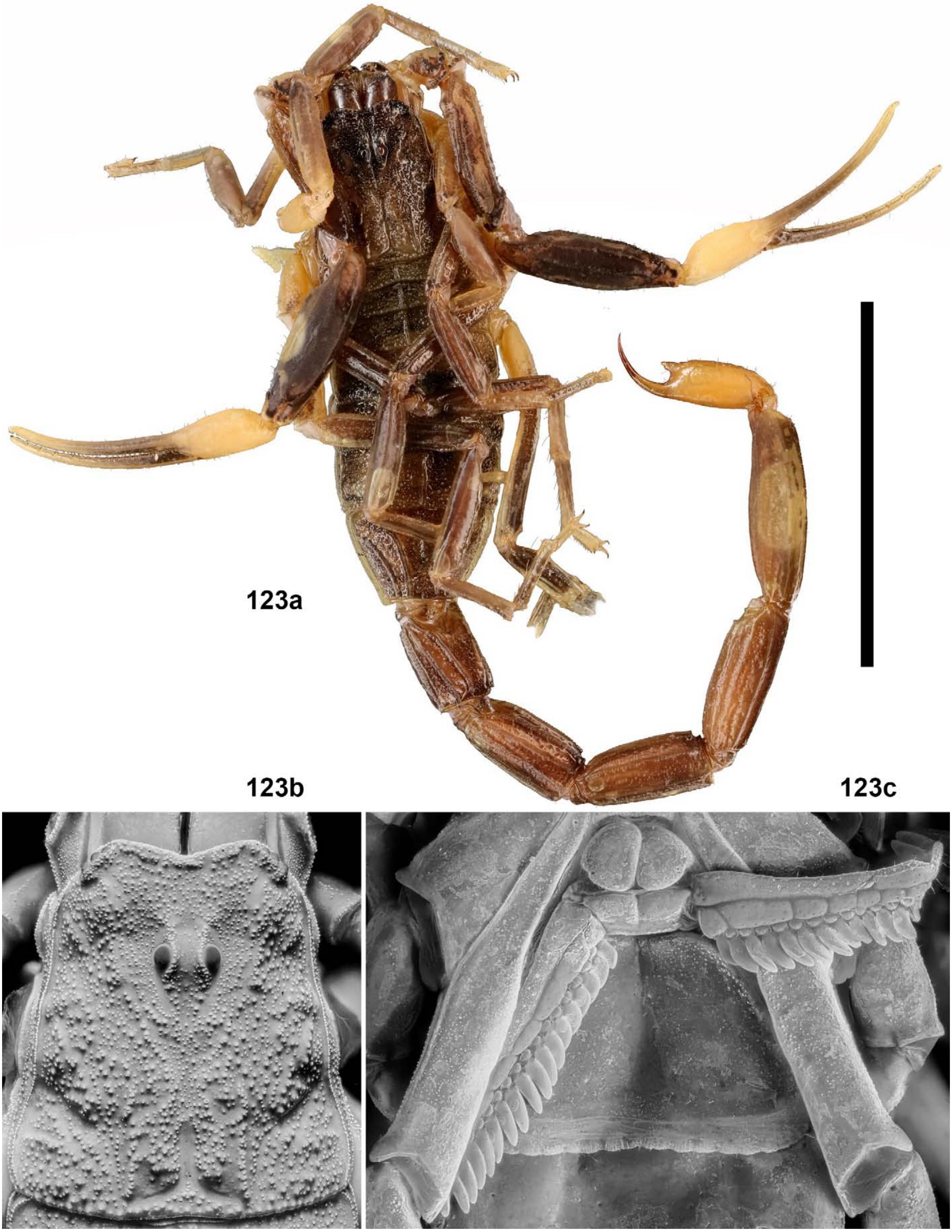

Figures 123a–**c**. *Langxie feti* **gen**. et **sp**. **n**., female paratype no. F15, habitus (123a), carapace (123b) and sternopectinal area (123c). Scale bar = 10 mm (123a).

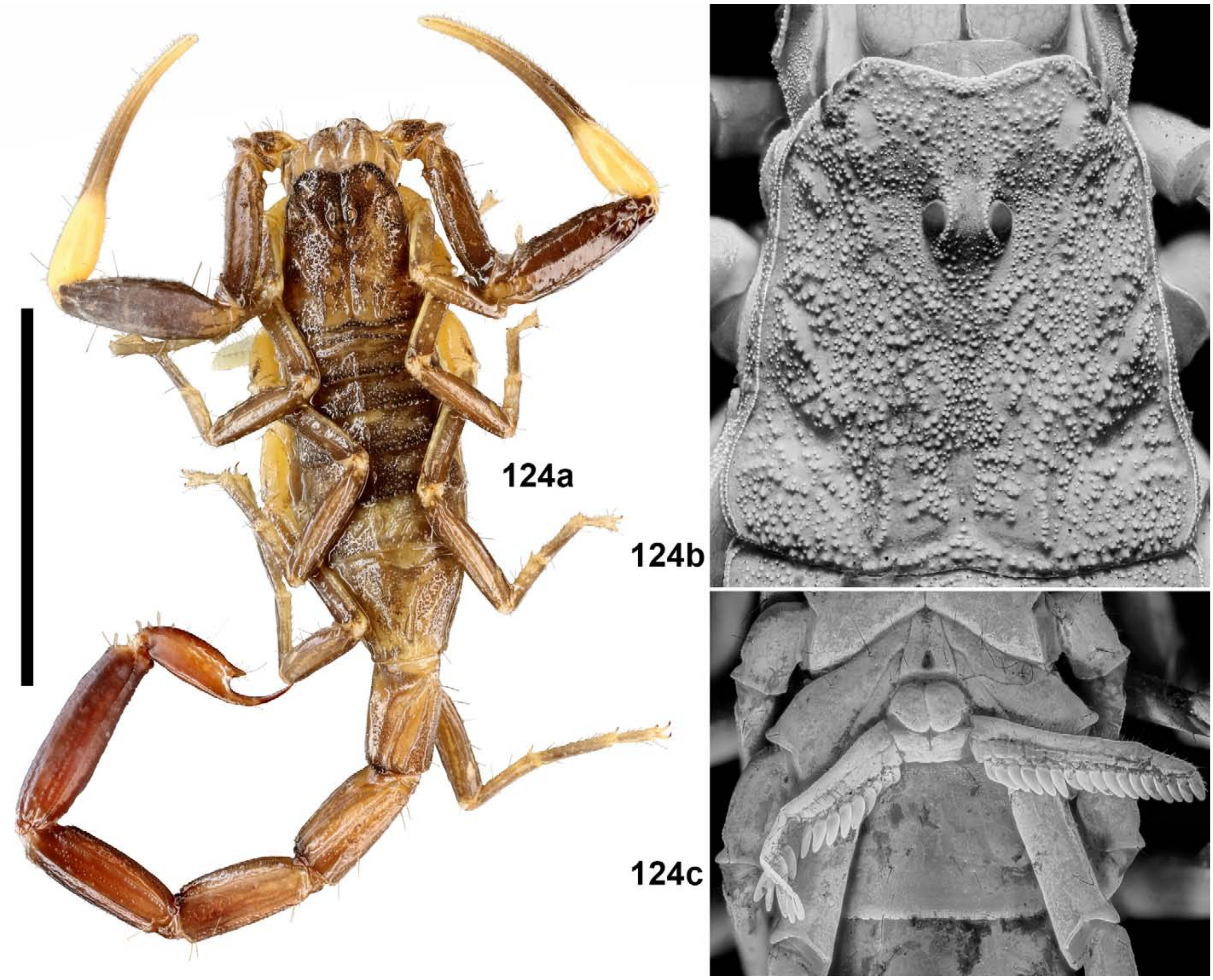

Figures 124a–**c**. *Langxie feti* **gen**. et **sp**. **n**., female paratype no. F16, habitus (124a), carapace (124b) and sternopectinal area (124c). Scale bar = 10 mm (124a).

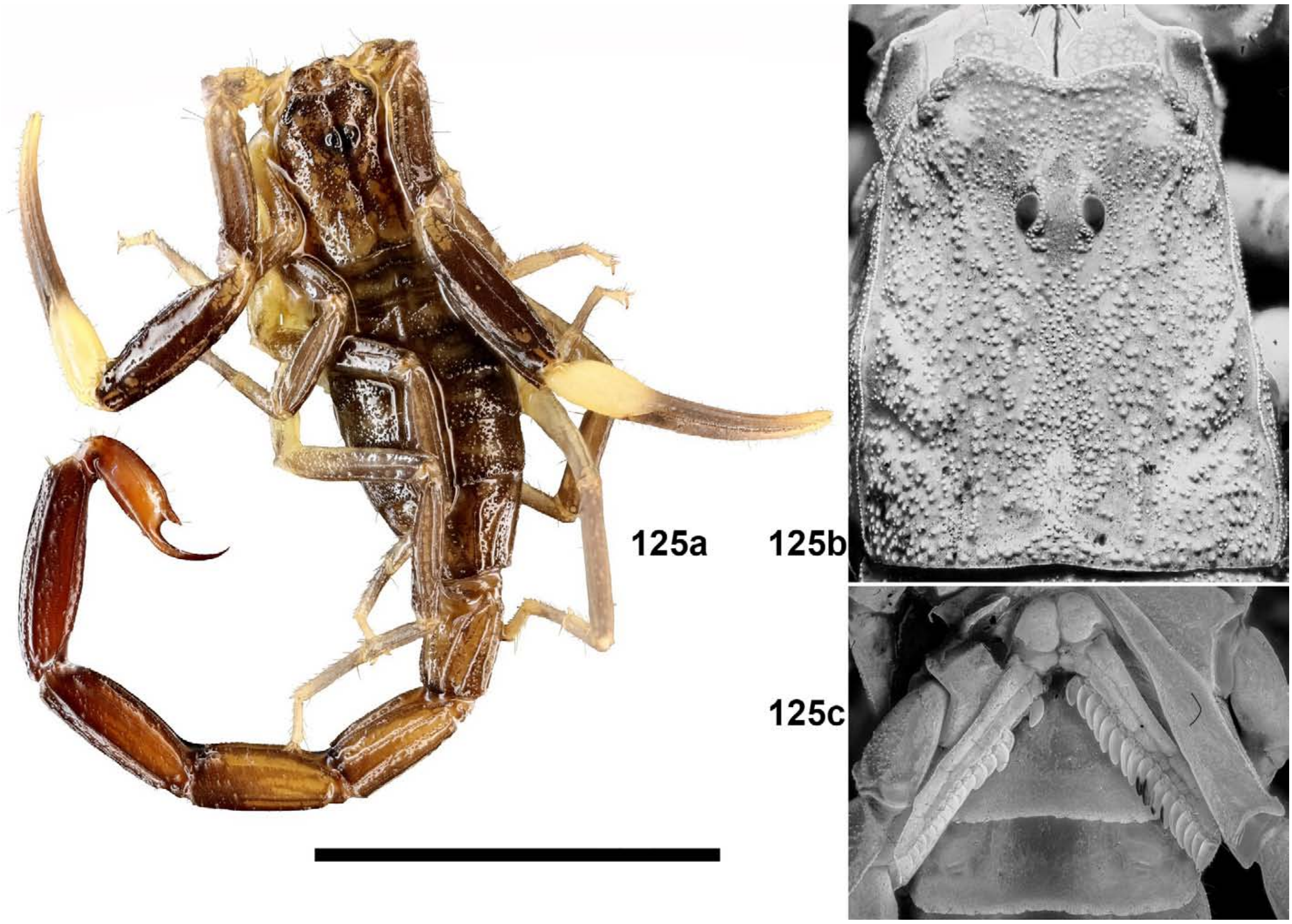

Figures 125a–**c**. *Langxie feti* **gen**. et **sp**. **n**., female paratype no. F17, habitus (125a), carapace (125b) and sternopectinal area (125c). Scale bar = 10 mm (125a).

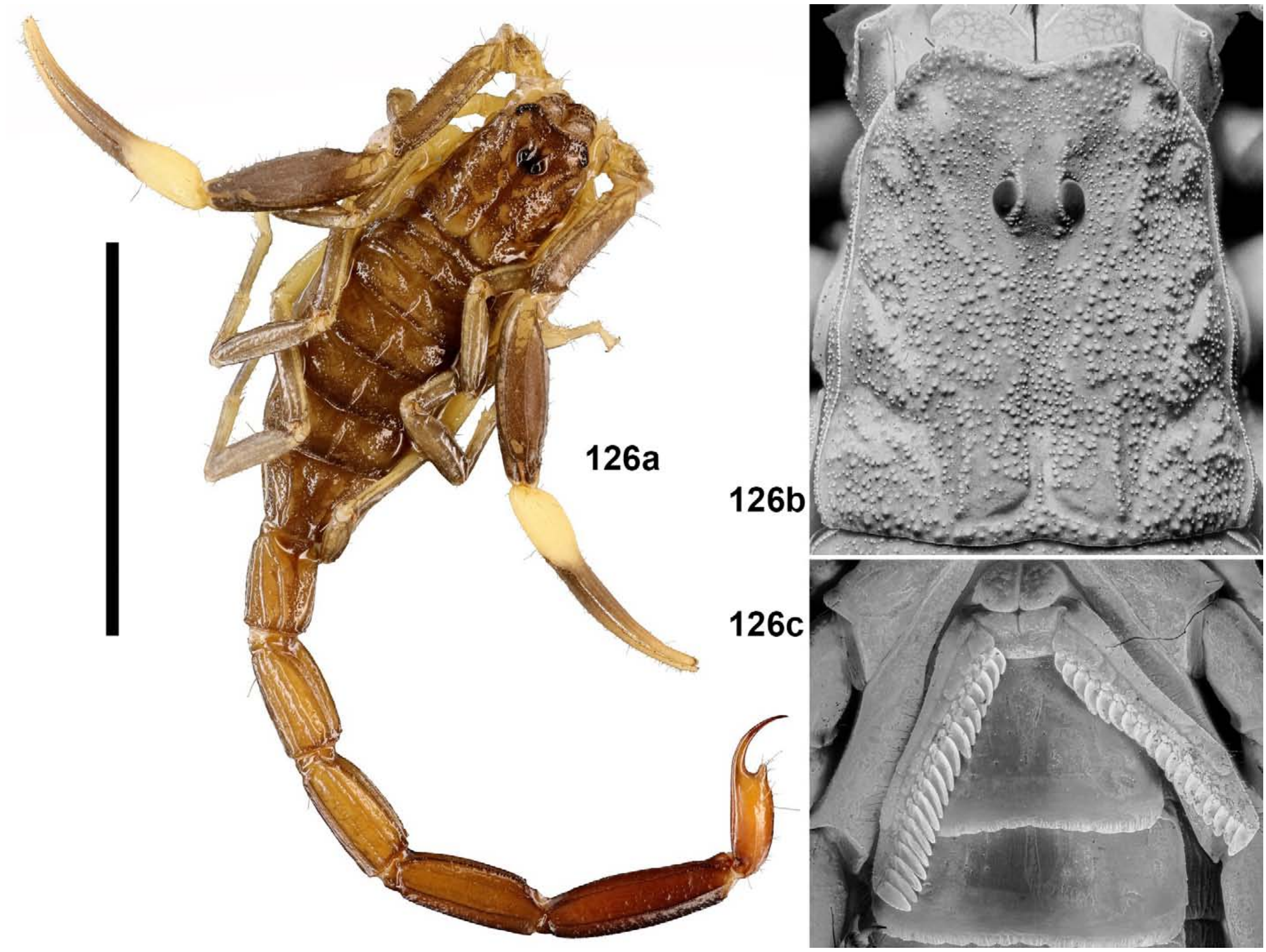

Figures 126a–**c**. *Langxie feti* **gen**. et **sp**. **n**., female paratype no. F18, habitus (126a), carapace (126b) and sternopectinal area (126c). Scale bar = 10 mm (126a).

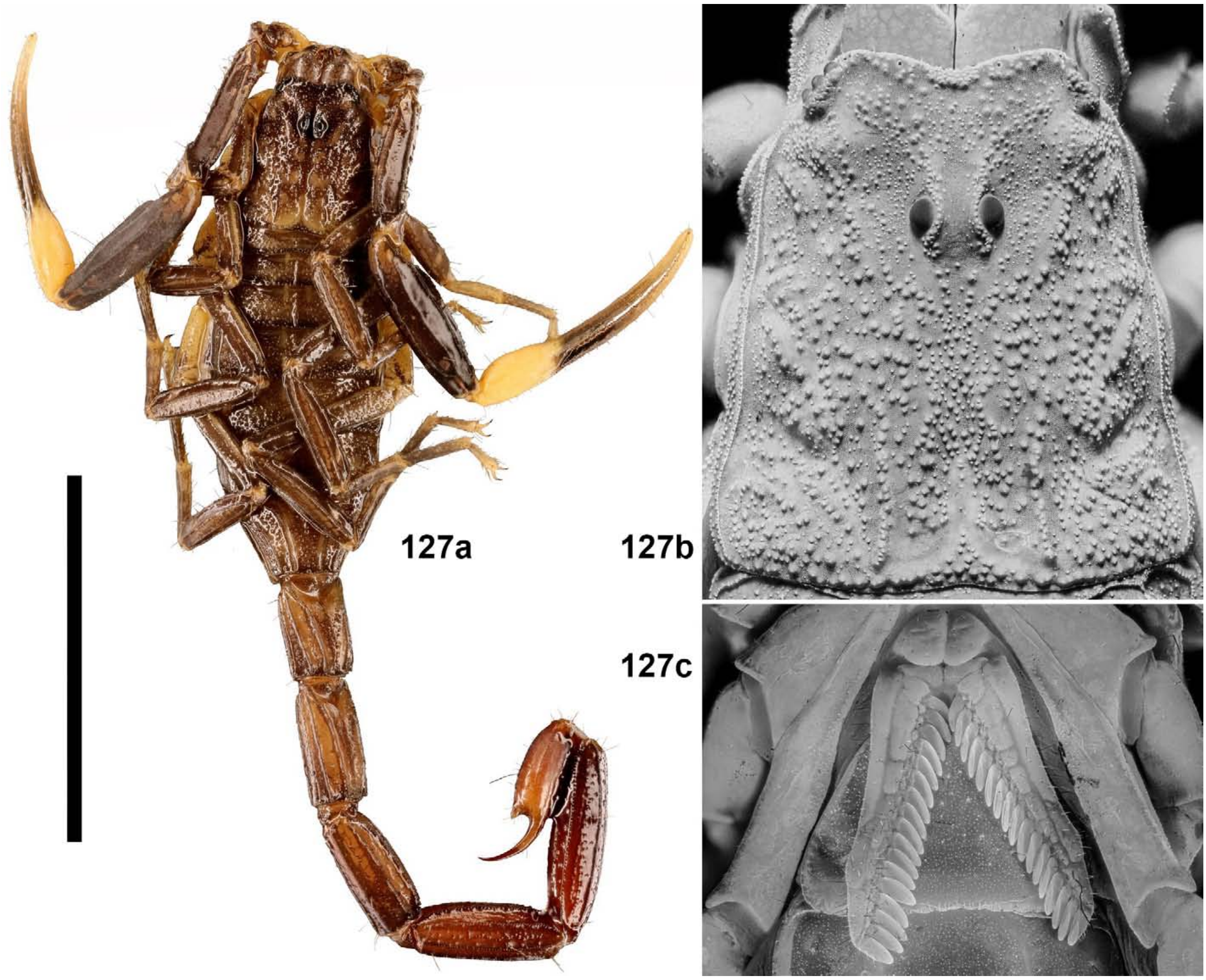

Figures 127a–**c**. *Langxie feti* **gen**. et **sp**. **n**., female paratype no. F19, habitus (127a), carapace (127b) and sternopectinal area (127c). Scale bar = 10 mm (127a).

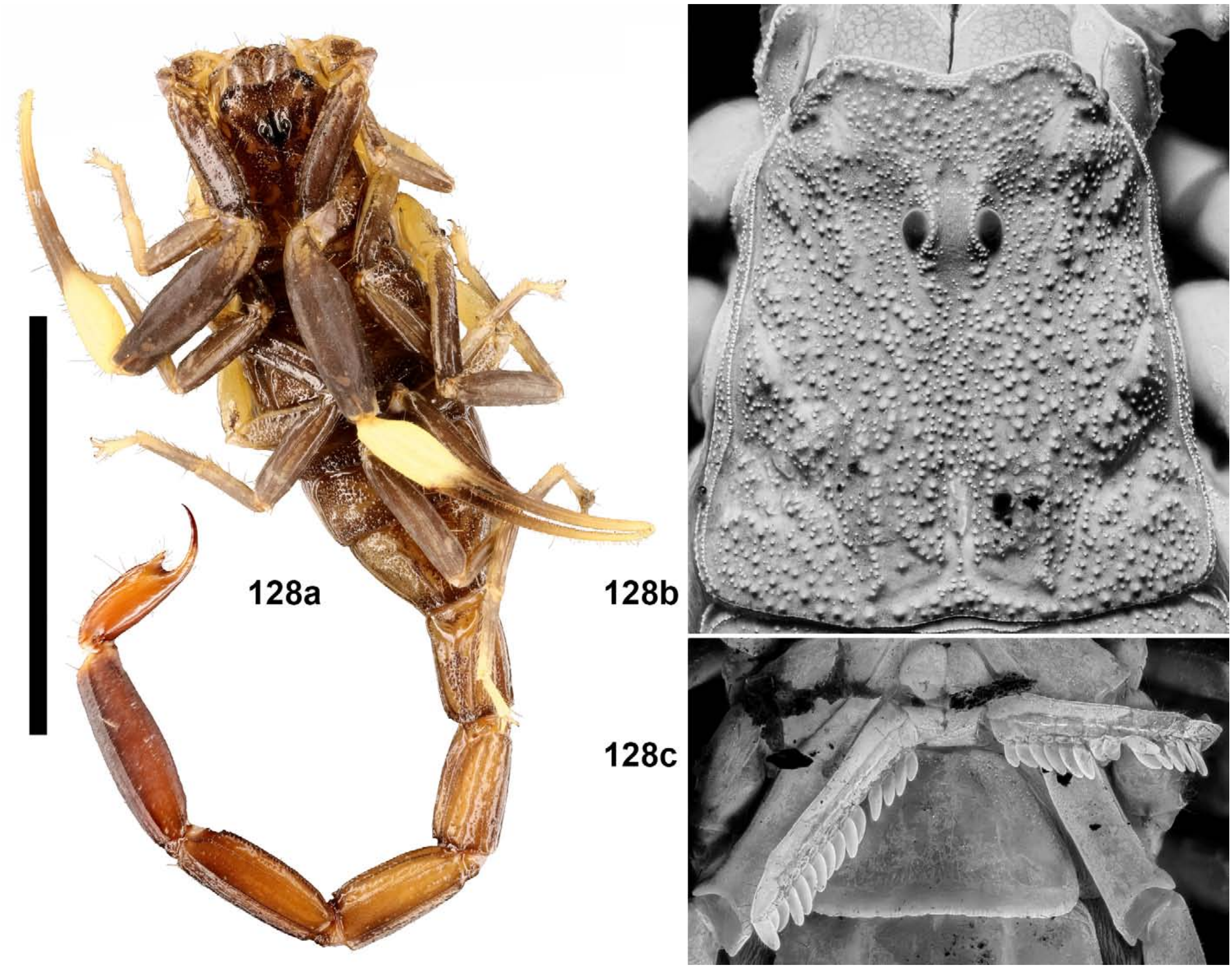

Figures 128a–**c**. *Langxie feti* **gen**. et **sp**. **n**., female paratype no. F20, habitus (128a), carapace (128b) and sternopectinal area (128c). Scale bar = 10 mm (128a).

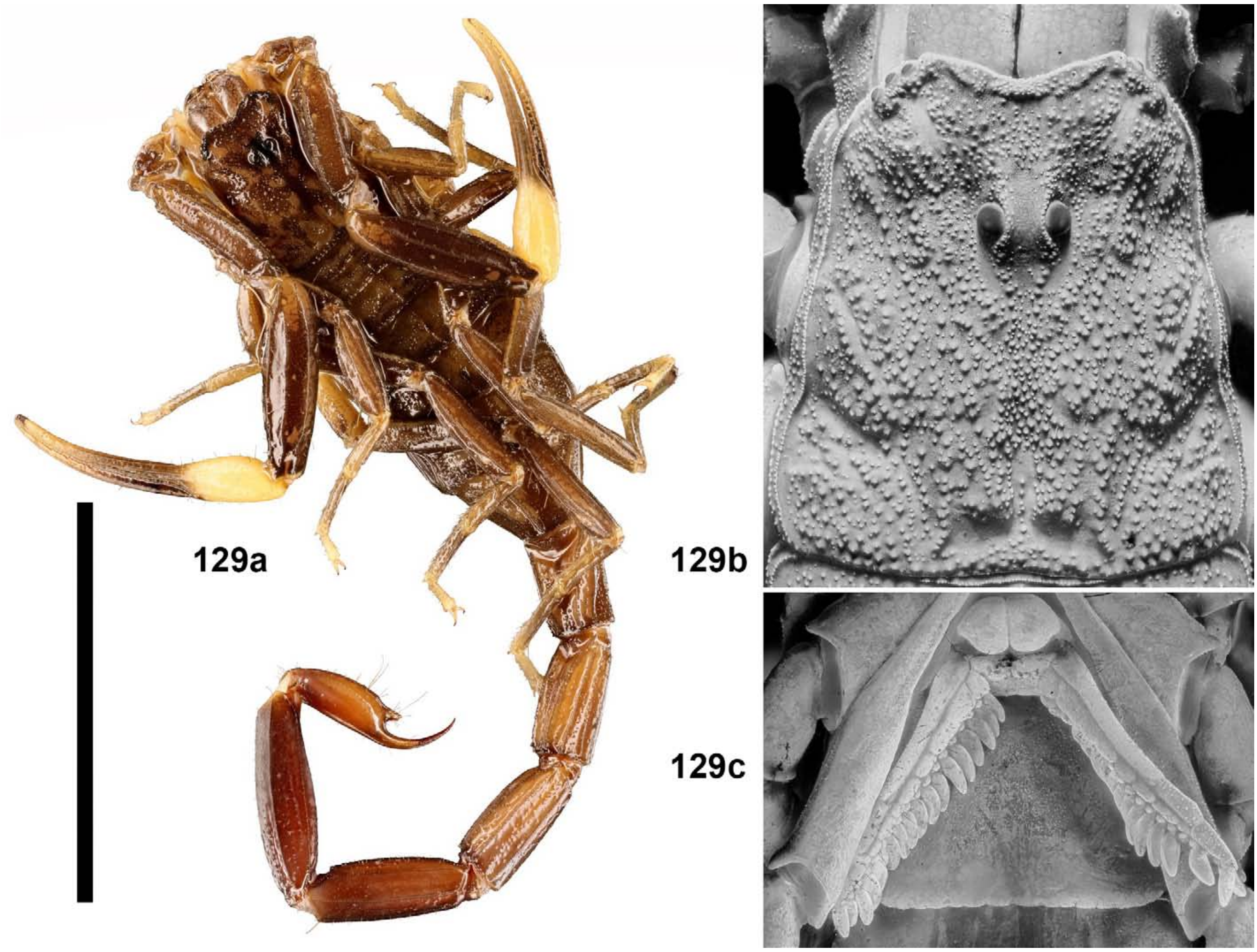

Figures 129a–**c**. *Langxie feti* **gen**. et **sp**. **n**., female paratype no. F21, habitus (129a), carapace (129b) and sternopectinal area (129c). Scale bar = 10 mm (129a).

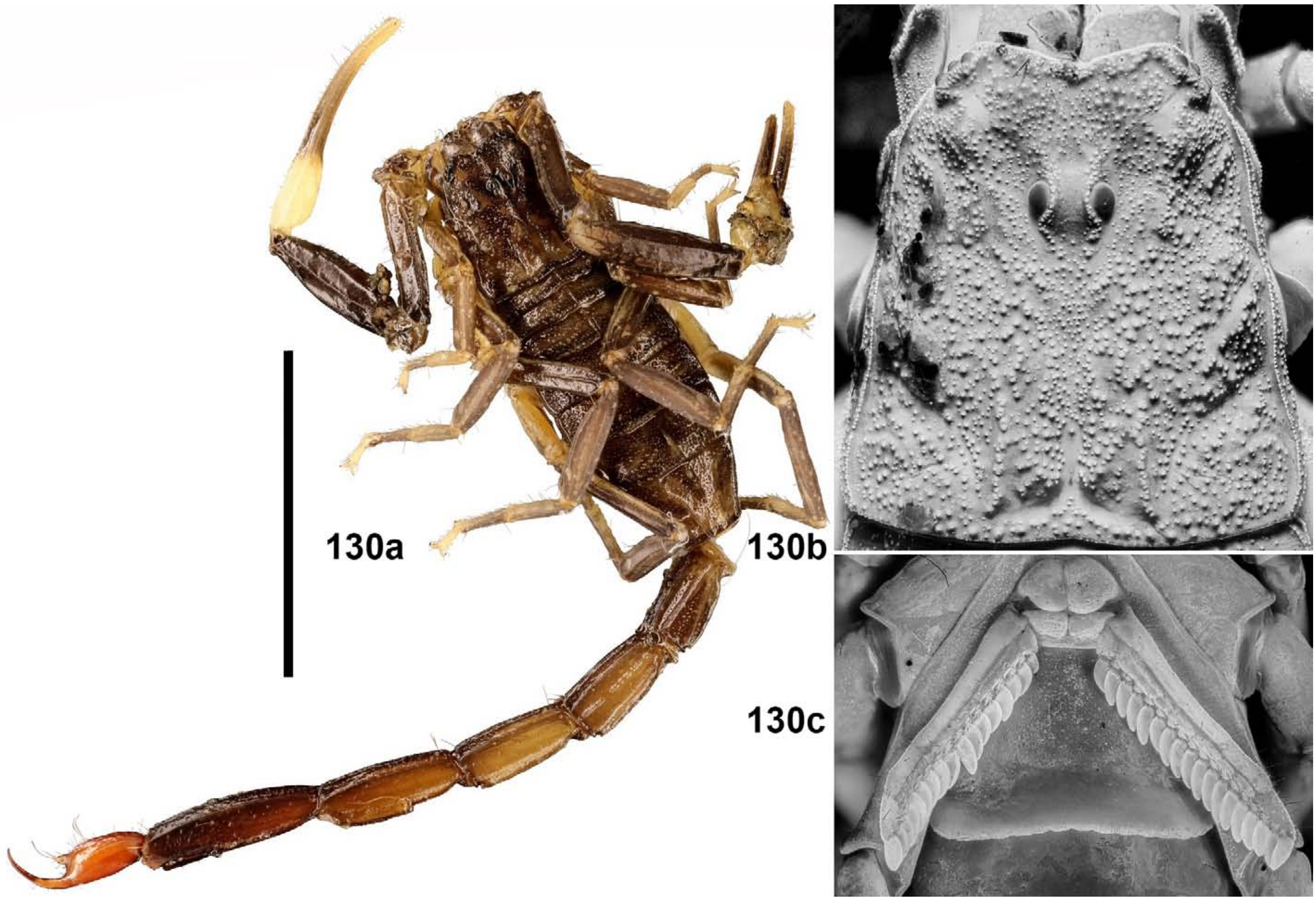

Figures 130a–**c**. *Langxie feti* **gen**. et **sp**. **n**., female paratype no. F22, habitus (130a), carapace (130b) and sternopectinal area (130c). Scale bar = 10 mm (130a).

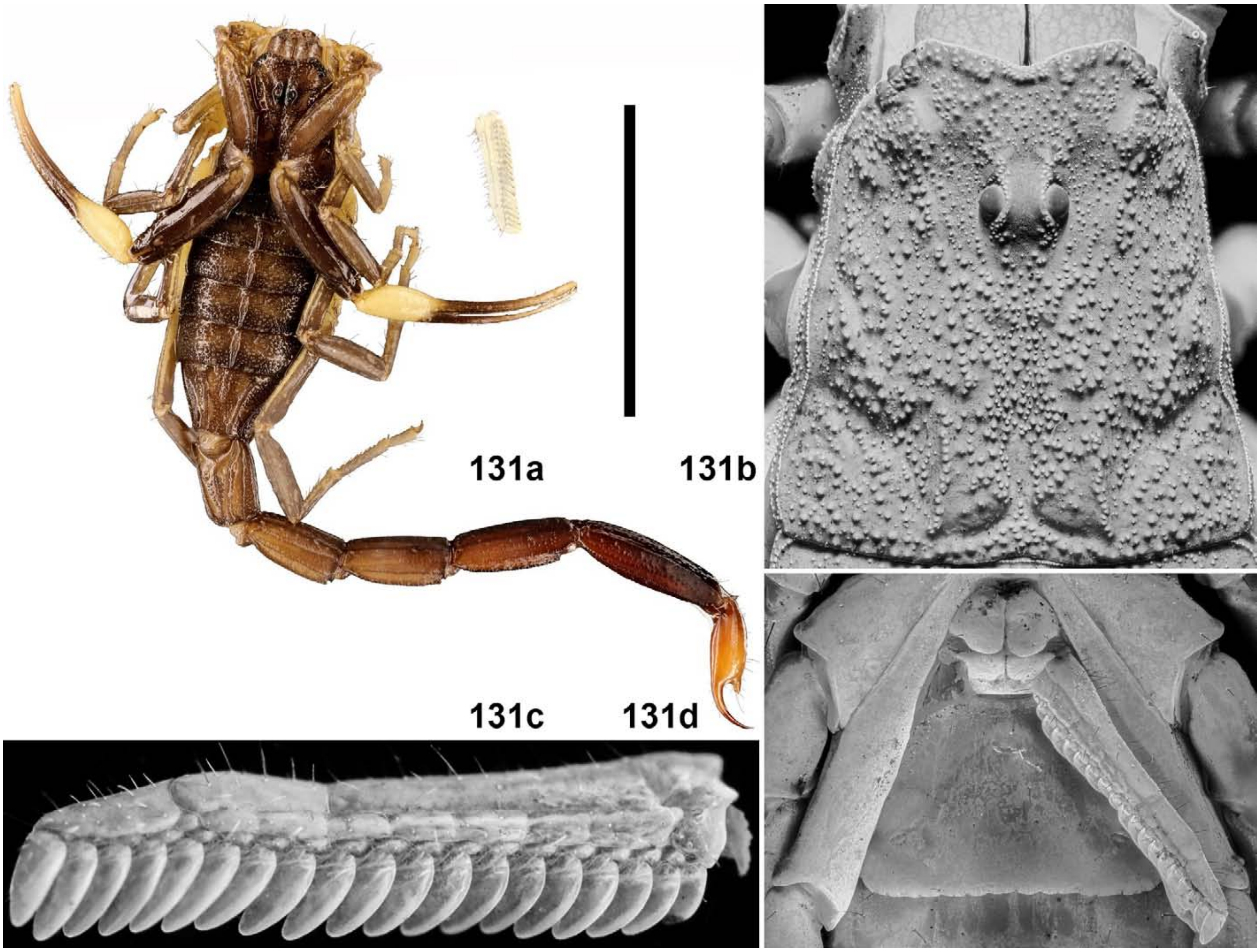

Figures 131a–d. *Langxie feti* **gen**. et **sp**. **n**., female paratype no. F23, habitus and left pectine (131a), carapace (131b), left pectine (131c) and sternopectinal area with right pectine (131d). Scale bar = 10 mm (131a).

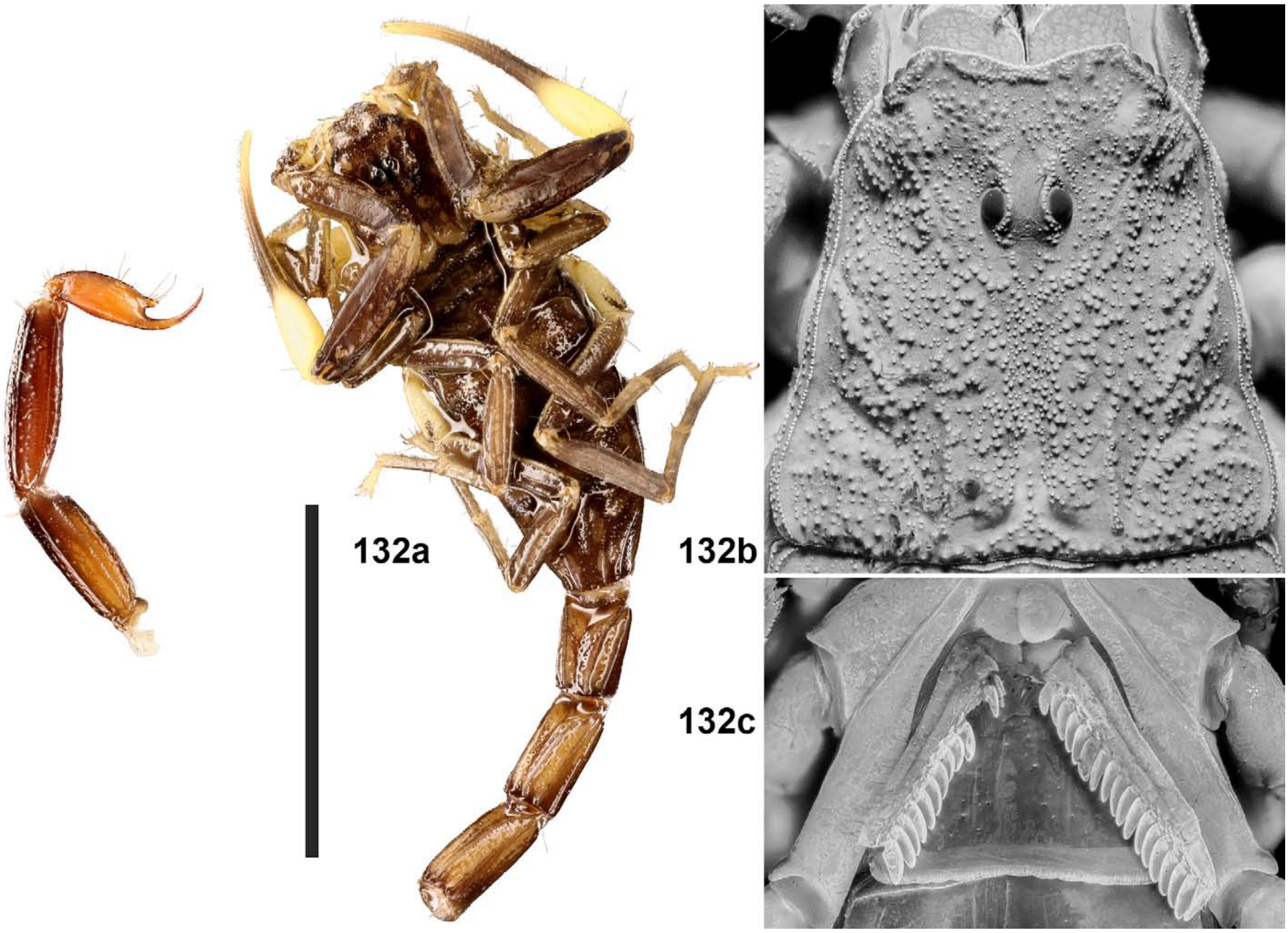

Figures 132a–**c**. *Langxie feti* **gen**. et **sp**. **n**., female paratype no. F24, habitus (132a), carapace (132b) and sternopectinal area (132c). Scale bar = 10 mm (132a).

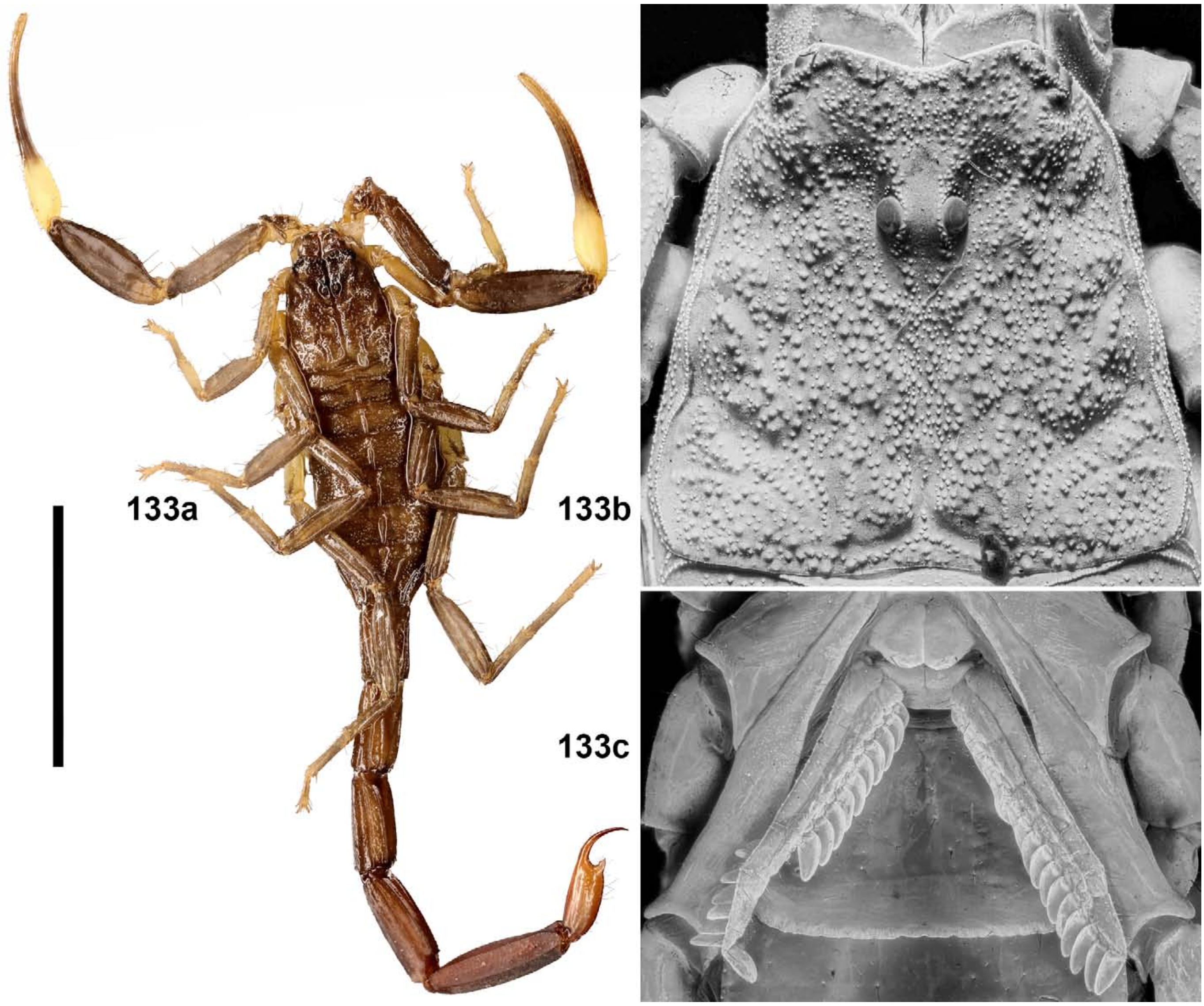

Figures 133a–**c**. *Langxie feti* **gen**. et **sp**. **n**., female paratype no. F25, habitus (133a), carapace (133b) and sternopectinal area (133c). Scale bar = 10 mm (133a).

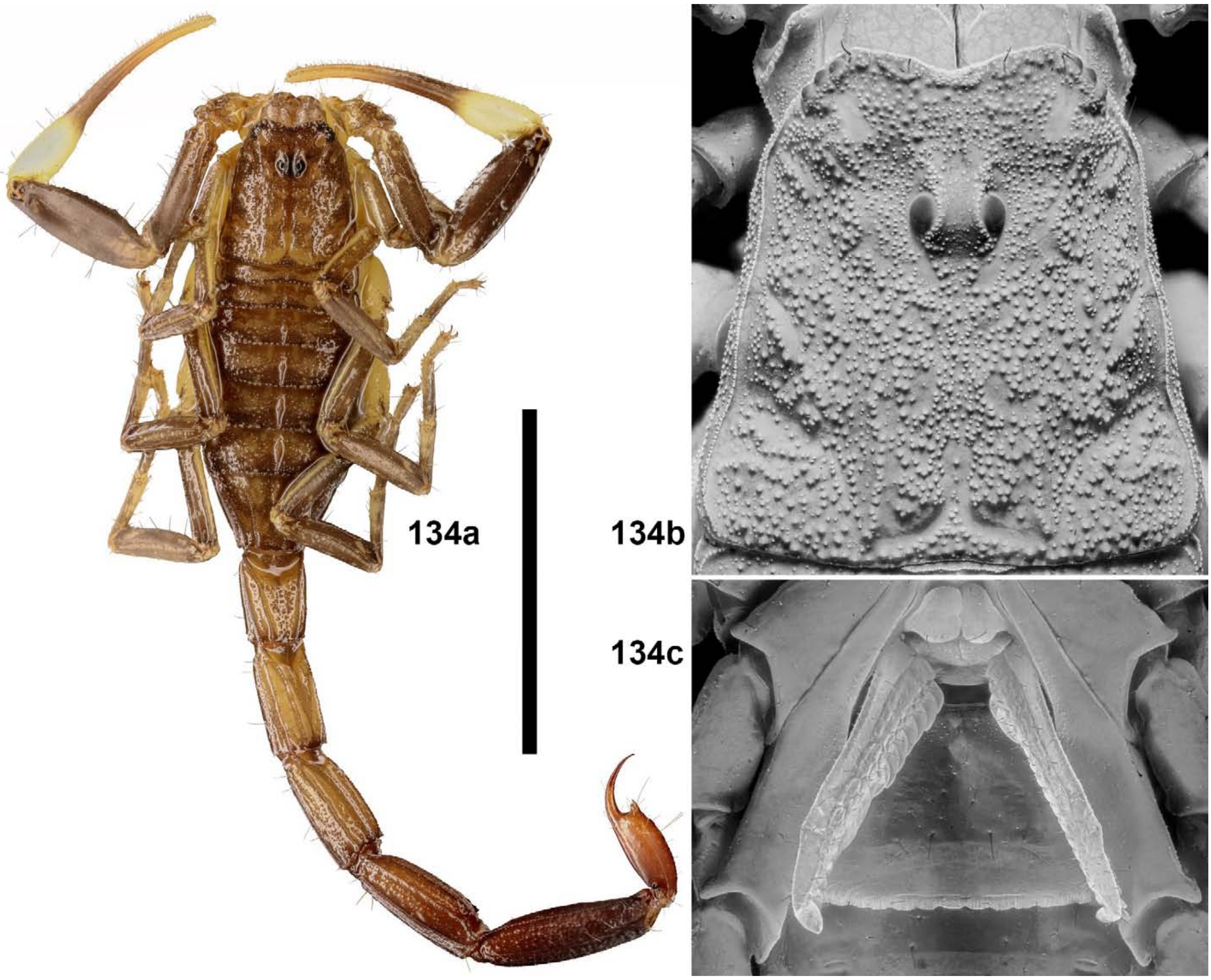

Figures 134a–**c**. *Langxie feti* **gen**. et **sp**. **n**., female paratype no. F26, habitus (134a), carapace (134b) and sternopectinal area (134c). Scale bar = 10 mm (134a).

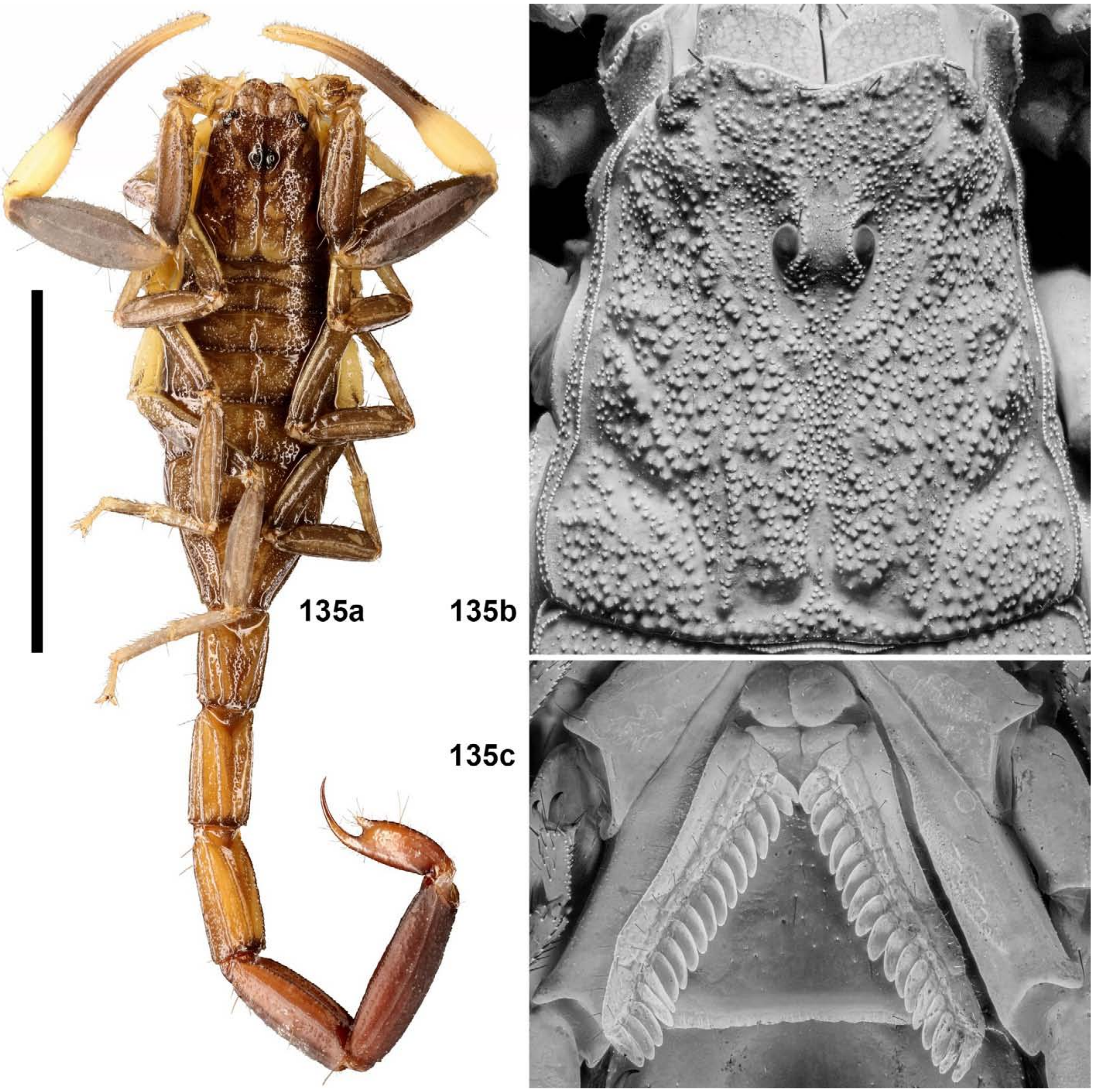

Figures 135a–**c**. *Langxie feti* **gen**. et **sp**. **n**., female paratype no. F27, habitus (135a), carapace (135b) and sternopectinal area (135c). Scale bar = 10 mm (135a).

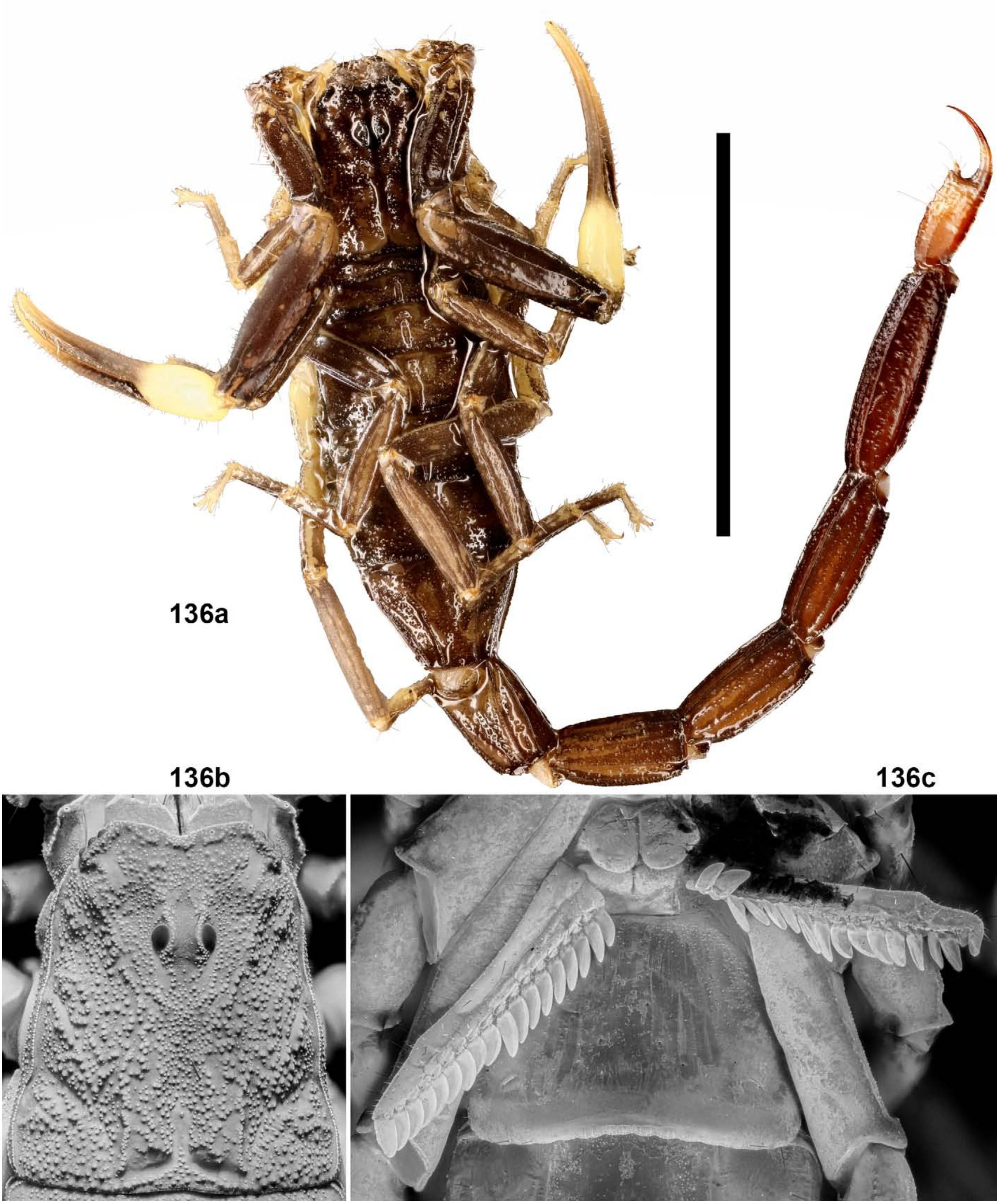

Figures 136a–c. *Langxie feti* **gen**. et **sp**. **n**., female paratype no. F28, habitus (136a), carapace (136b) and sternopectinal area (136c). Scale bar = 10 mm (136a).

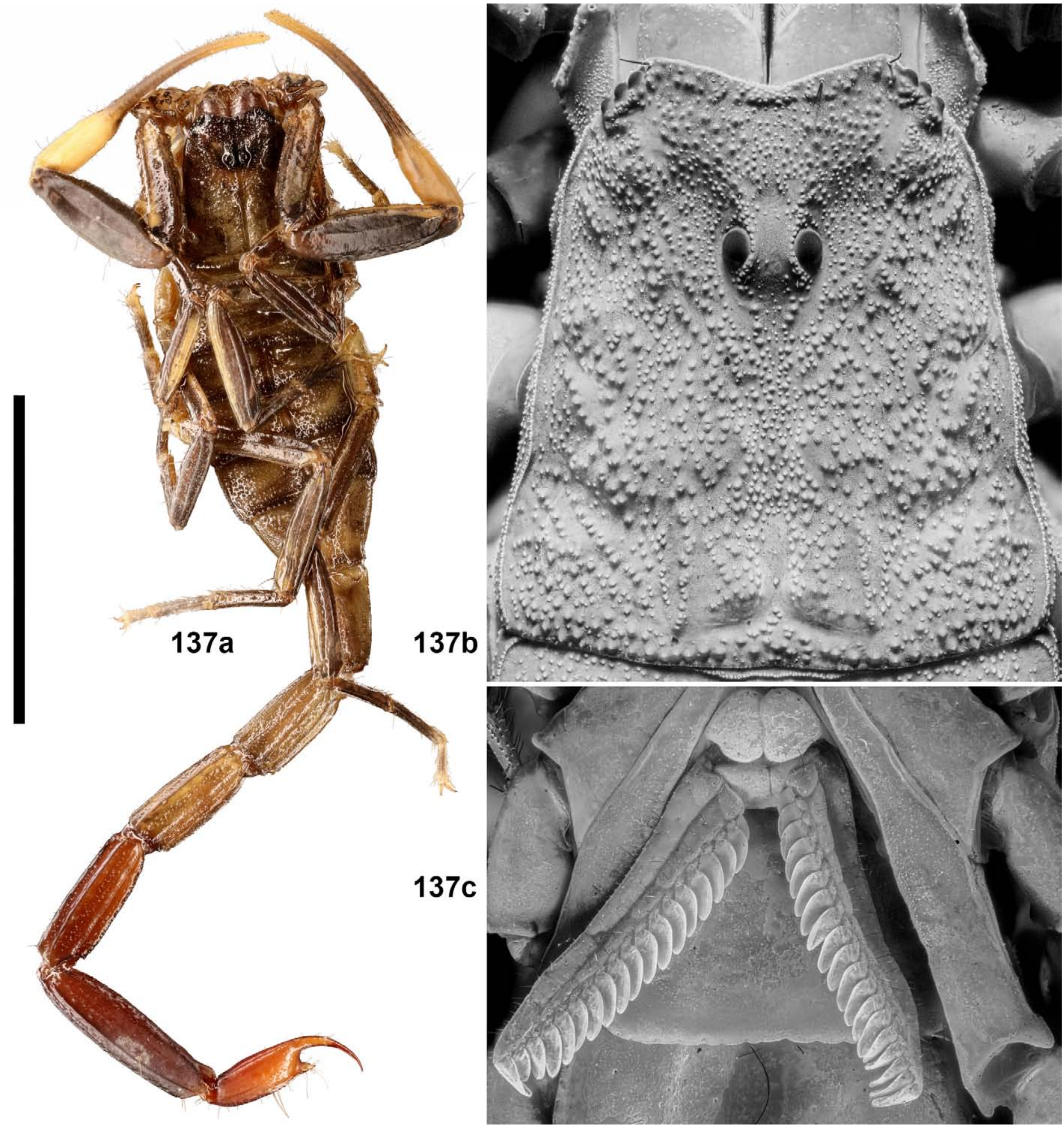

Figures 137a–**c**. *Langxie feti* **gen**. et **sp**. **n**., female paratype no. F29, habitus (137a), carapace (137b) and sternopectinal area (137c). Scale bar = 10 mm (137a).

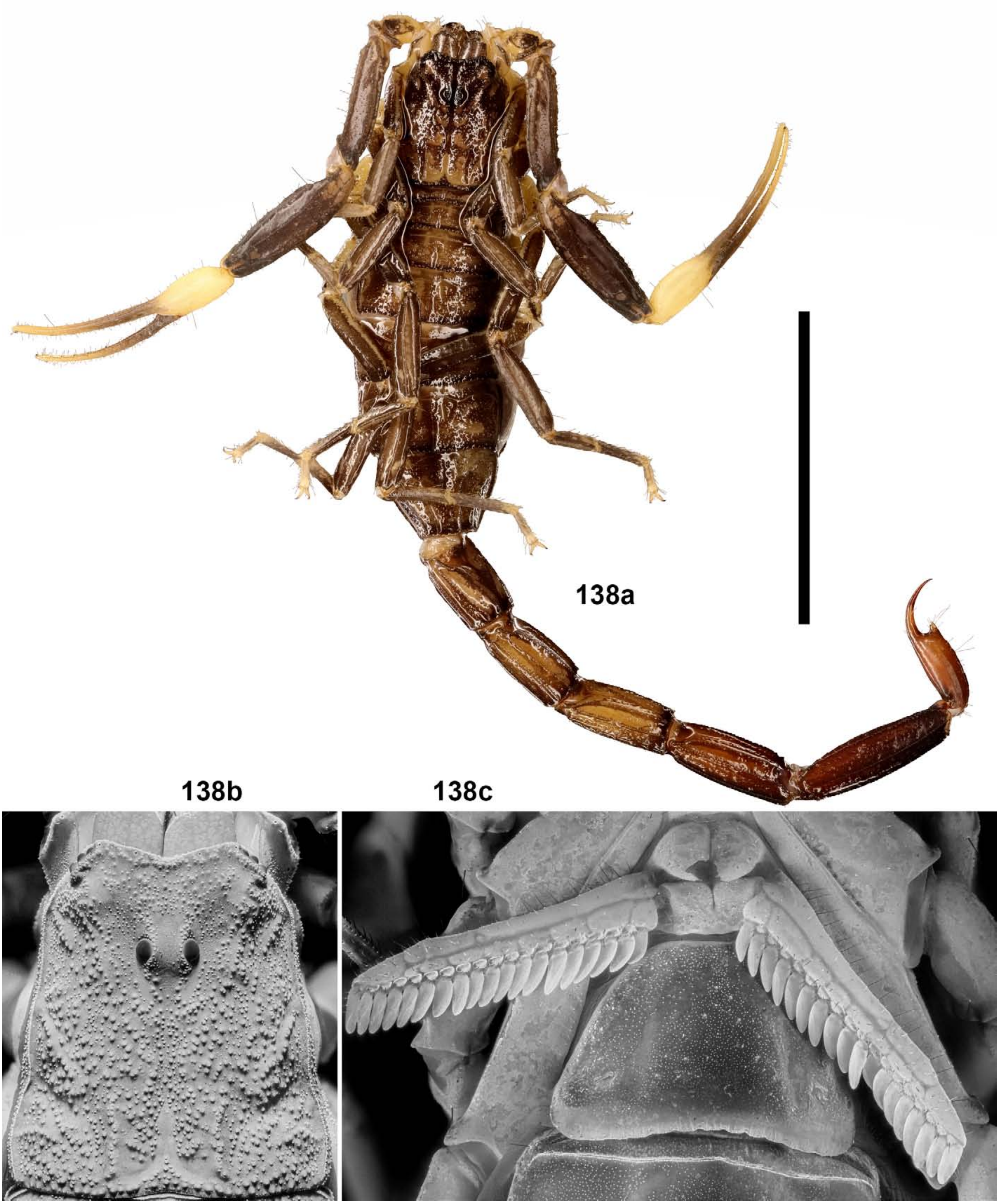

Figures 138a–**c**. *Langxie feti* **gen**. et **sp**. **n**., female paratype no. F30, habitus (138a), carapace (138b) and sternopectinal area (138c). Scale bar = 10 mm (138a).

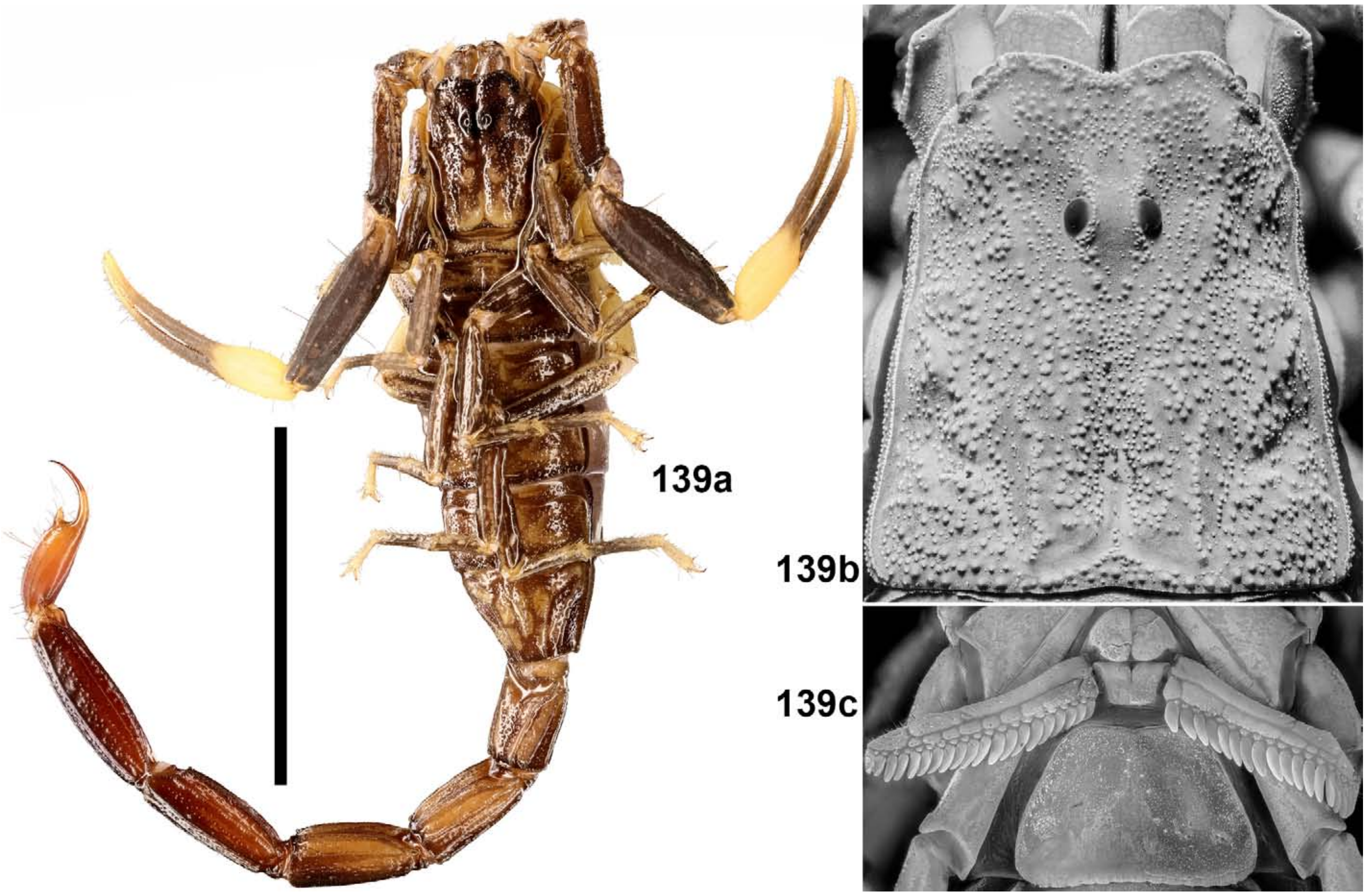

Figures 139a–**c**. *Langxie feti* **gen**. et **sp**. **n**., female paratype no. F31, habitus (139a), carapace (139b) and sternopectinal area (139c). Scale bar = 10 mm (139a).

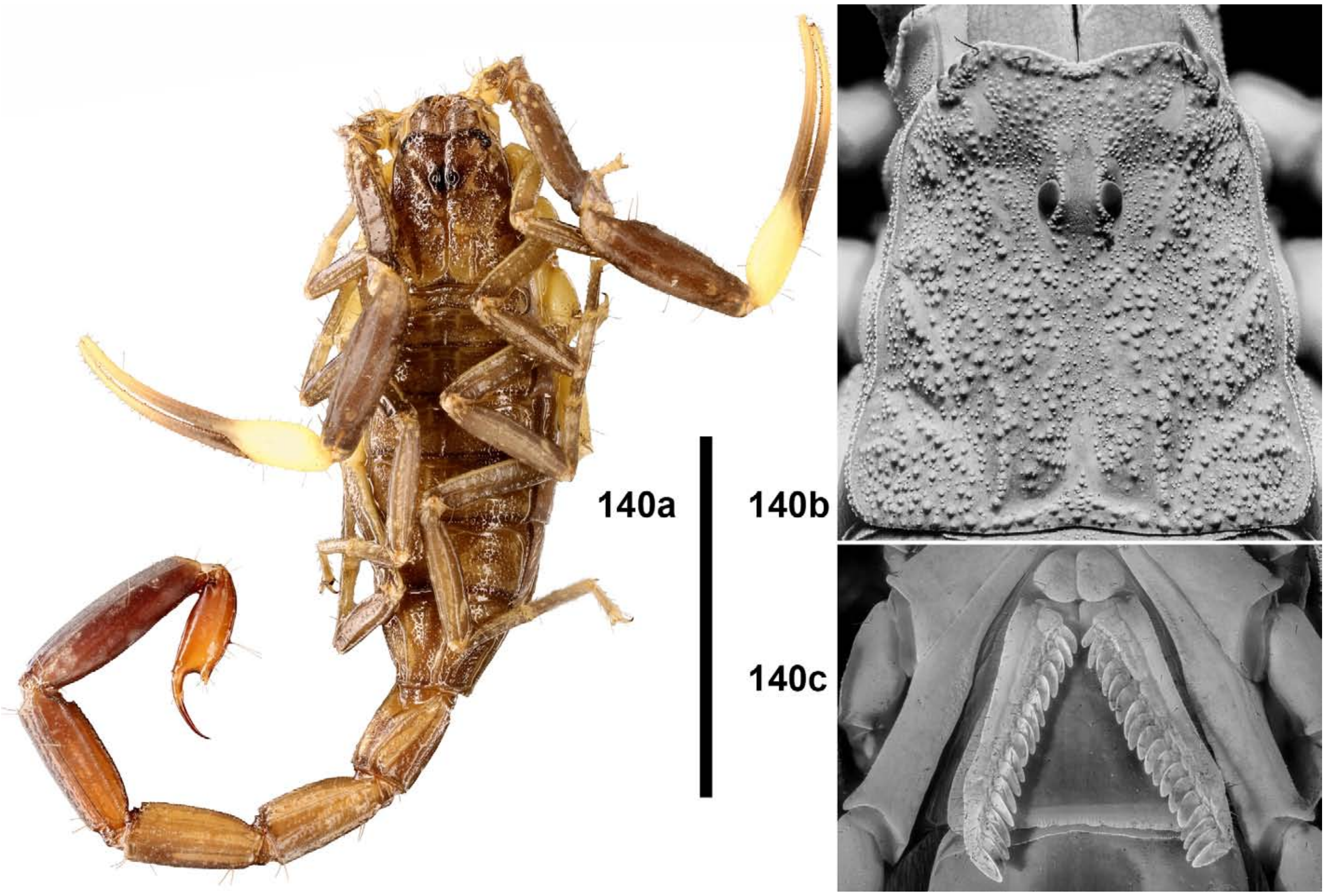

Figures 140a–**c**. *Langxie feti* **gen**. et **sp**. **n**., female paratype no. F32, habitus (140a), carapace (140b) and sternopectinal area (140c). Scale bar = 10 mm (140a).

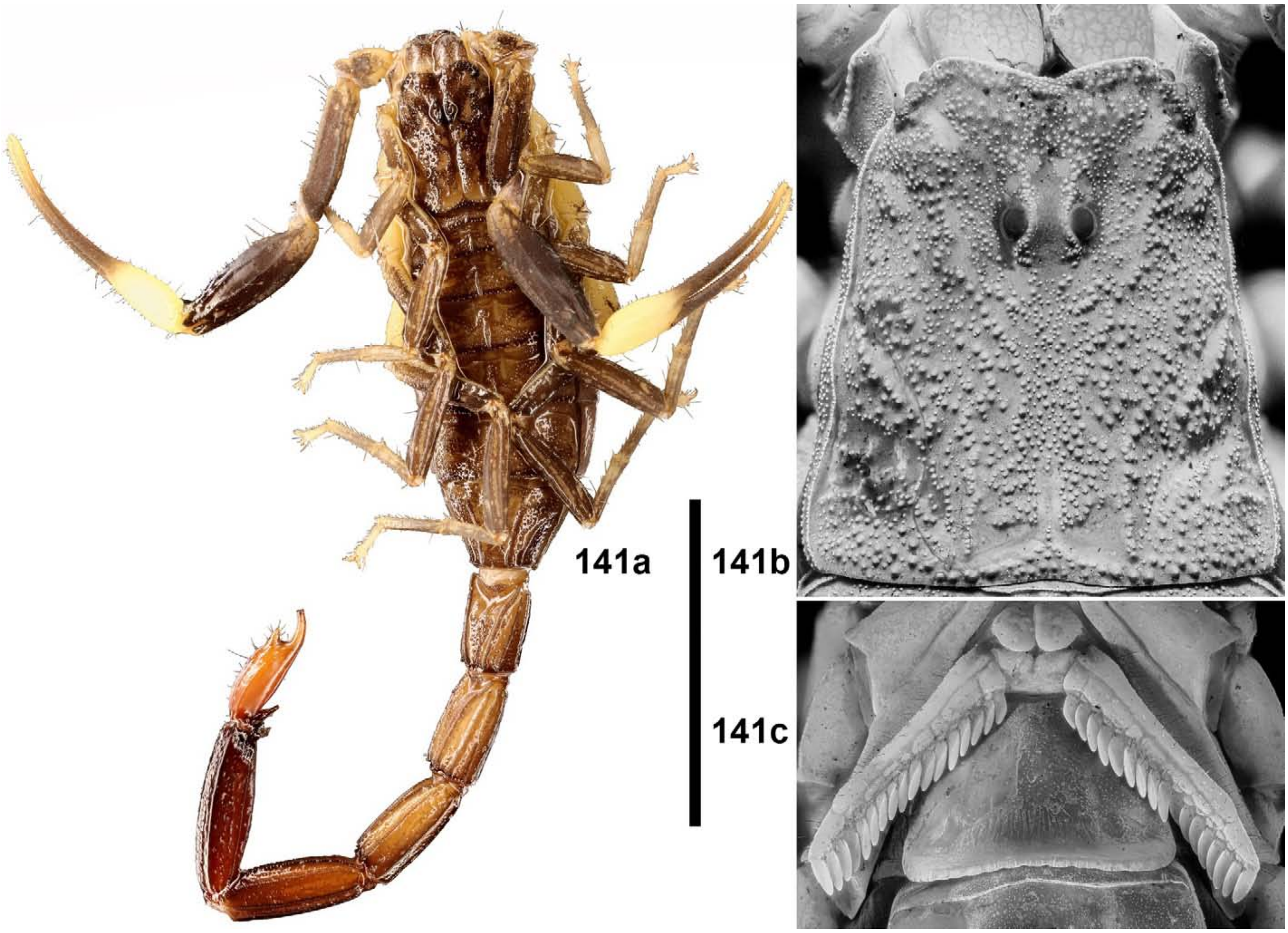

Figures 141a–**c**. *Langxie feti* **gen**. et **sp**. **n**., female paratype no. F33, habitus (141a), carapace (141b) and sternopectinal area (141c). Scale bar = 10 mm (141a).

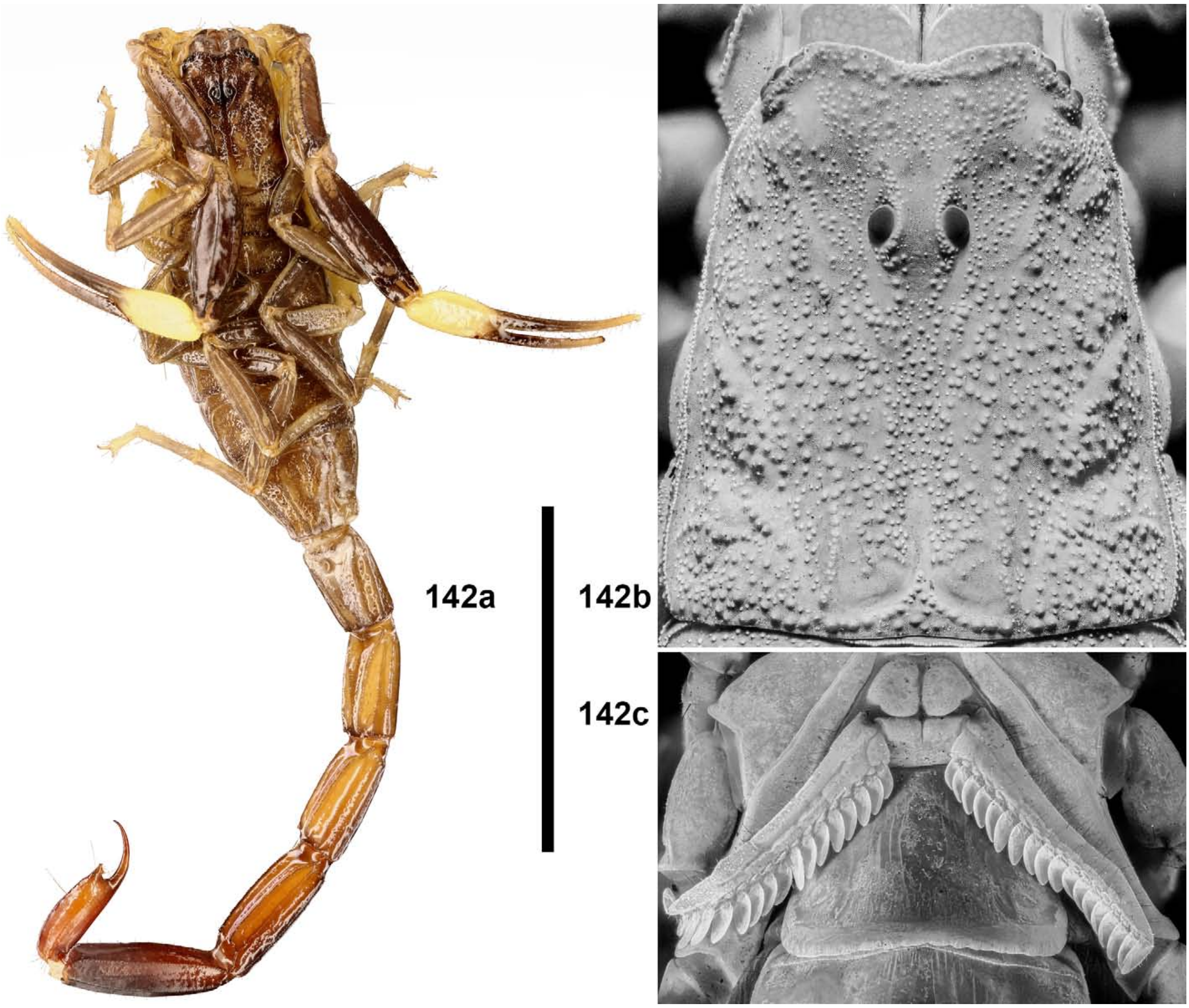

Figures 142a–**c**. *Langxie feti* **gen**. et **sp**. **n**., female paratype no. F34, habitus (142a), carapace (142b) and sternopectinal area (142c). Scale bar = 10 mm (142a).

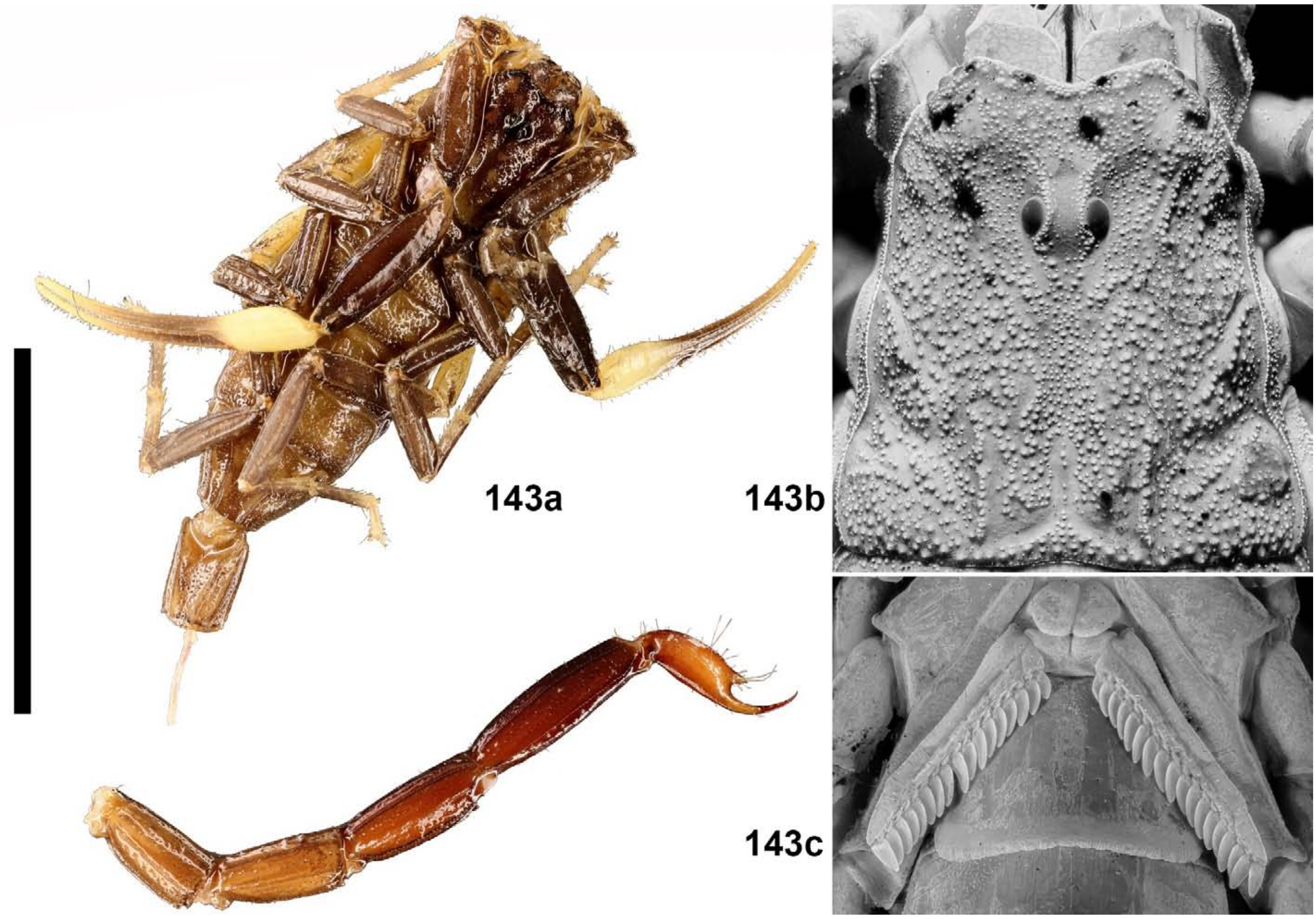

Figures 143a–**c**. *Langxie feti* **gen**. et **sp**. **n**., female paratype no. F35, habitus (143a), carapace (143b) and sternopectinal area (143c). Scale bar = 10 mm (143a).

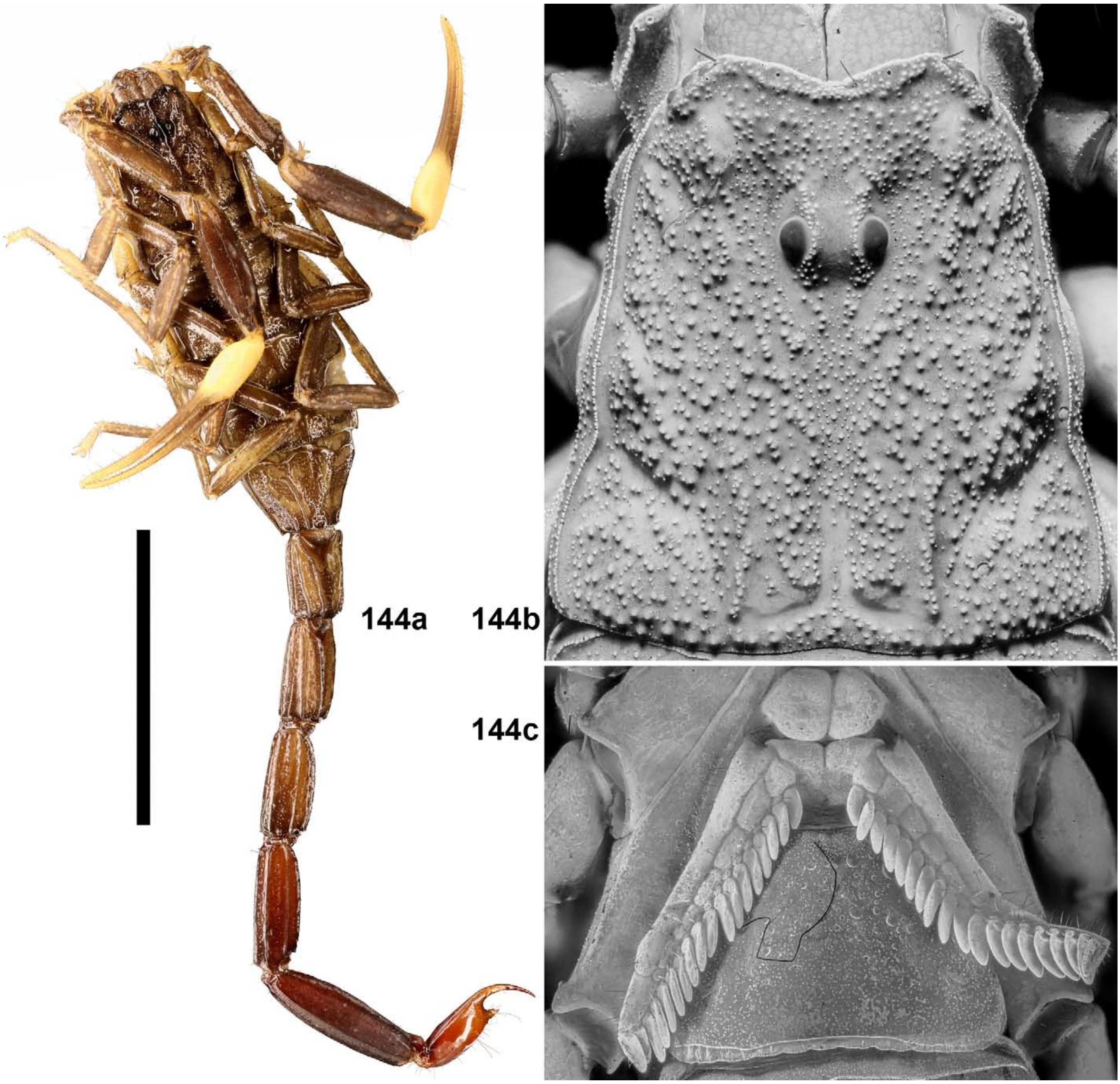

Figures 144a–**c**. *Langxie feti* **gen**. et **sp**. **n**., female paratype no. F36, habitus (144a), carapace (144b) and sternopectinal area (144c). Scale bar = 10 mm (144a).

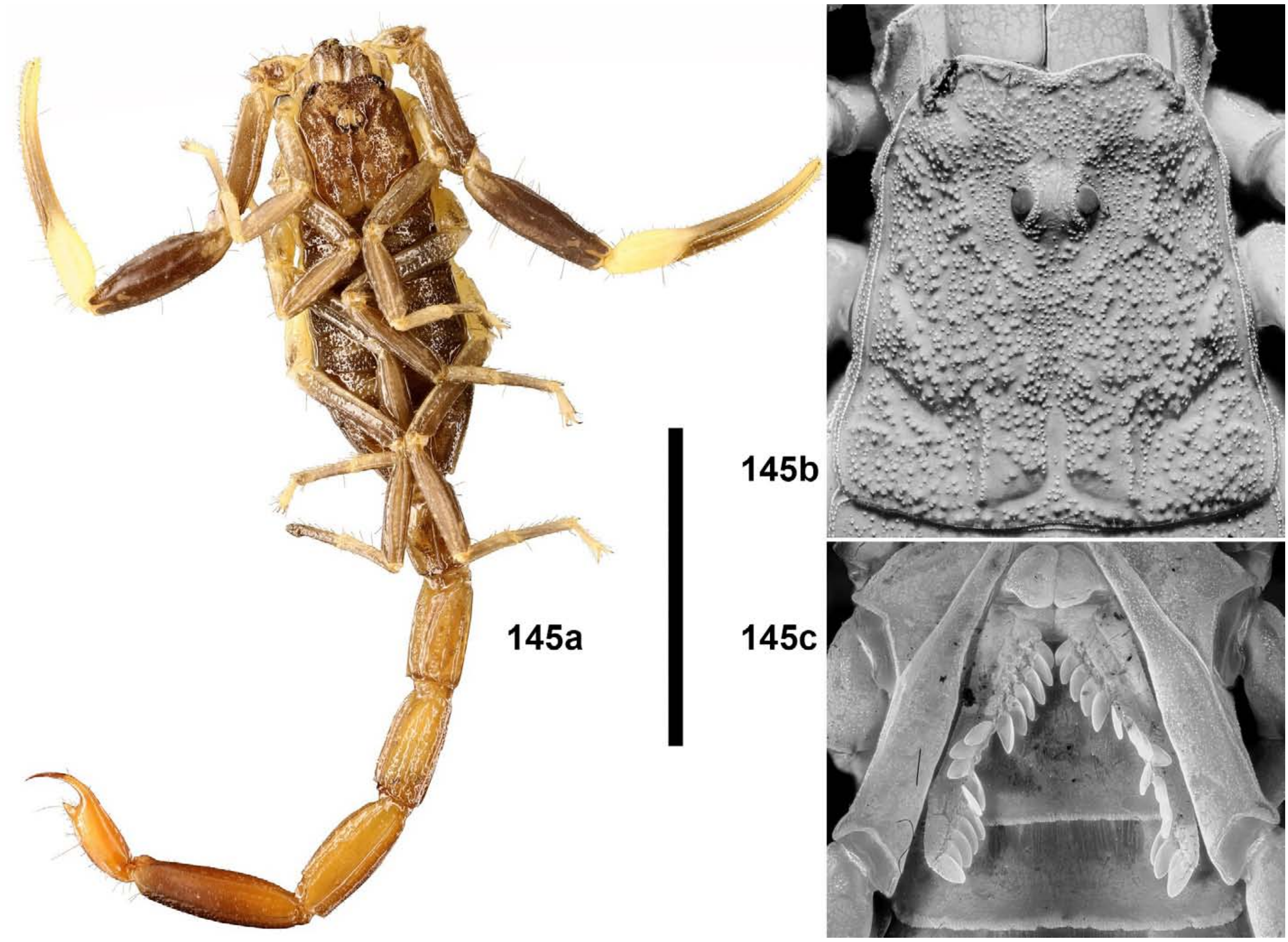

Figures 145a–**c**. *Langxie feti* **gen**. et **sp**. **n**., female paratype no. F37, habitus (145a), carapace (145b) and sternopectinal area (145c). Scale bar = 10 mm (145a).

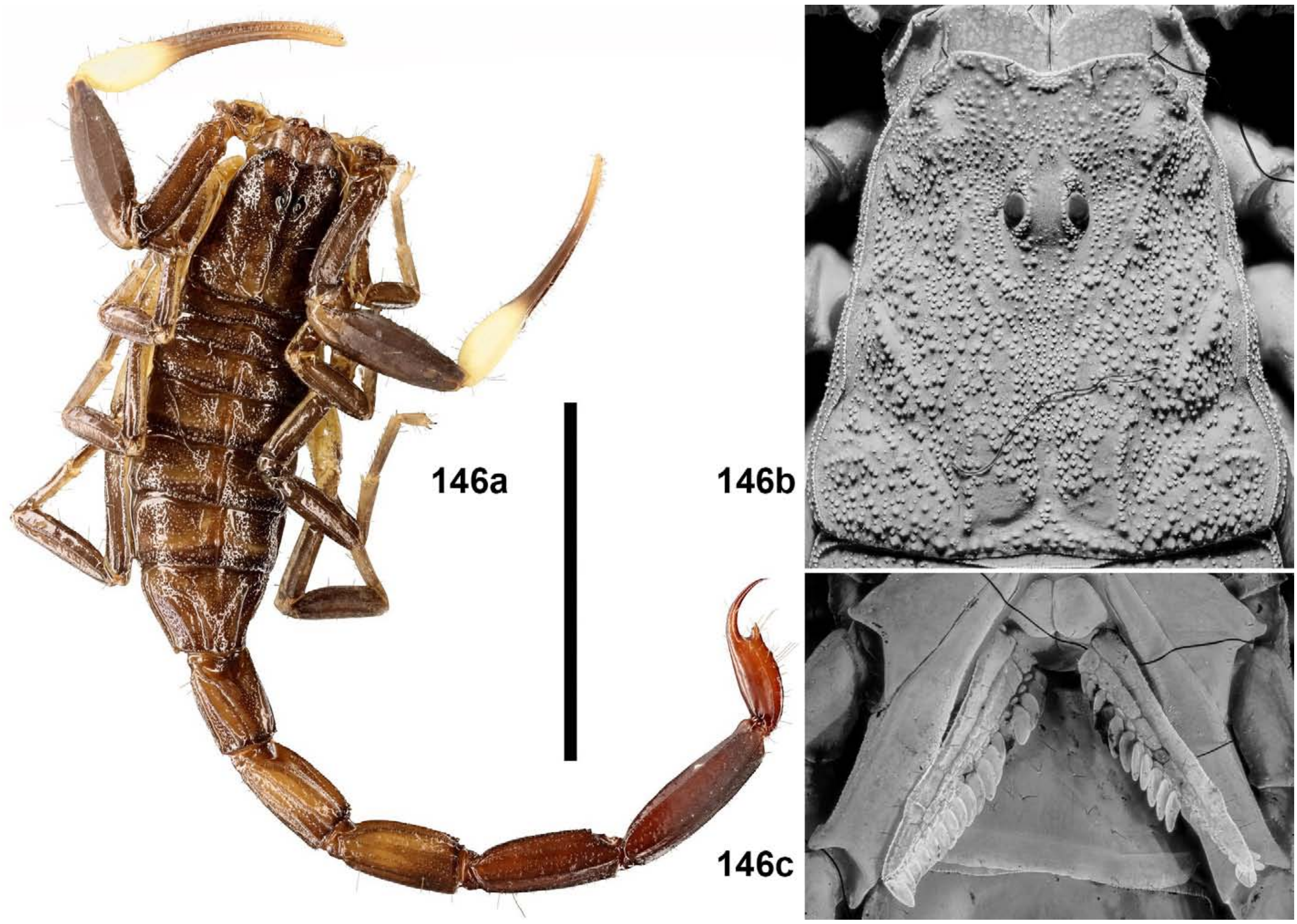

Figures 146a–**c**. *Langxie feti* **gen**. et **sp**. **n**., female paratype no. F38, habitus (146a), carapace (146b) and sternopectinal area (146c). Scale bar = 10 mm (146a).

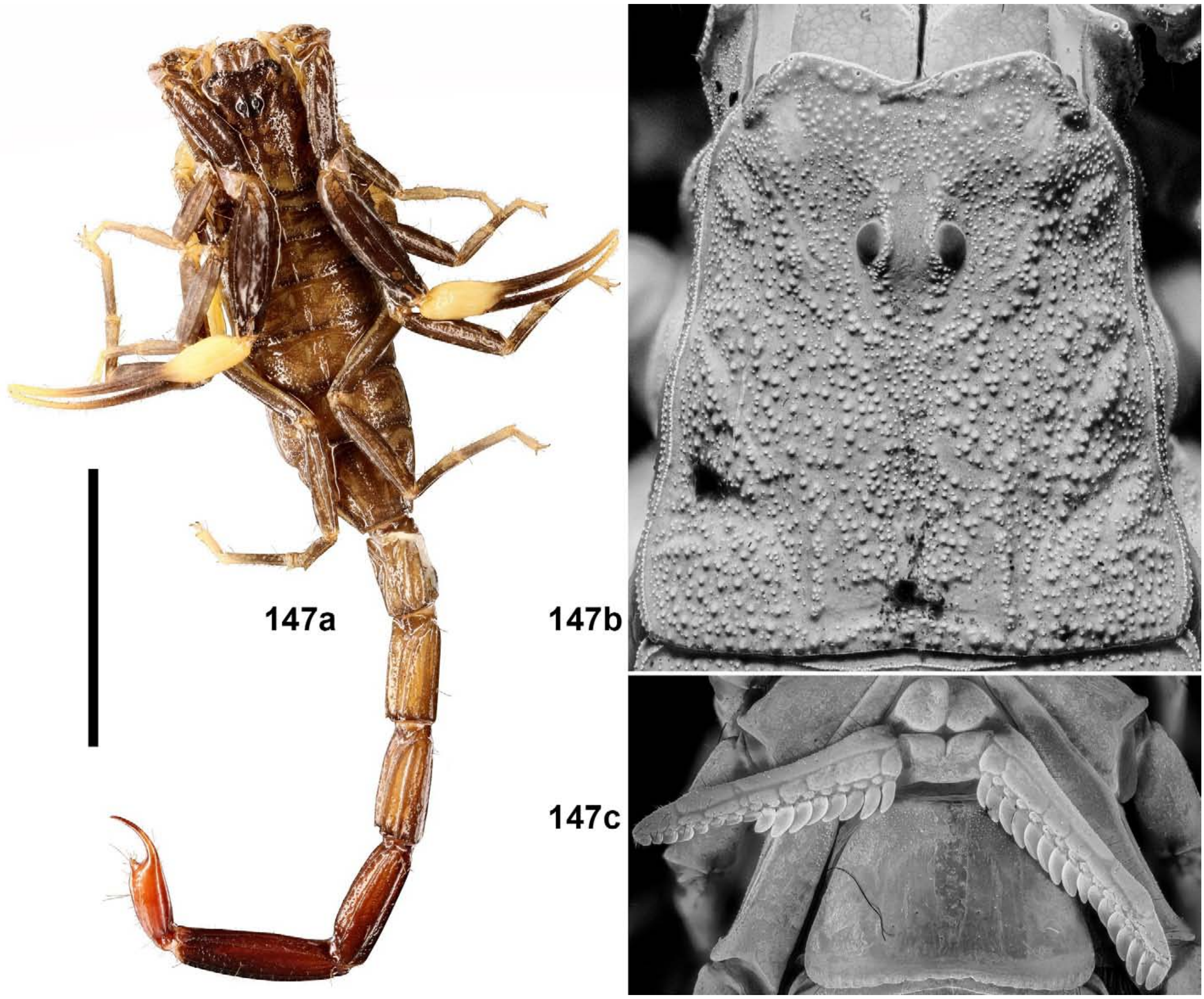

Figures 147a–c. *Langxie feti* **gen**. et **sp**. **n**., female paratype no. F39, habitus (147a), carapace (147b) and sternopectinal area (147c). Scale bar = 10 mm (147a).

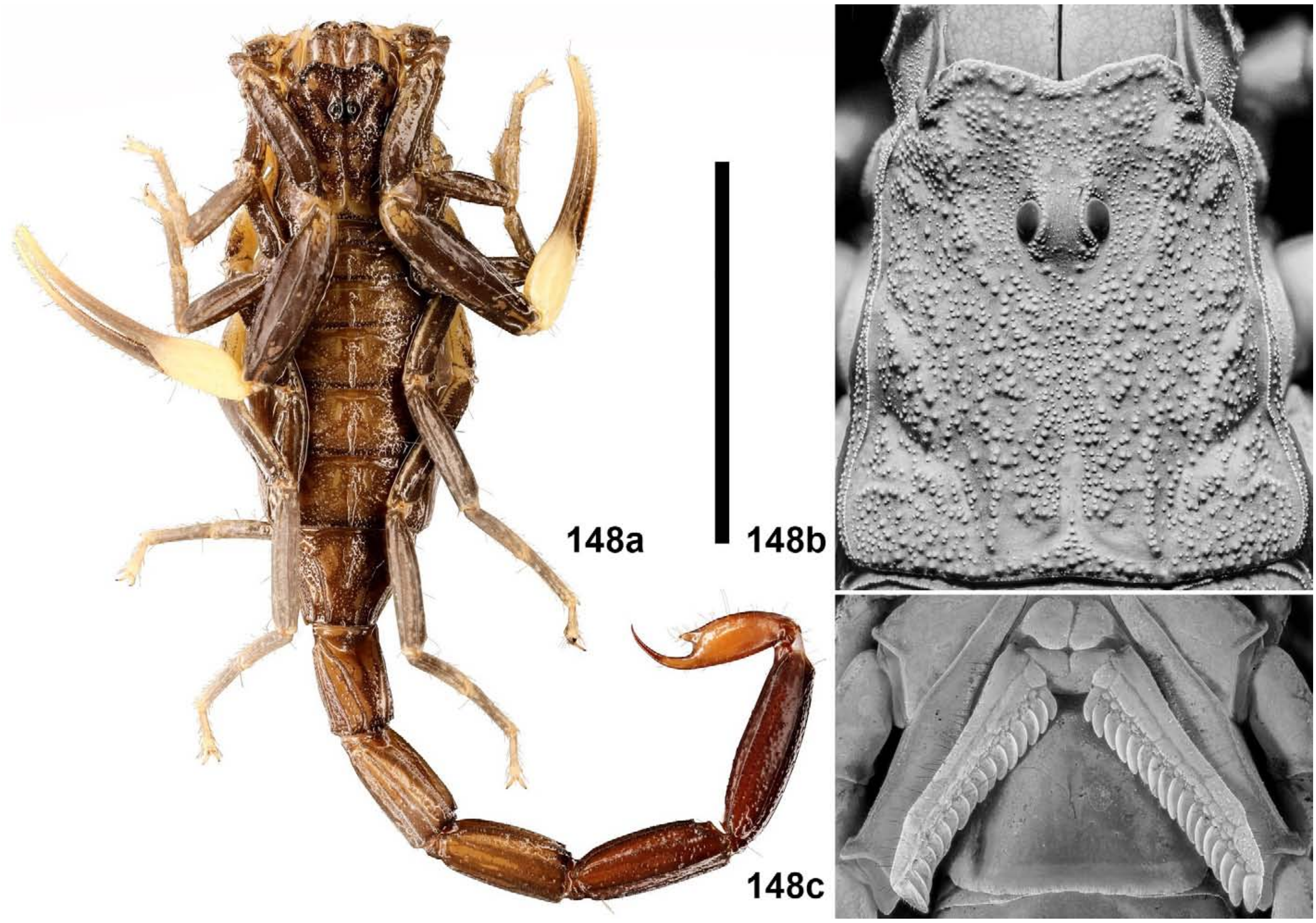

Figures 148a–**c**. *Langxie feti* **gen**. et **sp**. **n**., female paratype no. F40, habitus (148a), carapace (148b) and sternopectinal area (148c). Scale bar = 10 mm (148a).

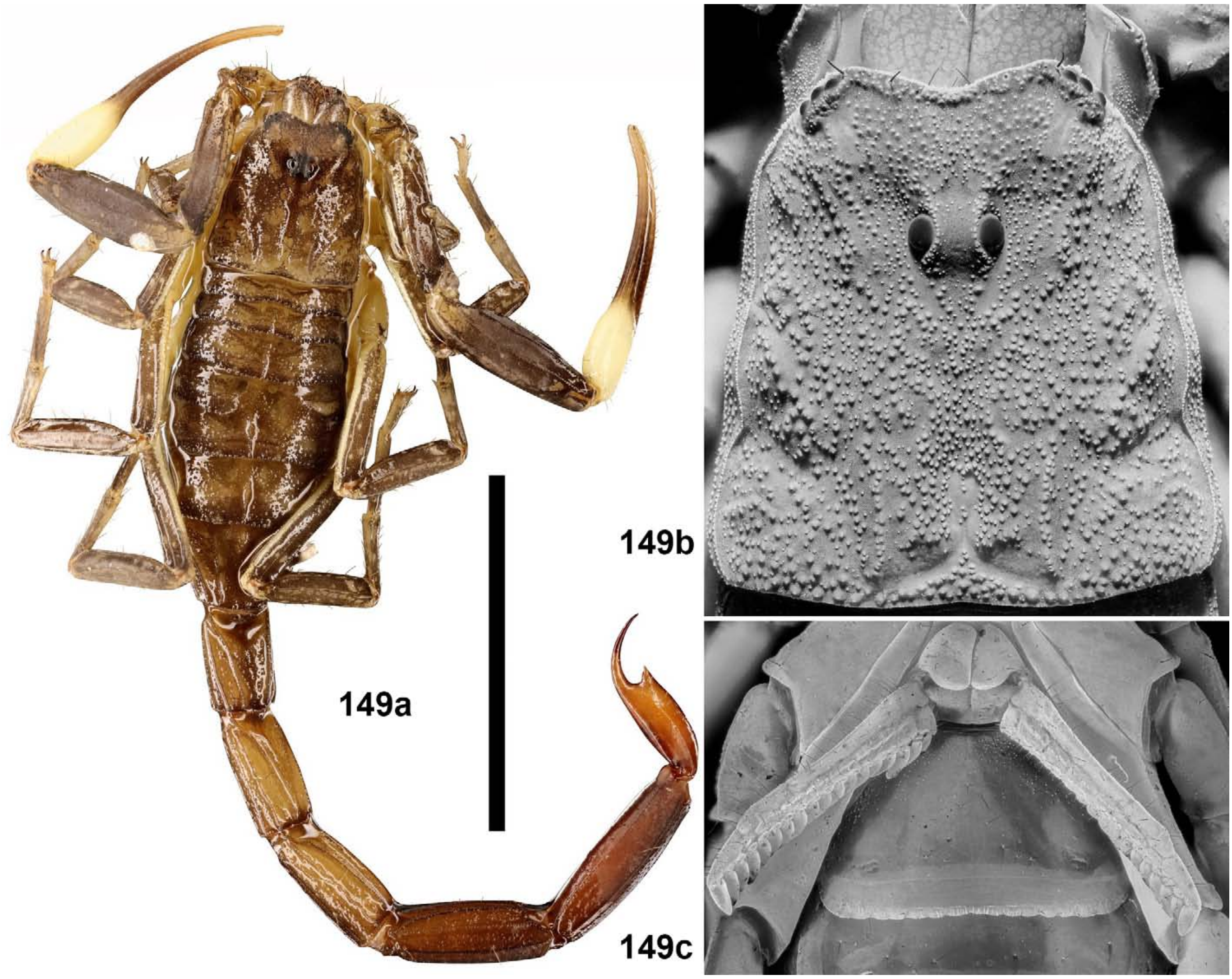

Figures 149a–**c**. *Langxie feti* **gen**. et **sp**. **n**., female paratype no. F41, habitus (149a), carapace (149b) and sternopectinal area (149c). Scale bar = 10 mm (149a).

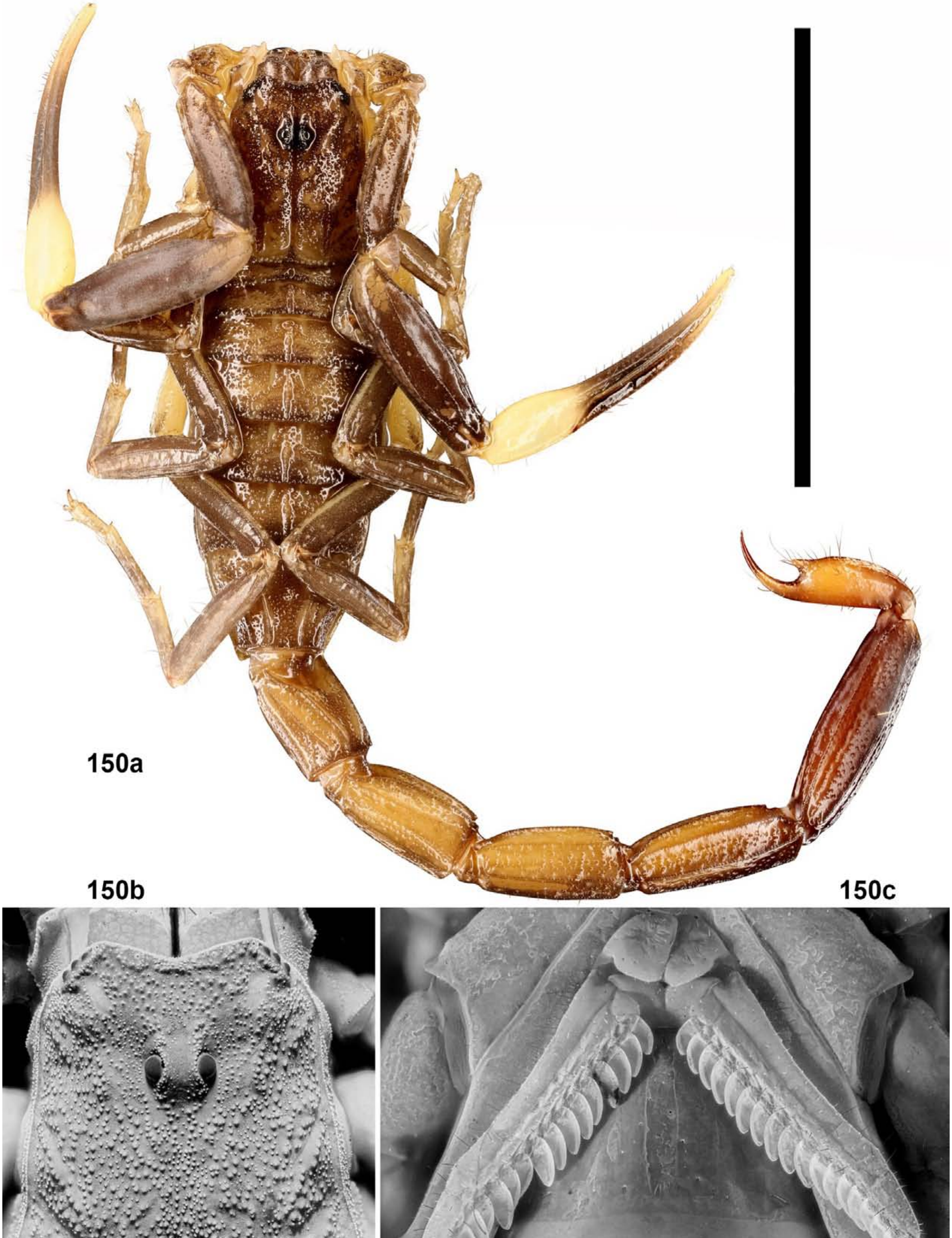

Figures 150a–**c**. *Langxie feti* **gen**. et **sp**. **n**., female paratype no. F42, habitus (150a), carapace (150b) and sternopectinal area (150c). Scale bar = 10 mm (150a).

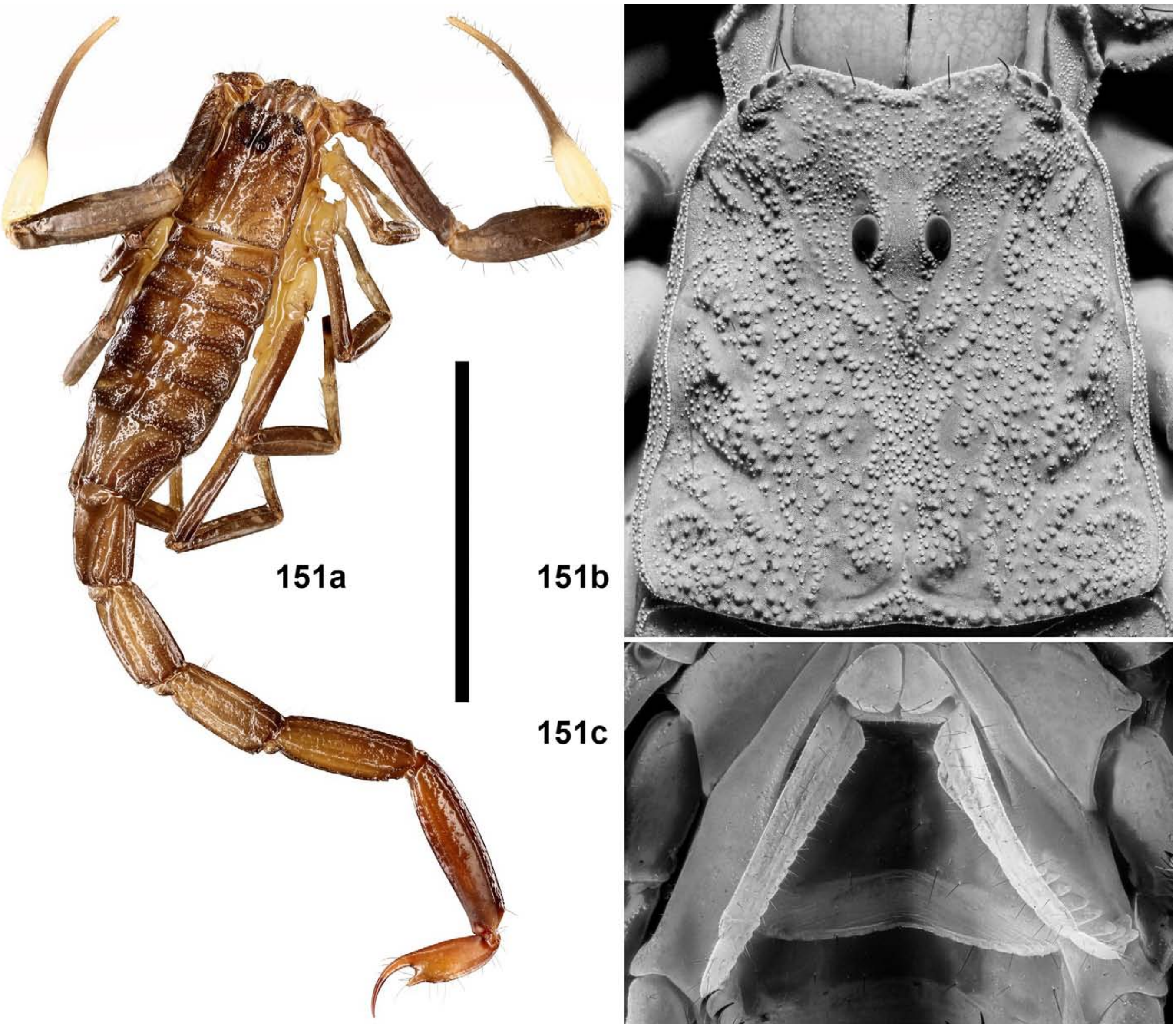

Figures 151a–c. *Langxie feti* **gen**. et **sp**. **n**., female paratype no. F43, habitus (151a), carapace (151b) and sternopectinal area (151c). Scale bar = 10 mm (151a).

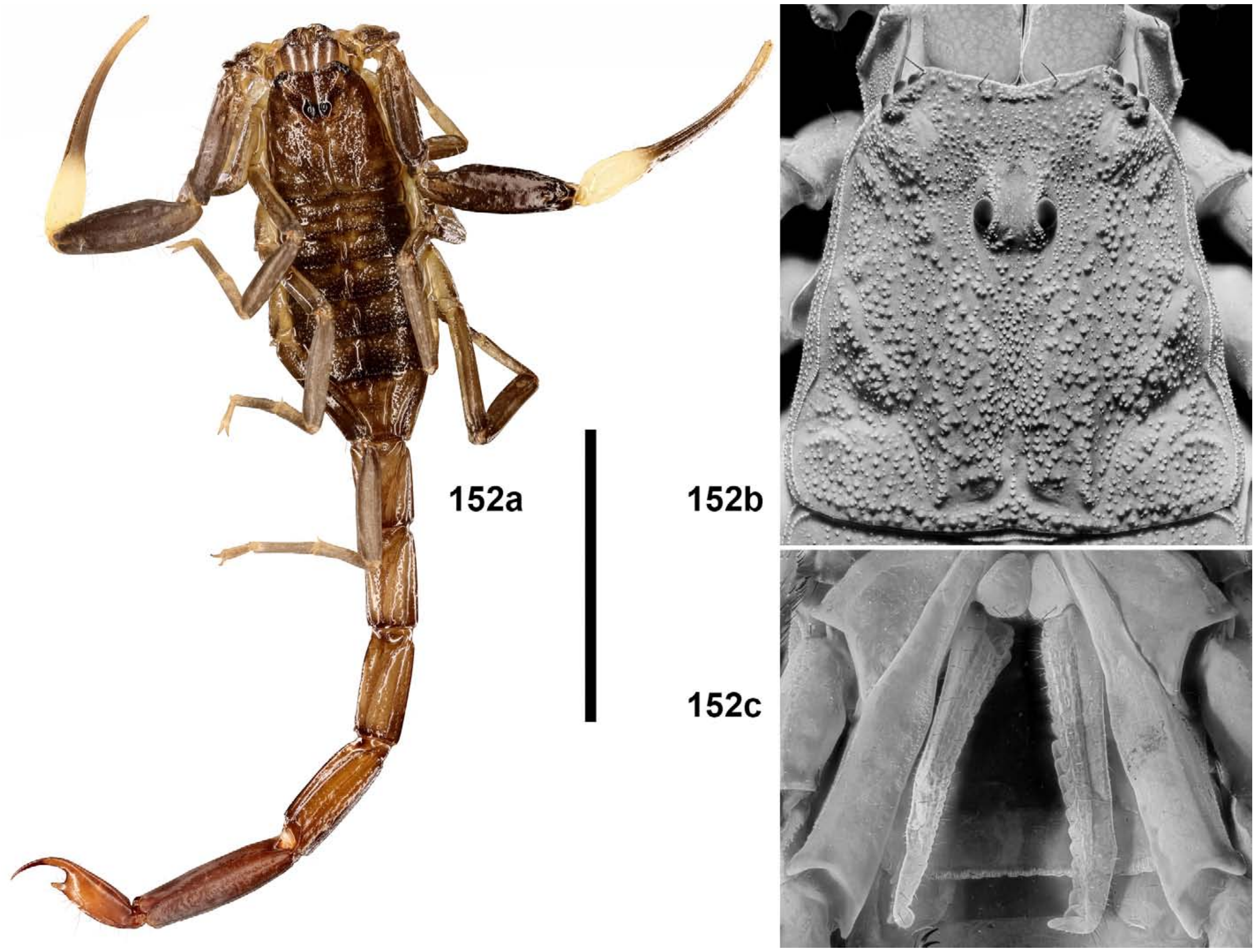

Figures 152a–**c**. *Langxie feti* **gen**. et **sp**. **n**., female paratype no. F44, habitus (152a), carapace (152b) and sternopectinal area (152c). Scale bar = 10 mm (152a).

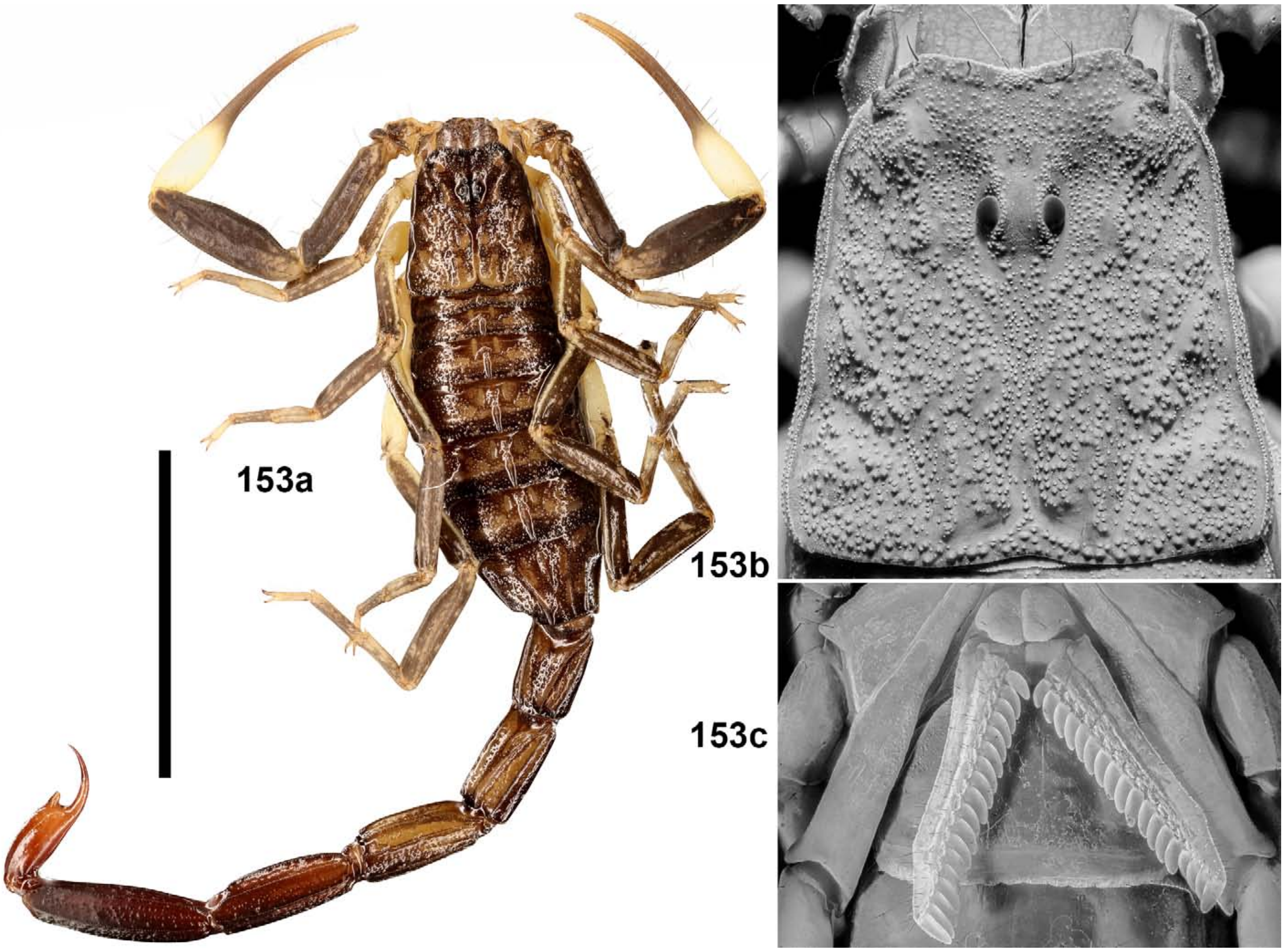

Figures 153a–**c**. *Langxie feti* **gen**. et **sp**. **n**., female paratype no. F45, habitus (153a), carapace (153b) and sternopectinal area (153c). Scale bar = 10 mm (153a).

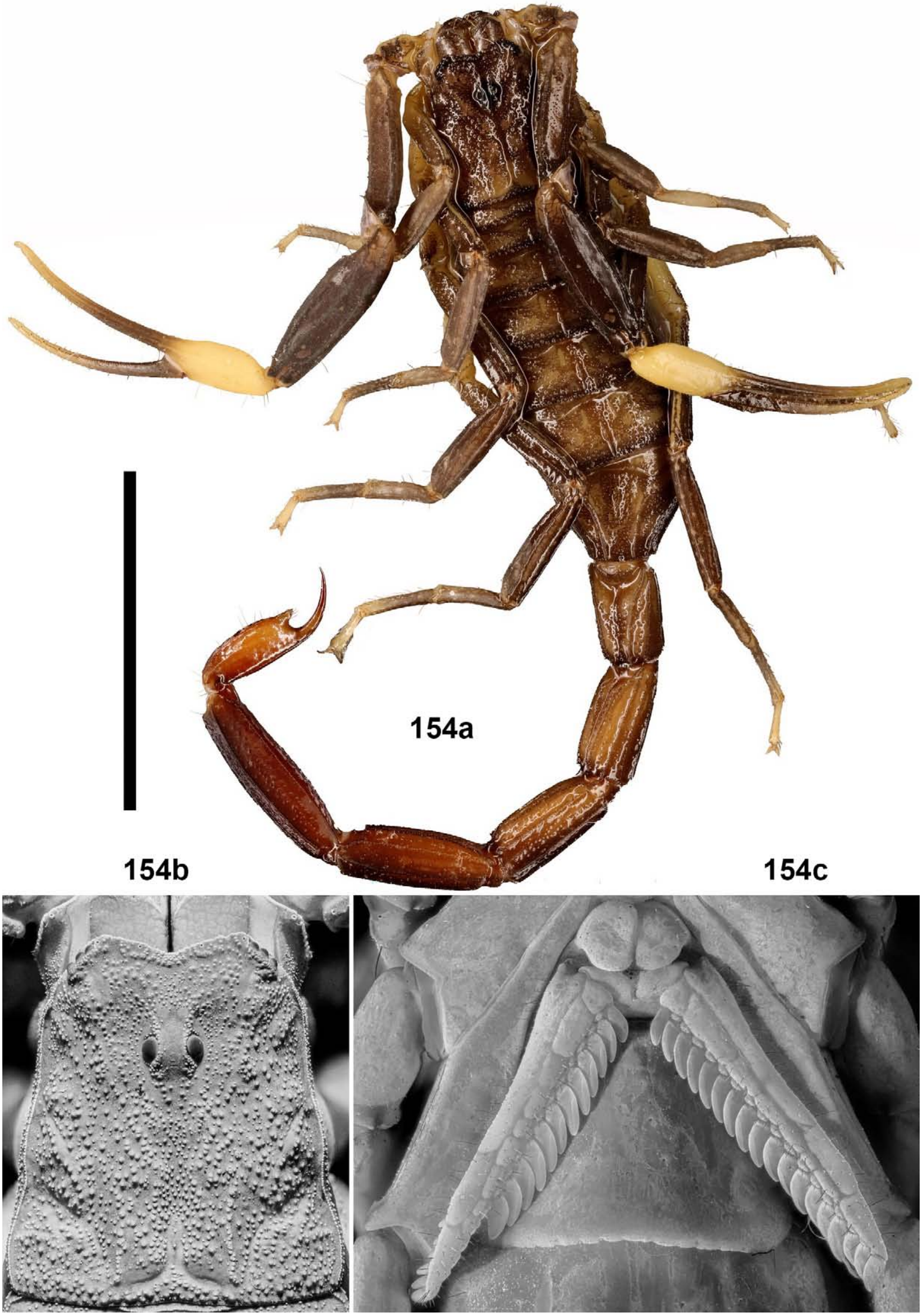

Figures 154a–**c**. *Langxie feti* **gen**. et **sp**. **n**., female paratype no. F46, habitus (154a), carapace (154b) and sternopectinal area (154c). Scale bar = 10 mm (154a).

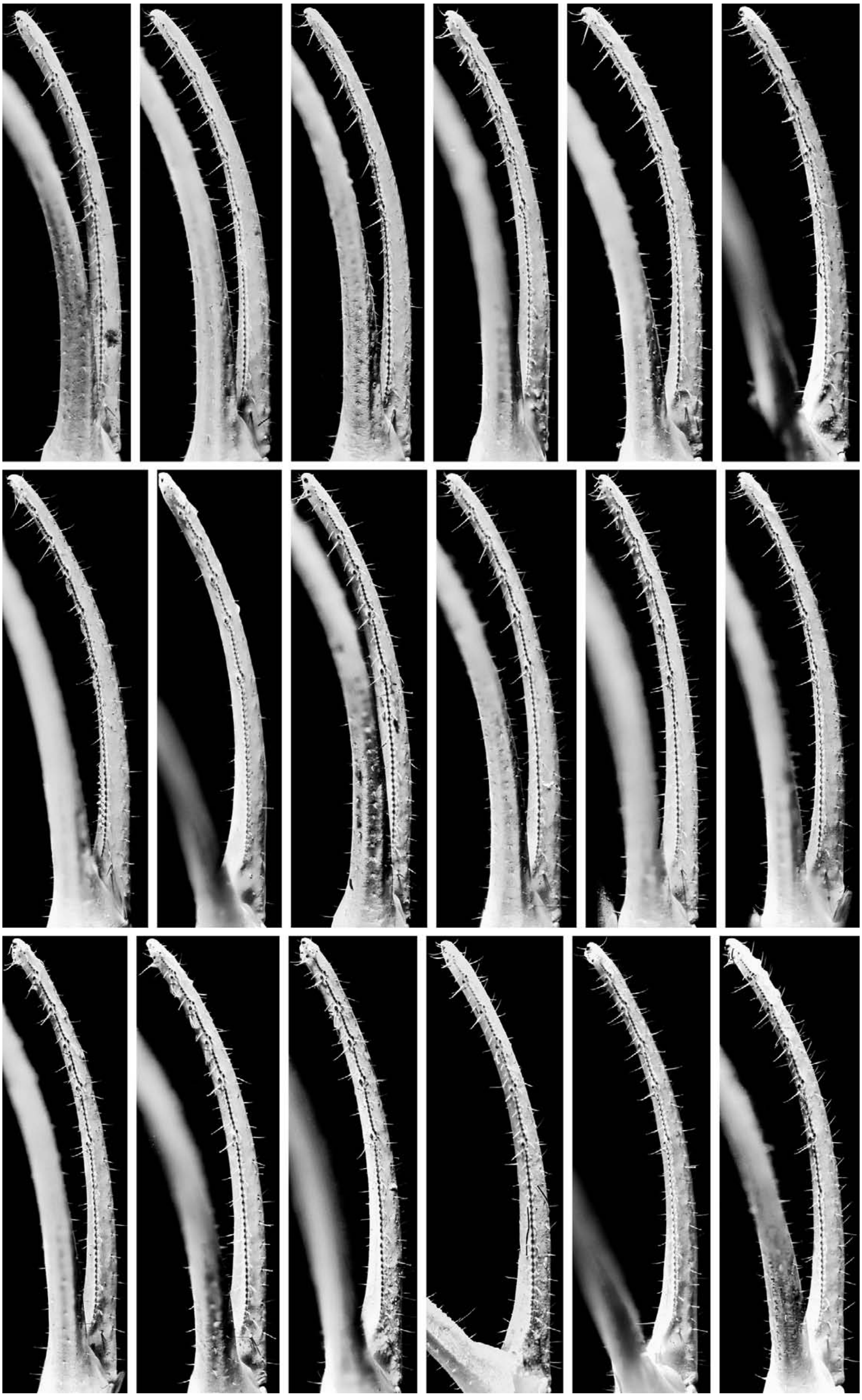

Figure 155. *Langxie feti* **gen**. et **sp**. **n**., paratypes, pedipalp movable fingers showing loss of all EADs.